UNIVERSITÁ DEGLI STUDI DI MILANO
FACOLTÁ DI MEDICINA E CHIRURGIA

DOTTORATO DI RICERCA IN FISIOLOGIA

SETTORE SCIENTIFICO DISCIPLINARE BIO-09

CICLO XXIII°

Tesi di Dottorato di Ricerca

Cost of transport, lower limbs asymmetry and the dynamics of running

Dottorando: Ing. Elena SEMINATI

Matricola: R07721

Tutor: Prof. Alberto E. Minetti
Dipartimento di Fisiologia Umana

Coordinatore: Prof. Paolo Cavallari

Anno Accademico 2009-2010

Tesi autorizzata dal coordinatore
Prof. Paolo Cavallari

Index

Summary

The main topic of my PhD project regards the effects of the human symmetry on energetic and locomotion.
The concept of symmetry, applied in many and different fields, from arts to physical sciences, has been always related to beauty, balance and equilibrium. Most individuals, animals and humans as well, are characterized by an almost complete morphological bilateral symmetry, and the deviation from it caused by environmental stresses, developmental instability and genetic problems, is called Fluctuating Asymmetry (FA). In numerous studies regarding FA, it has been demonstrated that this index is related to several different features, like sexual selection, body mass, running performance in humans and in racehorses.
Similarly, symmetry plays a key role in the maintenance and design of our vehicles. They are periodically inspected, to guarantee a wheel balance/alignment and homogeneous tyre wearing. In this way the fuel consumption can be reduced.
The main aim of this project has its origin from the comparison between mechanical vehicles and the human body. In human locomotion the skeletal muscles (the motor), and the limb lever system (the machine), interact together, in order to produce the movements of the whole body system. We assume that an anatomical or structural symmetry of the human body could have effects on the dynamic asymmetry during locomotion and also could be related to some metabolic energy saving.
Several authors studied symmetry in locomotion with different methodological approaches in human, but also in animals. Different symmetry indices were found in order to classify subjects in different categories, or for pattern identification and pathologies diagnosis, but the relationships between symmetry and the Cost of Transport were poorly investigated. Gait symmetry has been defined as a perfect agreement between the actions of the lower limbs and general this assumption was adopted to simplify data collection and analysis of the lower limbs. Gait asymmetry instead, does not appear to be the consequence of abnormality, but rather reflects natural functional differences between the lower extremities.
In the present study, we tried to validate our hypothesis, investigating anatomical and, dynamical symmetries, and the cost of transport in 19 different aged and trained male runners, in order to find out significant relationships between these parameters. Subjects were divided

in three categories: Occasional Runners (OR), Skilled Runners (SR) and Top Runners (TR), depending of their training/performance level.

Differently from others studies, we compare two different kinds of symmetries: the dynamic symmetry during running at different velocities (i.e. spatial differences, in Body Center of Mass (BCOM) trajectory, between two step), and the anatomical symmetry of the human lower limbs.

A Magnetic Resonance (MR) protocol was applied for each subject, to evaluate the anatomical symmetry of three different anatomical districts Pelvis district (PD), Upper-Leg district (UD) and Lower-Leg district (LD). All the recorded images were analyzed with a custom, ad hoc program that can identify the MR images and calculate a cross correlation index, between right lower limb and left lower limb. This anatomical symmetry index can assume values from -1 to 1 and it is bigger the more the subject's limbs are symmetrical. Level running at incremental velocities on a treadmill was performed in order to record kinematic functional symmetries. The human body was modelled as a series of linked, rigid segments with twenty reflective markers and their positions were captured by an optoelectronic system in order to evaluate trajectory of the BCOM. The coordinate describing this position were successively used to evaluate the main aspects of the gaits and the individual characteristics of movements, a sort of "*locomotion signature*" capable to reflect any significant change in the motion pattern. The time course of each of the 3 BCOM coordinates was fit by a *Fourier Series* and three single anatomical indices (one for each direction) were calculated.

To evaluate running economy, heart rate (HR) and oxygen consumption $\left(\dot{V}O_2\right)$ were measured continuously during level running/kinematic registration.

The hypothesis we assumed, arising from to the world of the motor vehicles, found some answers with the results obtained in this work.

The human body and the mechanical vehicle seem to have some similarity regarding the structure stability. In the human body, a high level of dynamical symmetry, during running locomotion is accompanied by structural/anatomical symmetry, but, differently from the motor vehicles, the energetic consumption doesn't change with the level of anatomical and dynamic symmetry. Furthermore, training seems to be an important element in the stability and in the dynamical symmetry of running, even if no relationship was found between training level and Cost of transport.

Also we found significant negative correlations between anatomical/structural symmetry and subject age. According to the literature asymmetry increase with the age of the subjects.

We can conclude that our body can be biased by asymmetrical anatomical structures of the lower limb in the dynamical symmetry of the BCOM displacement, but without changing the energetic cost of running. Maybe some physiological adaptations of the human machine can compensate for small imperfections in the mechanics of our legged system, with no influence on the metabolic cost of transport, while larger anatomical imperfection, like length legs discrepancy or a body mass not uniformly distributed, or also prosthesis and support for pathological situations, could have a significant effect on the energetic cost of transport.

This work brings new developments in the study of symmetry in locomotion, both for the introduced methods and for the presented result. Anyway further developments could be carried out in order to understand the already obtained results. The number of participants should increase and a longitudinal work could be carried out in order to find out differences between groups. Furthermore kinematic and energetic recording should be performed for a longer period. In this way the subjects could arise higher running velocity, and also we could observe new physiological parameters that we didn't notice in only some minutes of registration.

Prologue

Human physiology is the science of the mechanical, physical, and biochemical functions of human body, its organs, and the cells of which it is composed.

My PhD in human physiology was dedicated in particular to the study of the biomechanics and the energetic of human movements. I tried to combine my background in biomedical engineering with the science of physiology, in order to analyse, model and understand the human motion and its biomechanical and energetic features.

In these last three years I carried out three main projects regarding three different aspects of the biomechanics in locomotion, but also other forms of human movement.

The first project I took part, was an experimental study regarding a novel sport activity; running upstairs on the tallest buildings of the world. Its name is *Skyscraper Running* and in our work we delineated the metabolic and mechanical profile of this sport activity (Minetti et al. 2008; Minetti et al. 2009). While this study was focussed on the main features of running at extreme slopes uphill, in the second study I considered level running and its relationships with the cost of transport and the human symmetry. In this second work the in biomechanical variables describing the symmetry of running have been compared to the anatomical symmetry of the lower limbs, and to the metabolic cost of transport in running at different velocities.

Finally, the last period of my PhD, was addressed to the study of 3D biomechanics of the upper limbs, in particular of the shoulder of the volleyball players during typical movements in volleyball game. The aim of this study was to analyse quantitatively different training techniques for the volleyball players' shoulder, in order to prevent injuries and maintaining a high level of performance.

Each of the presented projects would deserve a complete description of the work done, but I decided to focus my PhD thesis on the study regarding human symmetry/asymmetry and the relationships with the cost of transport. Large part of my PhD was dedicated to this project. This topic involved different aspects of the human biomechanics and energetic that allowed me to increase my scientific knowledge and to acquire new experimental techniques adopted for the study of physiology.

Chapter 1

INTRODUCTION

1.1 Foreword

The term symmetry, applied in many and different fields, from arts to physical sciences, is of ancient Greek origin. It means "Harmonic arrangement of parts" and it has been always related to beauty, balance and equilibrium or even it became a symbol of seeking for perfection.

Most animals and humans as well, are characterized by an almost complete morphological bilateral symmetry with respect to the sagittal plane, and the deviation from it caused by environmental stresses, developmental instability and genetic problems, is called Fluctuating Asymmetry (FA), (Leary & Allendorf 1989; Manning & Chamberlain 1994; Van Valen 1962).

Many authors also identified low FA as an element of beauty and attractiveness, and they emphasized a strong relationship between FA and sexual selection (Gangestad & Thornhill 2003; Grammer & Thornhill 1994). Manning and collaborators, through anatomical measurements, demonstrated that FA was related also to several different features, like body mass (Manning 1995), and metabolic rate (Manning et al. 1997), while their most interesting papers are concerned with symmetry and running performance in humans (Manning & Pickup 1998), and in racehorses (Manning & Ockenden 1994), where FA was negatively correlated with the performance.

In the last two decades several authors studied symmetry in locomotion with different methodological approaches in human (Herzog et al. 1989; Liikavainio et al. 2007; Mattes et al. 2000; Maupas et al. 1999; Potdevin et al. 2008; VanZant et al. 2001), but also in animals (Halling Thomsen et al. 2010; Manning & Ockenden 1994). Different symmetry indices were found in order to classify subjects in different categories, or for pattern identification and pathologies diagnosis, even if the symmetry topic was introduced more than 70 years ago (Lund 1930): Lund showed the effects of structural/anatomical asymmetry on the human locomotion and the same experiments, were recently repeated by a German group (Souman et al. 2009).

The literature reviewed (Sadeghi et al. 2000), shows that symmetrical behavior of the lower limbs during gait has often been assumed, mainly for simplicity in data collection and analysis, while gait asymmetry seems to reflects a natural functional difference between the limbs (Maupas, Paysant 1999). This functional difference does not appear to be the consequence of abnormality, but rather relates to the contribution of each limb to propulsion and control tasks, or also related to the laterality that characterize each individual.

Also Cavagna, in his studies, introduced the concept of symmetry (Cavagna 2010; Cavagna 2009; Cavagna et al. 2008), even if he limited to consider only physical and physiological constrains resulting in the on-off-ground symmetry and the symmetry of rebound, without taking in account differences between right and left limbs.

Even if focussed on a single limb, the works of Cavagna highlighted the interesting idea that locomotion results from the interaction of a motor, represented by the skeletal muscles, and a machine, the limb lever system. This important comparison between the human and the world of mechanical vehicles is useful to better understand the main aims of this project.

1.2 Objectives

As the concept of symmetry has an important influence in human locomotion, it plays a key role in the maintenance and design of the vehicles. They were periodically inspected, to guarantee a wheel balance/alignment and homogeneous tyre wearing, in order to reduce the fuel consumption and ensure driving safety.

Raibert, in 1986, explained that the symmetry used for controlling legged robots, giving them the ability to run and to maintain a stable upright posture, could help in elucidating the legged behaviour of animals (Raibert 1986).

It is the same for human locomotion? Can an anatomical or structural asymmetry of the human body cause a dynamic asymmetry during locomotion? (e.g. unbalanced musculo-skeletal structures, or the effect of unilaterally adding limb orthoses or prostheses can increase the risk of wearing). Also, can a symmetric pattern/structure be related to some metabolic energy saving?

In the present study, we tried to answer these questions, investigating the possible interactions between running economy, anatomical/structural symmetry and dynamical symmetry (i.e. spatial differences, in Body Center of Mass (BCOM) trajectory, between the two steps). We analysed a group of differently aged and trained athletes, in order to take in account also the performance. Differently from others studies, we compare two different kinds of symmetries: the dynamic symmetry of the BCOM trajectory, during running at different velocities, and the anatomical symmetry of the human lower limbs.

In order to find possible relationships between variables these two levels of symmetry will be compared together and also with the Cost of Transport (C), a parameter that can be associated with the machine fuel consumption.

In particular differently from other studies, where anatomical symmetry was measured only with anatomical/anthropometrical data, in this study we will consider for the anatomical symmetry the whole structures of the lower limbs, from bones to muscles, analysed by using Magnetic Resonance Imaging (MRI) techniques.

1.3 Thesis Layout

In these first introduction pages (*Chapter 1*), we described the general idea of our project, introducing the main elements (biomechanical variables, indices and techniques), involved and analysed in this thesis. The following chapters then will discuss the background theory, the methods employed and the results obtained using these methods. In particular

- *Chapter 2* introduces the parameters listed in this first chapter, explaining their meaning, their application and their use in literature, focussing on the main objectives of the project.

- *Chapter 3* explains the methods adopted to find the relationships between anatomical symmetry, dynamical symmetry and the cost of transport. The protocol characteristic, together with the features of the instrumentation utilised are presented. Also this chapter introduces background theory, necessary for an understanding the symmetry indices calculation. In particular, in order to understand some mathematical steps, we help the reader with three different appendices, positioned at the end of the last chapter.

- *Chapter 4* presents the results obtained after the experimental sessions. Firstly we illustrate the single analysed parameters; secondly the same variables are presented together with their statistical results, in order to explain their respective relationships. The results presentation is accompanied by the statistical analysis performed on the processed data. Tables and graphs collecting the analysed data help the reader to better understand the outcomes of this work.

Chapter 5 finally contains a discussion of the obtained results and also offers possible future developments and applications of the obtained results and of the implemented methods. The chapter ends with conclusions drawn from this entire work and recommendations for further work.

Chapter 2

SYMMETRY AND ENERGETICS COST: A REVIEW OF LITERATURE

In this chapter we will present the principal elements involved in this work of thesis. The concept of symmetry will be introduced in order to understand its meaning and its use in the different application fields. Also we will dedicate a paragraph of this chapter to give an explanation of the term “Cost of Transport” with some of its most important features and its relationships with the different biomechanical variables. The chapter ends with a section dedicated to the relationships between energetic cost of human locomotion, performance and symmetry, with some examples of studies present in the literature.

2.1 Symmetry, definition and applications

The meaning of the term symmetry went through a great transformation during its use along many centuries. The proper translation of the Greek term “*symmetria”* - (from the prefix *syn* [together] and the noun *metros* [measure]) - is 'measure that go together'. The Greeks interpreted this word, as the harmony of the different parts of an object, the good proportions between its constituent parts. In the Renaissance, Leonardo exemplified the blend of art and science, providing with the “Vitruvian Man”, the perfect example of his keen interest in proportion (see Figure 2.1). He was convinced that the proportions and symmetry characterizing the human body should also affect architecture and art production. In the centuries symmetry was not only related to such positive values, but it became even a symbol of seeking for perfection.

Symmetry occurs also in geometry, in statistics and in different branches of mathematics. It is actually the analogous of invariance under a set of transformations. The laws of mathematics regarding symmetry have been largely exploited to explain and describe phenomena in different research fields. Symmetry and the lack of symmetry characterize the phenomena in our natural and artificial environment. Likewise, there is a symmetry of many internal organs (kidneys, lungs, brain hemispheres, limbs, etc.) and of other natural phenomena, such as plants, animals and even geological formations.

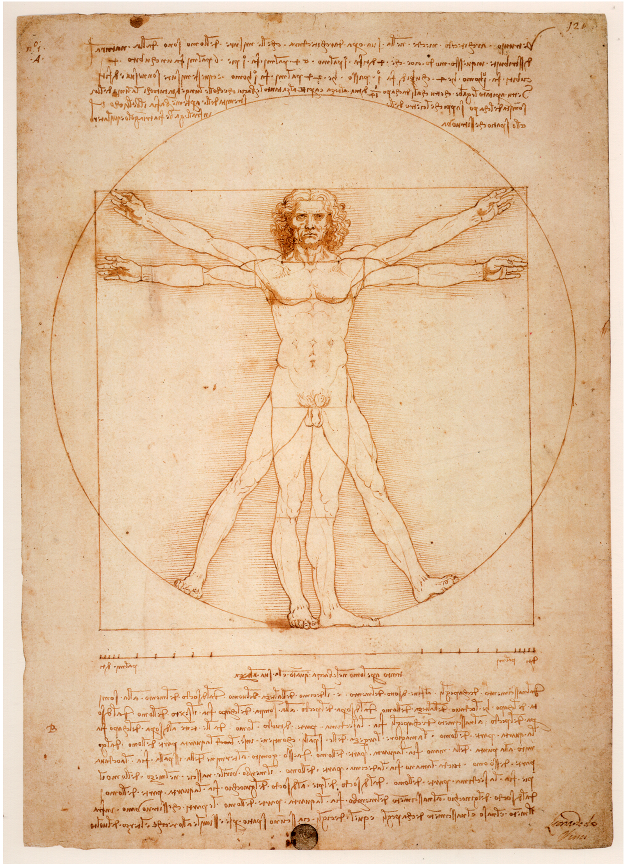

Figure 2.1: The Vitruvian Man, drawn by Leonardo (1487). The drawing is based on the correlations of ideal human proportions with geometry described by the ancient Roman architect Vitruvius. He described the human figure as being the principal source of proportion among the classical orders of architecture.

2.1.1 Fluctuating Asymmetry (FA)

Most animals and humans as well, are characterized by a bilateral symmetry, i.e. their body could be divided into matching halves by drawing a central axis (e.g. human faces, leaves of most plants, insects, spiders, worms and many other invertebrates). Indeed, this constitutes an indicator of developmental stability and the deviation from this almost perfect bilateral symmetry caused by environmental stresses, developmental instability and genetic problems, is called Fluctuating Asymmetry (FA), (Leary & Allendorf 1989; Manning & Chamberlain 1994; Van Valen 1962). It has been also suggested that fluctuating asymmetry (FA) reflects

an animal's ability to cope with the sum of challenges during its growing period and, thus, seems a promising measure of animal welfare (Knierim et al. 2007).
Furthermore many authors identified low FA as an element of beauty and attractiveness, and they emphasized a strong relationship between FA and sexual selection (Gangestad & Thornhill 2003; Grammer & Thornhill 1994). Grammer and Thornhill, in their studies, shown that both averageness and symmetry in faces would be preferred (figure 2.2), and, successively, it has been verified that the magnitude of the negative correlation between fluctuating asymmetry and success related to sexual selection was greater for males than for females (Moller & Thornhill 1998).

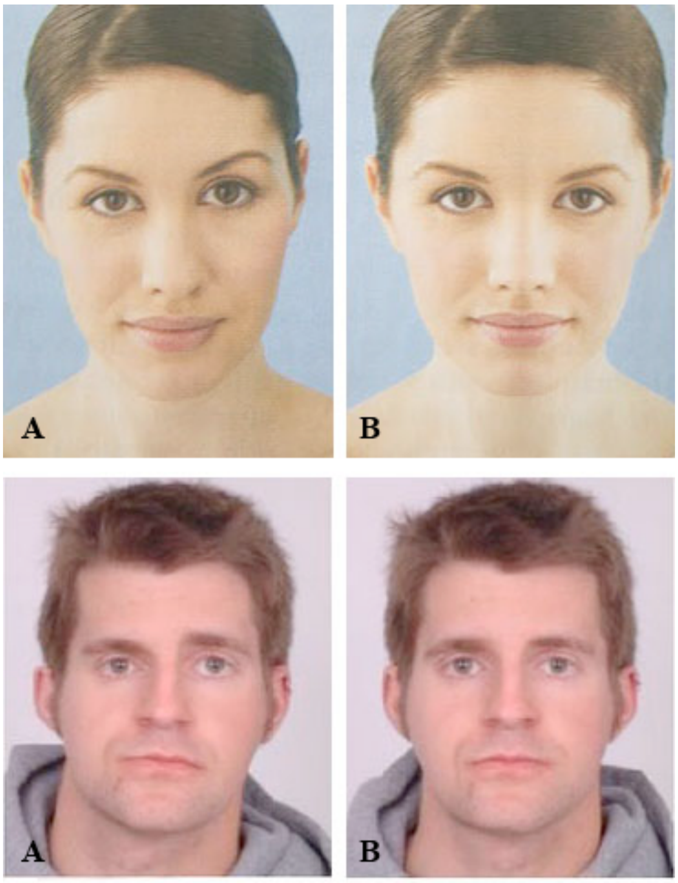

Figure 2.2: An example of computer generated symmetrical faces (B) compared with the original one (A). The experiment of Grammer and Thorhill in 1994, shown that symmetry and averageness were preferred in human faces.

Nowadays, it has been sought to establish which aspects of attractive bodies are more predictive of lower fluctuating asymmetry (Brown et al. 2008). Strong negative correlations between fluctuating asymmetry and bodily attractiveness (both sexes) have been found. Further, gender-specific body size and shape characteristics were treated as attractive and correlated negatively with fluctuating asymmetry. Among the numerous authors who focussed on FA, Manning presented FA as an important factor in human sexual selection. Through anatomical and anthropometrical measurements he demonstrated that FA was related to several and different features, like body mass (Manning 1995), and metabolic rate (Manning, Koukourakis 1997), although his most interesting papers are concerned with symmetry and running performance in humans (Manning & Pickup 1998), and in racehorses (Manning & Ockenden 1994), where he showed that FA was negatively correlated with locomotion performance.

2.1.2 Symmetry in locomotion

Natural locomotion involves a variety of different mechanisms, in particular in legged locomotion symmetry plays an important role in describing the features of a specific paradigm, in humans, but also in animals. The locomotor paradigms are different according to the age, to the environments and to the individuals necessities, and different energies are involved in them (Saibene & Minetti 2003). Individuals can intentionally manipulate bipedal coordination patterns in order to gallop, hop, or skip in sports or for various dance forms. While for children skipping is a typical exploited locomotion pattern, adults could gallop or unilaterally skip when on the moon or when descending slopes or stairs (Minetti 1998).

Hildebrand began studying symmetry in animal locomotion more than 20 years ago, explaining that there are two principal class of gaits. *Symmetrical gaits* have the footfalls of a pair of feet evenly spaced in time (the pace, various walks and running walks, and the trot), while *asymmetrical gaits* have the footfalls of a pair of feet un evenly spaced in time as gallops and bounds (Hildebrand 1977). Some years later Raibert suggested that while symmetric motion accounts for nominal, steady-state behaviour, asymmetry accounts for the forces required to stabilize the system against external disturbance and for the accelerations needed to change running speed, posture or direction. Asymmetric leg and body motion can also compensate for imperfections in the mechanics of the legged system, such a friction in the joins, unsprung mass in the legs, and body mass not uniformly distributed (Raibert 1986).

One of the first studies about the asymmetric legs was performed in 1930 by Lund. He showed the effects of a structural/anatomical asymmetry on human locomotion (Lund 1930). In his experiments, blindfolded subjects were required to walk straight on from point O to point P, like shown in figure 2.3. Without visual information, human subjects were not able to maintain a straight active displacement. In particular subjects veered in the direction corresponding to their shorter leg, both in forward and backward walking.

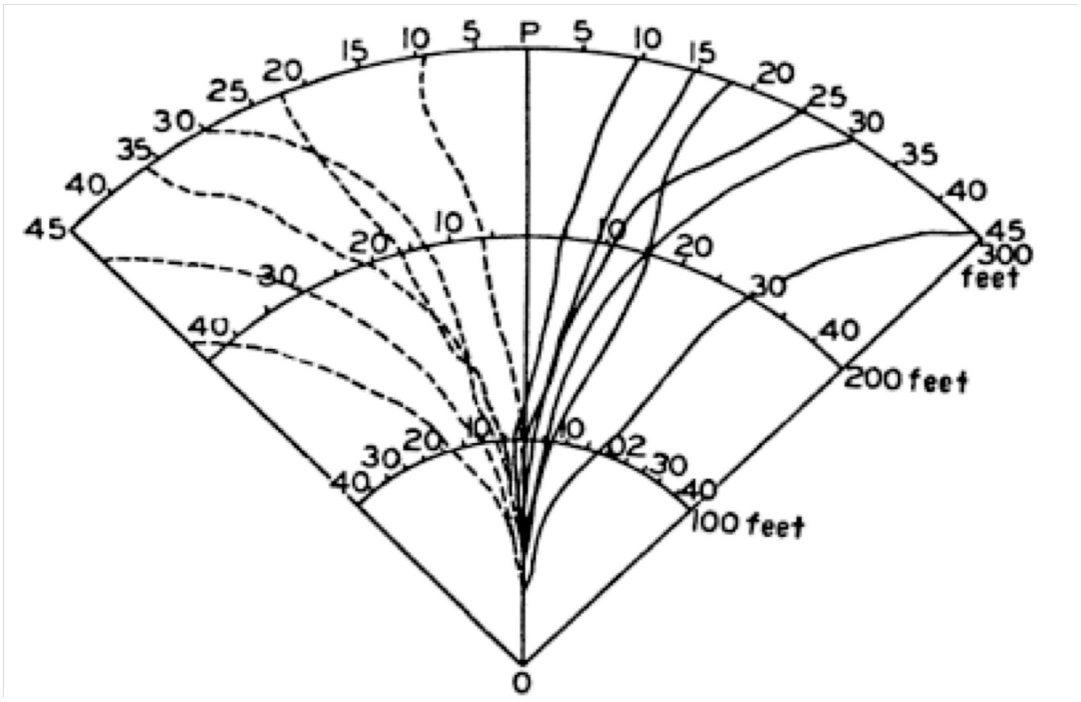

Figure 2.3: Diagram for the experimental field used by Lund in 1930. O is the start point, P is the final point the subject had to reach. The continuous lines to the right (walking forward) and the dotted lines to the left (walking backward) indicate the performance of a "Left-dominance" subject.

The same kind of experiments, were successively repeated (Boyadjian et al. 1999; Souman, Frissen 2009), concluding that systematic deviations occurring in two-limb displacements originate from a peripheral mechanism (slightly different properties of the right and left limbs) rather than a central mechanism (systematic bias in the perceived body trajectory), but no significant correlation was found between leg dominance length and the veering direction. Laterality has been cited as an explanation for the existence of functional differences between the lower extremities (Gentry & Gabbard 1995; Whittington & Richards 1987), although a number of studies do not support the hypothesis of a relationship between gait symmetry and laterality (Armitage & Larkin 1993; Gabbard C & Hart 1996; Katsarkas et al. 1994; Rudel et al. 1984). Further investigations are needed to demonstrate functional gait asymmetry and its relationship to laterality, taking into consideration the biomechanical aspects of gait.

Anatomical or physiological criteria have been used to describe symmetrical or asymmetrical gait behaviour. It seems that the common idea in the different definitions is that the term 'gait symmetry' can be applied when both limbs behave identically (Sadeghi, Allard 2000).

In the last two decades several authors studied symmetry locomotion (in human and animals) with different methodological approaches, e.g. with force platforms (Herzog, Nigg 1989), by electrogoniometry recordings (Maupas, Paysant 1999), with plantar pressures measurements (VanZant, McPoil 2001), using optoelectronic systems (Potdevin, Gillet 2008), or adopting a combination of the different listed instrumentations (Liikavainio, Isolehto 2007).

Sometimes symmetry was simply evaluated from the measured physiological or anthropometric values in the two different human limbs (Herzog, Nigg 1989; VanZant, McPoil 2001). In other cases a symmetry index was calculated starting from biomechanical measured variables (step length, swing time, stance time), in order to classify subjects in different categories, for pattern identification or for pathologies diagnosis (Halling Thomsen, Tolver Jensen 2010; Mattes, Martin 2000).

The symmetrical behaviour of the lower limbs during gait has often been assumed in literature mainly for simplicity in data collection and analysis, while gait asymmetry seems to reflect a natural functional difference between the limbs. This functional difference does not appear to be the consequence of abnormality, but rather relates to the contribution of each limb to propulsion and control tasks. Laterality may be another explanation for the presence of functional differences between the lower extremities. Basically, the preferred limb carries out an action towards a goal, while the other limb provides support. However, more work is needed to evaluate gait symmetry and to determine its possible relationships to other physiological and biomechanical parameters.

2.2 The cost of Transport

The Cost of Progression (metabolic or energy Cost of Transport, C) is a parameter that characterises any type of human/animal locomotion.

As underlined di Prampero (di Prampero 1986), the earliest attempts to describe quantitatively the energetic of human locomotion were devoted to walking, in the second half of the 19th century (di Prampero 1986). Some years later, some authors determined a value for the energy cost of running, not far from the presently accepted ones (Waller 1919) (Liljestrand & Stenstrom 1920).

In 1950 the famed engineer and physicist von Kármán, together with his student Gabrielli put forward this concept, introducing a term called "economy of transport", describing how much power is needed to move the weight of the vehicle at its speed and presenting a chart on which the specific cost of transport of the various modes of transport is plotted against speed (Figure 2.4), (Karman & Gabrielli 1950). Successively, in 2005 a group of mechanical engineers revisited the work of Gabrielli-Kármán. They proposed a new graphical representation of the specific resistance for various transport, adding the improvement of the last decades, (figure 2.5).

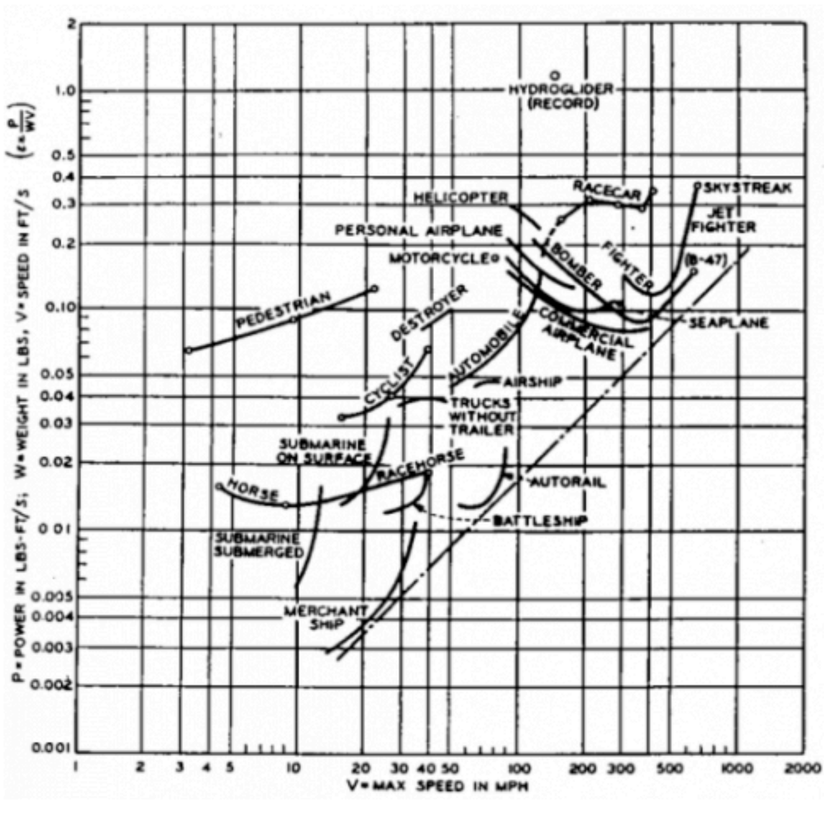

Figure 2.4: Specific cost of transport of the various modes of transport are plotted against their speed. The bulk of the data lies above a line of gradient 1, identified as the Gabrielli-Kármán line, which represents 'best performance'. (Karman & Gabrielli 1950).

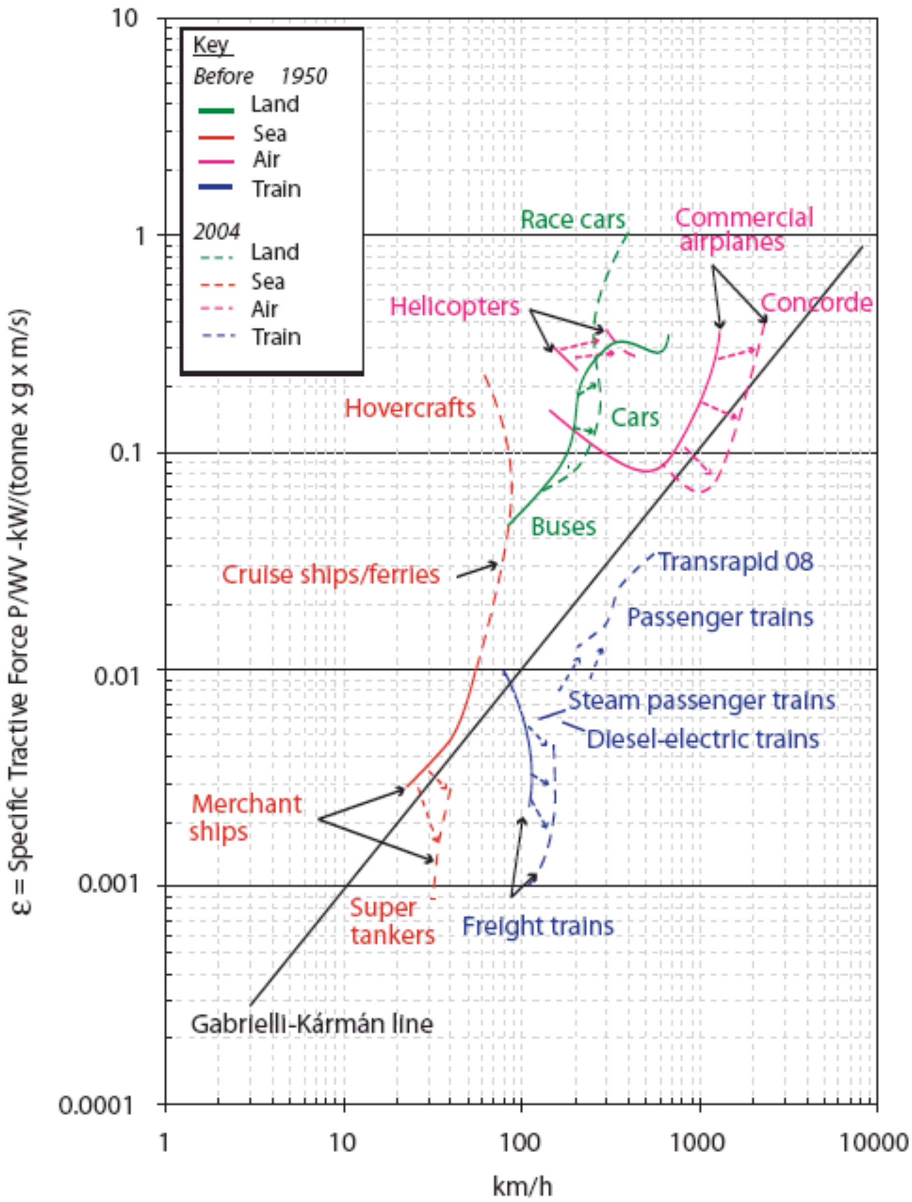

Figure 2.5: Updated specific Cost of trasport of various transport modes over the last 54 years. The data lines for sea, land and air transport have moved below the original Gabrielli-Kármán line (movement illustrated by arrows), which illustrates considerable performance improvement in all kinds of transport. From Yong et al. 2005.

A similar representation was suggested even earlier, in a classical study of the energy expenditure of walking and running at different speeds and on different gradients (Margaria 1938); as in the study of the1950, regarding vehicles, Margaria introduced the energy spent per unit distance covered, for human walking and running, at different slopes. Later, Schmidt-Nielsen (Schmidt-Nielsen 1972), called this parameter the ‘‘cost of transport’’ (C).

For a given subject C is the quotient of net metabolic power divided by speed, and as such has the physical dimensions of force. To compare subjects of different size, C is usually expressed

as the quotient of net metabolic power divided by the product of speed, times body weight (body mass times acceleration due to gravity), that has also the physical dimensions of power (mechanical power). As such, the quantity becomes dimensionless and can be viewed as the reciprocal of efficiency.
In this work we considered C as the amount of oxygen consumed to move 1 Kg of body mass 1 m distance and we calculated it as

$$C = \frac{\left(\dot{V}O_2 - \dot{V}O_{2rest}\right) \cdot Eq}{Vel \cdot m}$$

where $\dot{V}O_2$ and $\dot{V}O_{2rest}$ expressed in ml O_2 $\cdot$(Kg min)$^{-1}$, are the O2 uptake consumed during the run (stationary conditions) and at rest respectively. *Eq* is the Energetic Equivalent, i.e. the amount of energy burned per litre of O2 consumed. We considered for *Eq* a value of 20.9 J$\cdot$ml^{-1}. The net metabolic power is represented by the difference $\left(\dot{V}O_2 - \dot{V}O_{2rest}\right)$, *Vel* represents the running velocity (m $\cdot$ s^{-1}) and *m* (Kg) is subject mass.

2.2.1 Cost of Transport features

The Cost of transport of different modes of human locomotion was thoroughly and extensively reviewed years ago by di Prampero (di Prampero 1985; di Prampero 1986) and it has been linked to a number of anthropometric and kinematic characteristics. These include factors such as size, slope, body mass distribution, stride length and/or stride frequency, air resistance, age and training.
In the next pages we will analyse some of these variables in relationship with the cost of transport, being one of the most important feature of the energetic Cost of transport its independence from the running speed, (see Figure 2.6).
Differently to what happens in human walking (Anderson & Pandy 2001; Cotes & Meade 1960; Ralston 1958) and in other sports such as skiing, country-cross skiing and skating as represented in figure 2.6, human running at steady state is not characterized by a speed at which running is optimally efficient (Bramble & Lieberman 2004; Cavagna et al. 1964; Di Prampero et al. 1993; Mayhew 1977; Steudel-Numbers & Wall-Scheffler 2009).

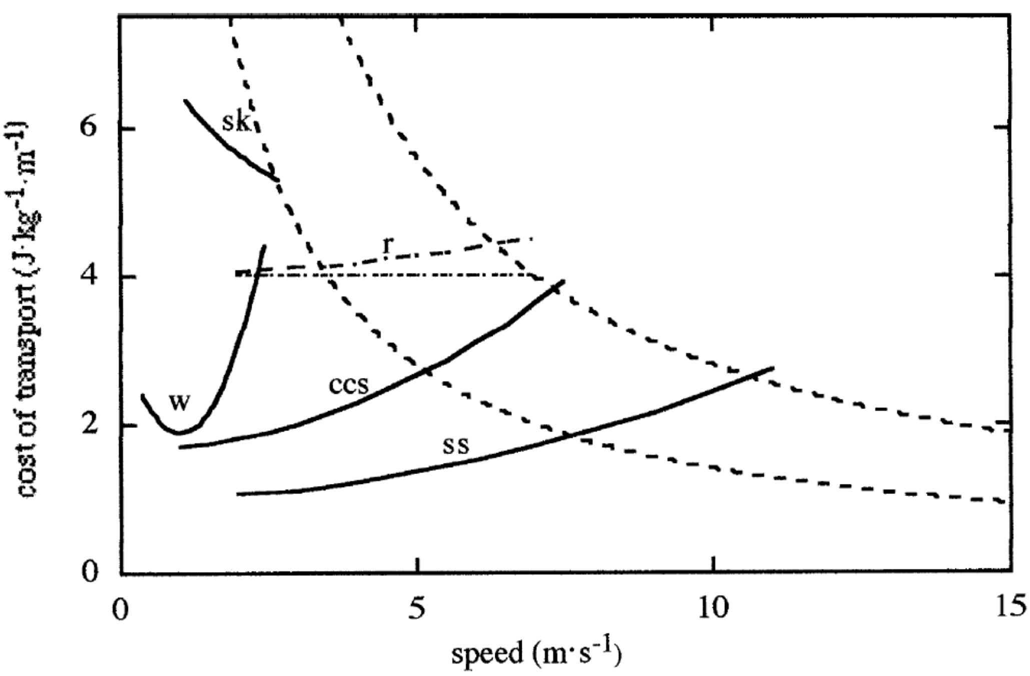

Figure 2.6: Cost of transport as a function of the speed for different types of human locomotion. w walking, r running, ccs crosscountry skiing, ss ice skating, sk skipping. The dashed curves represent the iso-metabolic power limit for a healthy normal subject (14 W.kg–1, lower curve) and an athlete (28 W.kg–1, upper curve), from Saibene and Minetti 2003.

In walking, the relationship between the energy expenditure above that at rest and speed can be empirically described using a quadratic equation. In fact, as it is shown in figure 2.6, C presents a minimum at an intermediate speed, called "the optimal walking speed", very close to the spontaneous walking speed. Furthermore, at each walking speed there is an optimal stride-frequency, corresponding to the freely chosen stride frequency, which minimizes C (Zarrugh & Radcliffe 1978; Zarrugh et al. 1974). As the speed increases the cost of walking attains and even exceeds that of running. The latter, as already stated, is almost constant and independent of the speed. As in walking, the stride frequency that is freely chosen in running is the least metabolically expensive (Kaneko 1990).

The independence between metabolic cost and running speed has been verified both in level and in slope locomotion (di Prampero 1985; di Prampero et al. 2009; Saibene & Minetti 2003). Furthermore energy cost of walking has a minimum at an optimal speed which is smaller the steeper is the slope uphill. Also, as shown in figure 2.7, the energy cost of walking is lower than walking and the both C have an absolute minimum at a slope of about -10% (di Prampero 1986).

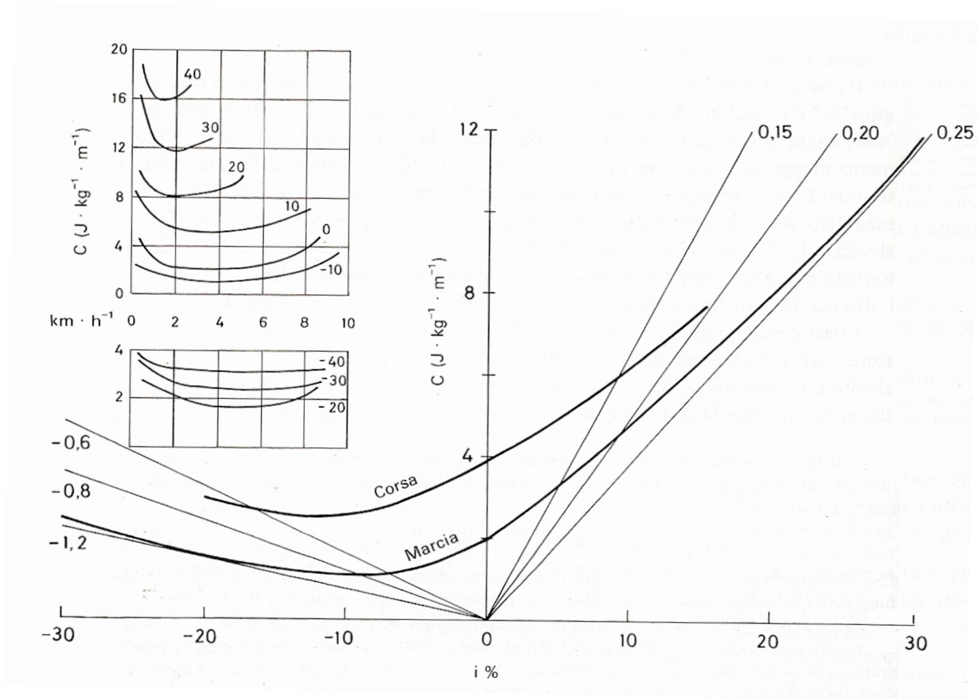

Figure 2.7: Energetic Cost above resting of walking ("Marcia") at the optimal speed, and of running ("Corsa"), (C, J · (Kg · m)$^{-1}$), as function of the incline (i, %) of the terrain. Every point on the abscissa is characterized by a given value of work performance against gravity per unit of distance. This allows construction of iso-efficiency lines (six of which appear on the graph) along which the ratio mechanical work/energy cost is constant. For down slopes, efficiency is negative since the mechanical work is performed by the gravitational field on the subject's body. The energy cost of running is independent of the speed at all slopes, that of walking is not. This last is indicated in the insert as a function of the speed, for different i values. From diPrampero 1985.

In addition, also in running children C (above resting) is essentially independent of the speed (MacDougall et al. 1983), even if it is larger than in adults (Daniels & Oldridge 1971) and decrease with increasing age, to achieve the adult values at 15-16 years of age (Daniels & Oldridge 1971).

2.2.2 Cost of Transport and training

From the first studies about the Cost of transport we know that C, is essentially the same in men and women (Bransford & Howley 1977; Daniels et al. 1977; Falls & Humphrey 1976) and in sedentary and athletic subjects (Allen et al. 1985; Conley & Krahenbuhl 1980; Margaria 1938; Margaria et al. 1963).

Regarding the effects of training on running economy the question has been largely discussed since a few decades ago (Daniels 1985), up to more recent years (Beneke & Hutler 2005).

Contradictory findings are due to the different methodological approaches. For instance, a range of different methods were used to assess running economy, a variety of training interventions were used, and groups of subjects were used that differed in terms of age and fitness.

Cross-sectional studies in general reported no training effect on C (Bourdin et al. 1993; Dolgener 1982; Margaria, Cerretelli 1963; McGregor et al. 2009; Slawinski & Billat 2004), while a longitudinal experimental design should either identify or exclude the potential effect of training. In this kind of study a decrease in C was observed following running training (Billat et al. 1999; Petray & Krahenbuhl 1985; Smith et al. 1999) but also in other studies no training effects on C was found (Beneke & Hutler 2005; Lake & Cavanagh 1996). Beneke tried to explain these results underlining that such findings do not necessarily mean that C does not respond to training at all, but rather is important to use specific training intensities to do so. Also he stated that

- Improvement of C is specific to the velocity domain emphasized during the running training
- Prolonged low-intensity running is less effective than high-intensity interval training at lowering C in endurance runners tested at race speed.
- Running performance could improve due to metabolic adaptations, independently of any effects on C that might be observed during the later training period.

Consequently, in order to be certain about training and the Cost of transport behaviour, we have to take into account several conditions and variables, in order to better understand every single situation.

2.2.3 Cost of Transport, performance and Symmetry

In order to discuss the relationships between Cost of transport, performance and symmetry it is useful to exploit an important comparison often mentioned in human physiology and biomechanics, i.e. human body and motor vehicles.

Locomotion results from the interaction of a motor, represented by the skeletal muscles, and a machine, the limb lever system. The muscles transform chemical energy of fuel into heat and positive mechanical work. The primary muscle shortening, similar to the motion of the piston in a car engine, is not suitable to sustain locomotion directly. Positive muscular work must be done on a lever system, which has the task to interact appropriately with the surrounding to promote locomotion (Cavagna 2010).

As for a car, also in human locomotion the main aim consist in minimizing the fuel consumption. As we saw before, indeed, during the different gaits patterns, individuals choose freely a stride frequency that is the least metabolically expensive. Similarly driving a car we should maintain a velocity that can minimize the fuel consumption, obtaining an optimal economy. The concept of symmetry also plays a key role in the maintenance and design of the vehicles. They are periodically inspected, to guarantee a wheel balance/alignment and homogeneous tyre wearing, in order to reduce the fuel consumption and to confer stability to the vehicle. In the present study we will try to investigate whether a structural asymmetry of the human body can cause a dynamic asymmetry during locomotion, like it could occur in a car. Also the relationship between a symmetric pattern/structure and some metabolic energy saving will be studied.

In 1986 Raibert, suggested that asymmetric leg and body motion could also compensate for imperfections in the mechanics of the legged system, such a friction in the joins, unsprung mass in the legs, and body mass not uniformly distribuited (Raibert 1986). In the previous section we spoke about experiments regarding discrepancies in the lower limbs (see section 2.1.2), showing the relationship between structural asymmetry and locomotion asymmetry, but there was no correlation with the energetic cost. In 2001, Gurney presented a study about the effect of limb-length on gait economy. He showed that both oxygen consumption and the rating of perceived exertion were greater with a 2-cm artificial limb-length discrepancy. Also he stated that a 3-cm artificial limb-length discrepancy was likely to induce significant quadriceps fatigue in the longer limb and elderly patients with substantial pulmonary, cardiac, or neuromuscular disease might have difficulty walking with a limb-length discrepancy as small as 2 cm, see figure 2.8 A and 2.8 B (Gurney et al. 2001).

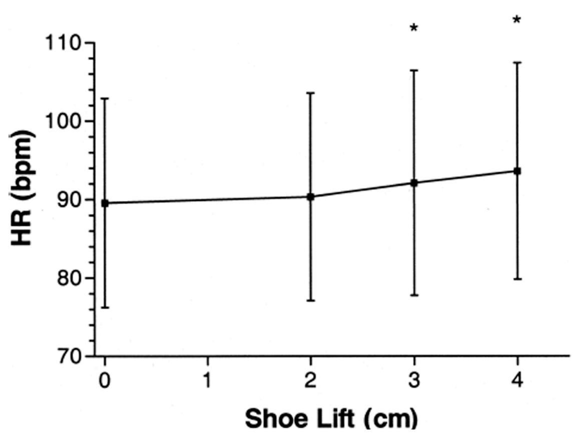

Figure 2.8 A: Relationship between The response of heart rate (HR) to artificially induced limb-length discrepancy. The asterisks indicate a significant difference compared with the value with no discrepancy (Gurney, Mermier 2001).

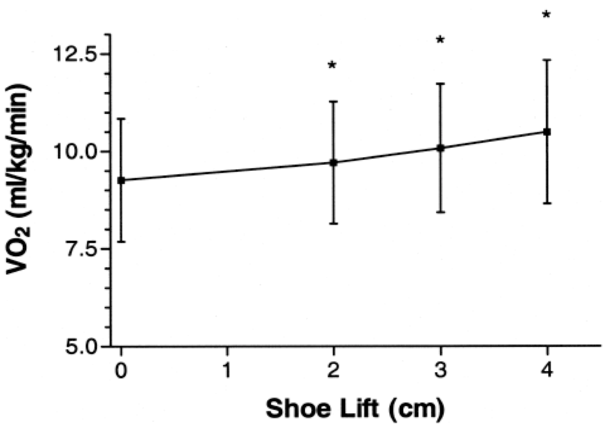

Figure 2.8 B: The response of oxygen consumption (VO2) to artificially induced limb length discrepancy. The asterisks indicate a significant difference compared with the value with no discrepancy (Gurney, Mermier 2001).

Also another study reported the relationships between structural asymmetry and changes in the energetic cost of transport (Mattes, Martin 2000). They investigated the effects of increasing the mass and moment of inertia of the prosthetic limb of people with unilateral, transtibial amputations on symmetry and on the energy cost. They founded that the loading configuration required to produce a match in the moments of inertia of the prosthetic and intact lower legs, resulted in greater gait asymmetry and higher energy cost.

Although these reported studies tried to correlate symmetry and the energetic variables related to the cost of transport, they didn't consider the subjects performance.

The first studies about symmetry and performance were performed by Manning and collaborators about two decades ago. In their works, through anatomical measurements, they demonstrated that FA was related to several and different features as we saw in the previous section.

The first work about symmetry and performance was performed on horses (Manning & Ockenden 1994). The authors measured 10-paired characters on 73 flat-racing thoroughbreds and calculated the relative asymmetry (FA) for each character. The averaged asymmetry value of the 10 measured anthropometric features is plotted against the racing ability in figure 2.9. They showed that FA in thoroughbred racehorses had an effect on racing ability and could therefore be a predictor of future performance in young horses.

Some years later Manning and Pickup repeated the experiments in humans. The purpose of that work was to examine the association between human symmetry and athletic performance with particular reference to middle distance runners (Manning & Pickup 1998).

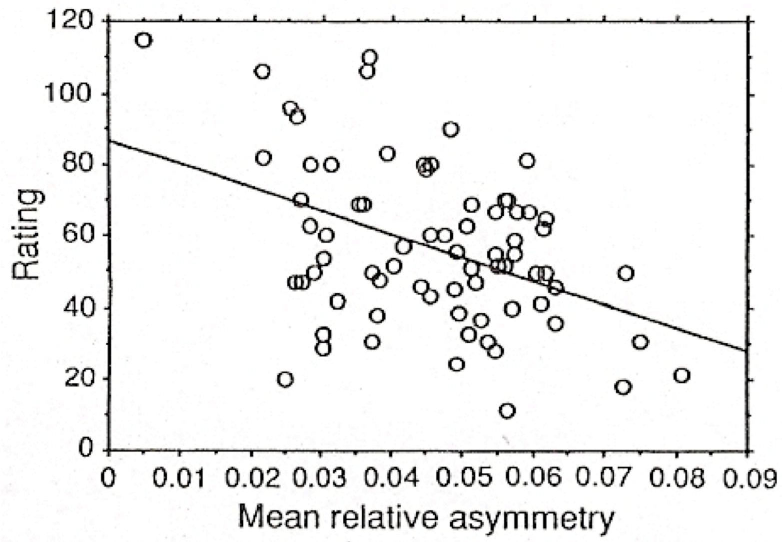

Figure 2.9: Relationship between the racing ability of 73 thoroughbred racehorses as measured by the ratings of the British Horseracing Board and overall mean FA (10 paired characters), per horse ($r^2 = 0.18$, $P = 0.0002$)

As in the previous study, seven anatomical traits were measured and the results suggested that symmetric athletes run faster than asymmetric athletes and the best predictors traits of speed were nostril and ears, as it is shown in figure 2.10.

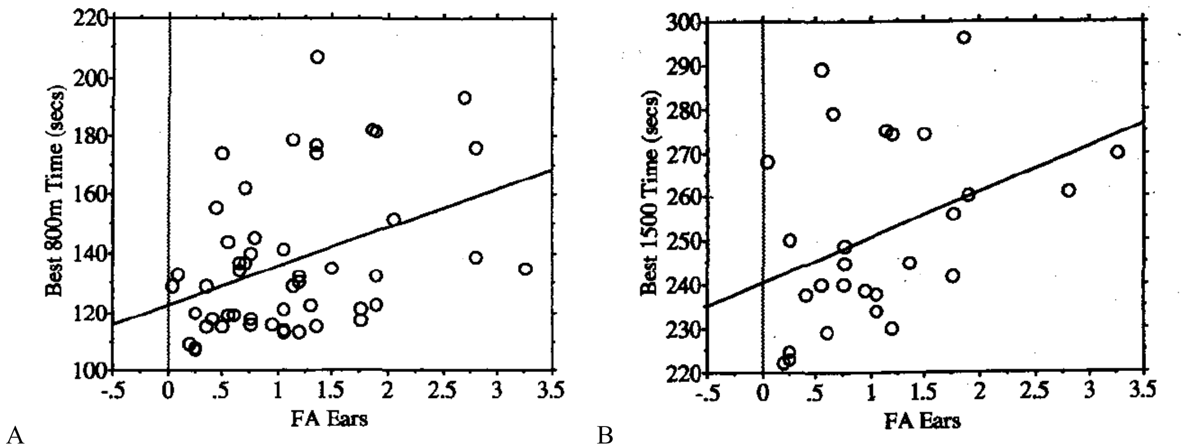

Figure 2.10: Relationships between: A) best 800 metre times and ear symmetry, B) best 1500 metre times and ear asymmetry.

Thought these last results were encouraging in order to consider FA as a predictor of performance, the work was only a pilot study and the author also suggested further developments, in order to examine relations between symmetry and other variables such as maximal oxygen consumption $\dot{V}O_{2\max}$ and Heart Rate (HR).

As suggested by Manning et al., the studies we mentioned, were only preliminary works; they limited their analysis to single anatomical/anthropometrical measures, without considering the whole individuals structure.

Also they evaluated the individuals' performance only from the subject record race times, or from questionnaires and interviews, without the evaluation of some important physiological and energetic measurements, necessary to describe quantitatively the athletes' performance.

For this reasons we based our study on different techniques and measurements, in order to evaluate not only global anatomical symmetries, but also dynamical symmetries, related to the three-dimensional (3D) displacement of the Body Centre of Mass (BCOM), the imaginary point where the whole body mass could be located to preserve the body dynamics (Winter 1979).

To complete the experiments we also evaluated physiological parameters like the Heart Rate (HR) and the Cost of Transport (C), in order to estimate the subject performance and its relations with the evaluated symmetries.

Chapter 3

MATERIALS AND METHODS

3.1 Subjects

Participants in this investigation were nineteen volunteered healthy male subjects of different ages (from 20 to 55 years).

Exclusion criteria included neurological or musculoskeletal pathologies affecting running ability. The institutional ethics committee had approved all methods and procedures and subjects gave informed consent prior to participation (see the attached informed consent format at the end of this paragraph).

We stratified participants into three different groups, based on their specific running ability:

- group 1, (n=7): Occasional Runners (OR), who practiced sport (not specifically running) 3 times *per week* (less than 2 hours *per week*)
- group 2, (n=7): Skilled Runners (SR), fit athletes, in prevalence triathletes, who trained more than 3 times *per week*, (between 2 and 6 hours *per week*). Each of them had already took part to a national competition (marathon, half marathon or 10 Km competition)
- group 3, (n=5): Top Runners (TR), who trained more than 3 times *per week* (at least 6 hours *per week*); they were marathon runners and with a mean performance time of 2 h 44 min 24 sec ± 10 min 12 sec.

Anthropometric characteristic of the different populations are shown in Table 3.1.

	Occasional Runners (±SD)	**Skilled Runners (±SD)**	**Top Runners (±SD)**
Participants (n)	7	7	5
Age (yrs)	33.1 ± 13.2	31.9 ± 11.8	42.6 ± 7.4
Body Mass (Kg)	70.6 ± 3.4	67.3 ± 6.1	68.2 ± 4.9
Height (cm)	175.9 ± 4.7	177.3 ± 4.0	177.8 ± 4.4

Table 3.1: Number of participants, mean ± standard deviation (SD) of age (yrs), body mass (Kg), and height (cm) of the 3 different groups

Informed Consent

Thank you for your taking part in this scientific experiment. Before starting, you will be given some information about why the exam is being carried out.

The main aim of this project is to verify both static anatomical and kinematic functional symmetries as important and relevant determinants of running economy.

To reach this goal, you will be expected to run on a treadmill, on level conditions, at 6 different incremental speeds (from 2.22 to 5.00 m/s; step 0.56 m/s).

20 reflective markers will be placed on the anatomical landmark points. A motion capture system will record kinematic data, in order to specify kinematic anatomical symmetries. At the same time, running economy will be recorded with the portable metabolic system $K4b^2$ (Cosmed). To analyse static anatomical symmetries, a MRI (Magnetic Resonance Imaging) will be carried out.

All running testing will be performed utilising the Biomechanics Laboratory of the Faculty of Exercise and Sport Science at Verona University. All MRI will be carried out in the general hospital of Borgo Roma in Verona.

We assure you that all data will remain anonymous and privacy will be guaranteed. Furthermore, data will only be utilized as regard this scientific research project.

Verona, date ………………

Tester's signature

………………………………………………………………

Researcher's signature

………………………………………………………………

3.2 The design of the experimental protocol

The protocol we adopted for this project is structured in three principal steps; each subject took part in kinematic analysis, energy cost measurements, and Magnetic Resonance (MR) examinations. Level running was performed in order to record both kinematic functional symmetries and running economy. These first two steps were carried out utilising the Biomechanics Laboratory of the Faculty of Exercise and Sport Science at Verona University, while the MR images were recorded in the radiological ward of the University Hospital of Borgo Roma, in Verona.

3.2.1 Kinematics

Level running on a treadmill (h/p/Cosmos Saturn 4.0, Germany), was performed in order to record kinematic functional symmetries.

The human body has been modelled as a series of linked, rigid segments: twenty reflective markers (Ø = 14 mm) were placed on anatomical landmark points (Figure 3.1), and their positions were captured at 100 Hz, using a eight-camera Vicon MX13 (1.3 million pixel) optoelectronic system (Vicon, Oxford, UK); eighteen markers were placed bilaterally, nine per each side (Koopman et al. 1995; Mian et al. 2006), two markers were placed asymmetrically because of Vicon system demands. In this way, 12 body segments were defined. In figures 3.1 and 3.2 we reported a list of all the markers and the segments included in our model.

After a brief period of familiarisation on the treadmill, at least 10 minutes, according to the documentation data (Lavcanska et al. 2005), each subject ran at six different incremental speeds: from 2.22 m/s to 5 m/s; step was 0.56 m/s. Each speed was maintained for at least 5 min, a time long enough to record an acceptable number of gait strides and corresponding physiological variables (Chen et al. 2009; Jones & Doust 1996; Minetti & Saibene 1992). Also a rest period of at least 5 min was proposed among the selected speeds.

During each test, the subjects had to run as naturally and regularly as possible. They also had to keep to in the middle of the treadmill, looking straight ahead (see Figure 3.3).

The test running session took 3 hours and each subject carried out at least 6 trials. To sum up, 400 trials/conditions were examined, in total.

Only five skilled runners and five top runners were able to complete all the running protocol (up to 5.00 m/s). Other subjects stopped at the speed of 4.44 m/s.

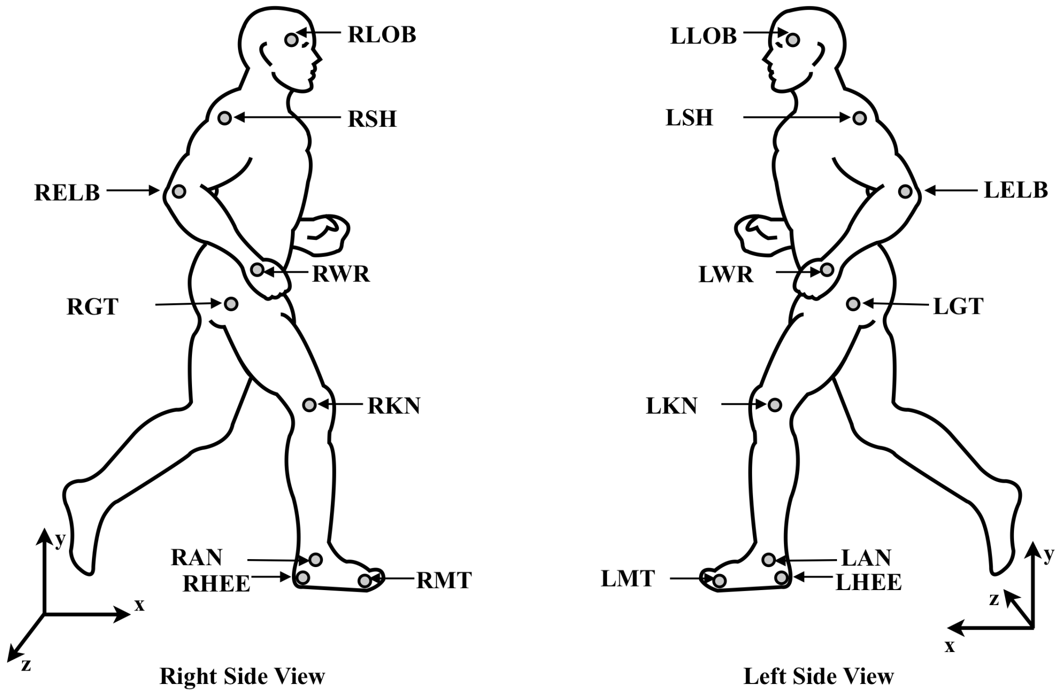

Figure 3.1: List of the twenty markers used for the kinematic protocol. We also indicated the convention we used for the reference system: x for forward, y for vertical and z for lateral direction.

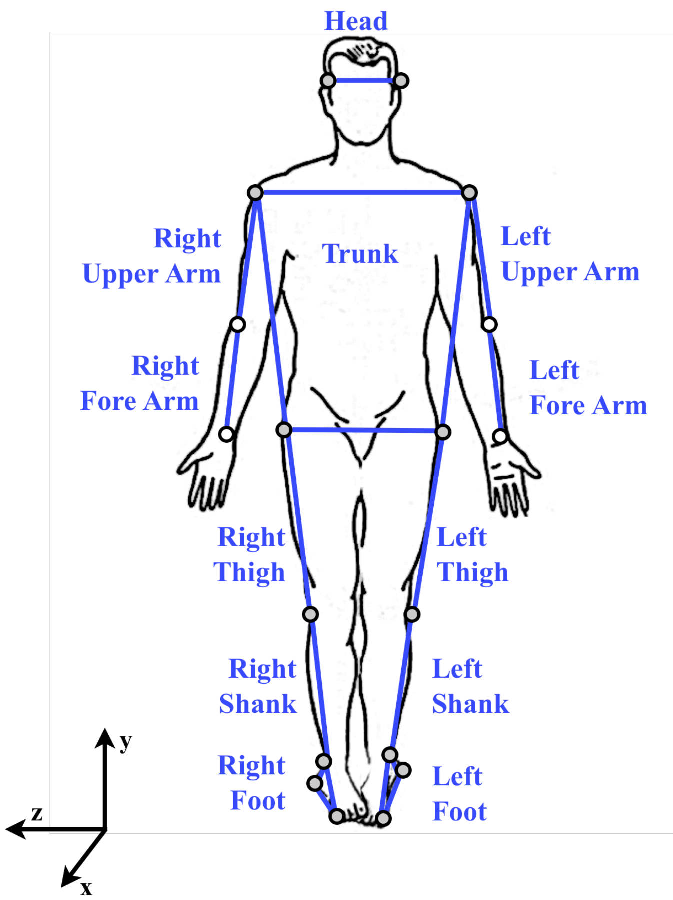

Figure 3.2: List of the twelve body segments used for the kinematic protocol.

For two runners (one OR and one SR), only one kinematic registration was performed at each speed. However, for all the others, during each run, three consecutive kinematic registrations were carried out: a) one at the end of the first minute (from 0.30 seconds to 1.00 minute); b) one in the middle of the test (from 2.30 to 3.30 minute); and c) one at the end of the last minute (from 4.30 to 5.00 minute). Their average value was used successively to compute the experimental trajectory of the Body Centre of Mass (BCOM). The 3D recorded coordinates of the 12 segments, together with the anthropometric tables (Dempster et al. 1959), were used in the mathematical method proposed by (Minetti 2009), simultaneously capturing the spatial and dynamical features of that 3D trajectory, in order to evaluate the dynamical symmetry indices (see paragraph 3.3).

3.2.2 Energy cost Measurement

To evaluate running economy, oxygen consumption $\left(\dot{V}O_2\right)$ was measured with a breath-by-breath gas analyser (Cosmed K4b^2, Rome, Italy), continuously during level running/kinematic registration. Data, including heart ate (HR), were sent via telemetry to a computer and recorded at each progression speed, after that the metabolic steady state had been achieved (3 min) for further 2 minutes, for averaging.

Before the familiarisation period on the treadmill, 6 minutes of basic routine was proposed, according to the most typical energy cost measurements protocols (Ardigo et al. 2005; Doke et al. 2005; Minetti et al. 2001; Sawicki & Ferris 2008; Zamparo et al. 2008). The subjects had to remain in a natural upright posture (Lejeune et al. 1998; Mahaudens et al. 2009) to calculate $\dot{V}O_2$ at resting.

The progressive incremental order for the velocity was respected. According to the literature (Mahaudens, Detrembleur 2009; Mian, Thom 2006; Ortega & Farley 2007), before continuing the test, some conditions had to be observed:

1. The heart rate, HR, before starting, had never to exceed 100 bpm.
2. Respiratory Exchange Ratio (RER)[1] was controlled in order never to be higher than 1 to confirm the aerobic metabolism as the main metabolic pathway. In this way we could express the metabolic Cost (C), i.e. the oxygen consumed to move 1 Kg of body mass 1 m distance in J (Kg m)$^{-1}$, by dividing the net $\dot{V}O_2$, (measured - resting), [ml (Kg min)$^{-1}$], by the progression speed (m min^{-1}), assuming an energy equivalent *Eq* of 20.9 J ml^{-1} (see chapter 2).
3. The individual shown predisposition to continue and conclude the test.

If only one of these conditions failed, the test was stopped.

In order to avoid external influences on individual patterns of walking and running, subjects were never aware when each registration data began and/or stopped. Physiological parameters were continuously recorded by means of the telemetry portable metabograph K4b[2].

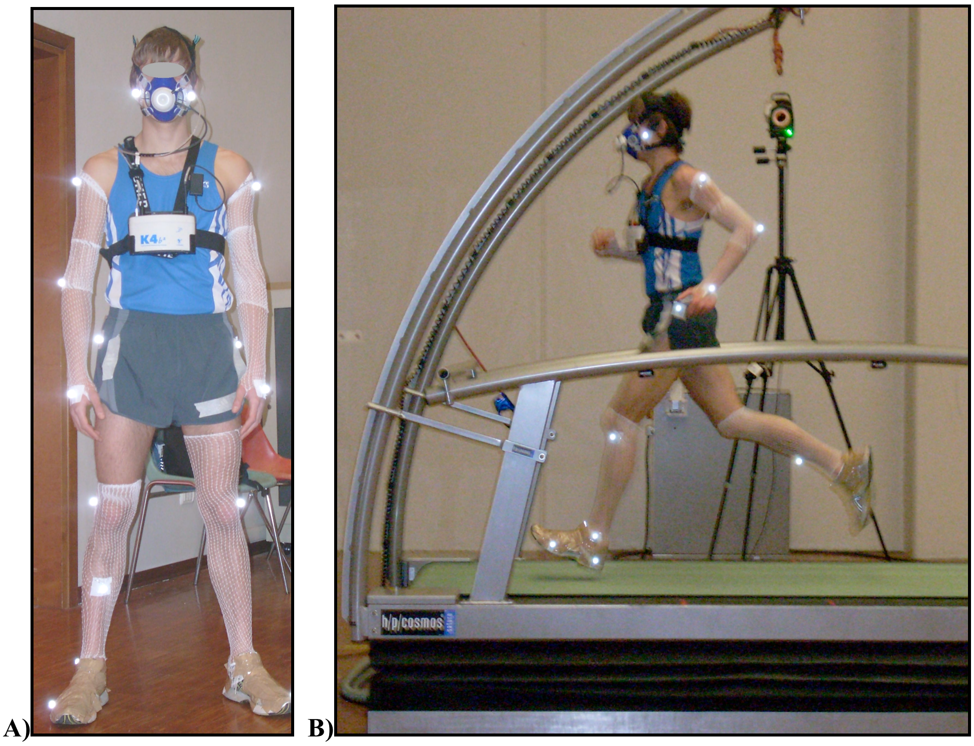

Figure 3.3: Typical subject experimental setup: A) Resting, B) Running.

[1]*Respiratory exchange ratio* (RER). The ratio between CO2 produced ($\dot{V}CO_2$) and O2 inspired ($\dot{V}O_2$) represents the Respiratory Quotient (RQ). It is an indicator of which fuel is being metabolized to supply the body with energy. At the equilibrium conditions, (steady-state), the RQ externally measured correspond to the Respiratory Exchange Ratio (RER), which assume a value lower than 1 for aerobic metabolism (Agostoni 1996).

3.2.3 Discarded tests

During the kinematic data analysis it became evident that some tests had to be rejected due to various and unexpected reasons. Consequently, they were discarded. Particularly:

- Two kinematic recordings (from 2.30 to 3.30 and from 4.30 to 5.00 minute), in running at 3.33 m/s for 1 OR;
- The kinematic recording, in running at 3.89 m/s for 1 OR;
- Two kinematic recordings (from 2.30 to 3.30 and from 4.30 to 5.00 minute), in running at 3.89 m/s for 1 OR;
- One kinematic recording (from 4.30 to 5.00 minute), in running at 3.89 m/s for 1 OR;
- The kinematic recording, in running at 4.44 m/s for 1 OR;
- Two kinematic recordings (from 2.30 to 3.30 and from 4.30 to 5.00 minute), in running at 4.44 m/s for 2 OR;
- One kinematic recording (from 4.30 to 5.00 minute), in running at 4.44 m/s for 2 OR;
- One kinematic recording (from 4.30 to 5.00 minute), in running at 2.78 m/s for 1 SR;
- One kinematic recording (from 4.30 to 5.00 minute), in running at 4.44 m/s for 1 SR;
- One kinematic recording (from 4.30 to 5.00 minute), in running at 5.00 m/s for 2 SR;
- The kinematic recording, in running at 5.00 m/s for 1 SR;
- One kinematic recording (from 0.30 to 1.00 minute), in running at 3.33 m/s for 1 TR;
- One kinematic recording (from 2.30 to 3.30 minute), in running at 3.89 m/s for 3 TR;
- Two kinematic recording (from 2.30 to 3.30 and from 4.30 to 5.00 minute), in running at 4.44 m/s for 2 TR;
- One kinematic recording (from 0.30 to 1.00 minute), in running at 4.44 m/s for TR.
- Two kinematic recording (from 2.30 to 3.30 and from 4.30 to 5.00 minute), in running at 5.00 m/s for 2 TR.

On the whole, 28 out of 400 trials were deleted.

3.2.4 Patient MR dataset

In order to evaluate the static anatomical symmetries, each participant had to perform a Magnetic Resonance (MR) imaging protocol. All the test were carried out in the university Hospital of Borgo Roma in Verona with the kind collaboration of Dr. Faccioli and his staff.

MR examinations were performed with a 1.5-T superconductive magnet (Siemens, Erlagen, Germany). In all subjects multiplanar T1-weighted Spin-eco sequences were obtained (TE 11, TR 565, flip angle 90°), on a coronal plane for three different anatomical districts indicated in Figure 3.4: Pelvis district (PD), Upper-Leg district (UD), (thigh and knee), Lower-Leg district

(LD), (calf and ankle), with slice thickness of 4 mm. The matrix was 320 X 320 and the field of view (FOV) was 460 X 460. Total examination time was less than 7 minutes (36 coronal slices for each district).

All the recorded images were saved in DICOM format file and subsequently analysed with a custom, ad hoc program written in LabVIEW 8.6 (National Instrument, Austin, Texas, USA).

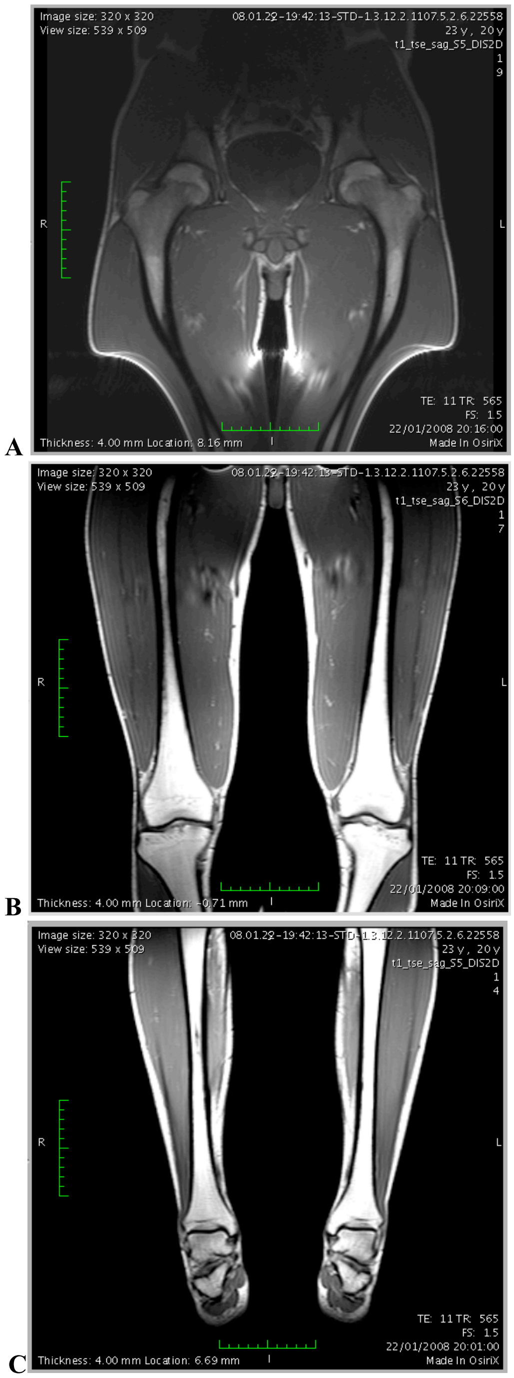

Figure 3.4: The three different analyzed anatomical districts, opened with the software Osiris v.3.3.2 (a classical viewer for biomedical images): A) Pelvis district (PD), B) Upper-Leg district (UD), and C) Lower-Leg district (LD).

3.3 Evaluation of the dynamic symmetry indices

A purposely designed set of equations was recently proposed by Minetti (Minetti 2009), to summarize both the general aspect of the gaits and the individual characteristics of movements, a sort of "*locomotion signature*" capable to reflect any significant change in the motion pattern. We exploited this method, implemented in a custom written program in LabVIEW 8.6 (National Instrument , Austin, USA), in order to calculate the dynamic symmetry indices, together with other biomechanical common parameters. To apply this method we need to know firstly the experimental trajectory of the BCOM, starting from the 12 segments coordinates sampled with the optoelectronic system, as documented in previous studies on human and horses (Minetti et al. 1999; Minetti et al. 1993; Saibene & Minetti 2003).

3.3.1 The BCOM experimental trajectory: the *.bcm file

The kinematic data, obtained from the optoelectronic recordings, are saved and exported in *.c3d file format. Successively all the following steps are carried out with the LabVIEW software in order to obtain the *.bcm file, containing the experimental BCOM trajectory for every trail.

- Each file *.c3d file is automatically converted in a similar *.txt file, containing the three-dimensional displacement of each marker.
- The *.txt format is analysed in order to check the *start* and the *end* frame for each trial. In this way it is possible also to count for each trial the number of strides and to determinate the stride frequency. The chosen trials are inserted in a new file characterised by the extension *.extr.
- This last file format (*.extr) is finally processed with the values of the anthropometric tables, reporting the fractional mass of the different segments and its relative position within them, (Dempster, Gabel 1959; Winter 1979; Winter 2005), in order to calculate the BCOM as the mass-weighted average of the position of all the body segments.
- Kinematics data are then low-pass filtered using a 'non adaptive' 5th order Butterworth filter with a 8.5 Hz cut-off frequency. This filter is used because of previous experiences with unfiltered spatial data manually digitized on analogue movie-frames (Minetti, Ardigo 1993; Minetti et al. 1994) and it seems to work well if compared both to no-filter and first-order filter conditions.

This last step provides the file *.bcm format, containing the three dimensional displacement (x, y and z) of the BCOM. This file is then analysed with the mathematical procedure proposed by Minetti in 2009, in order to evaluate the dynamics indices and other parameters included in the so-called "Locomotion Signature".

3.3.2 The "locomotion signature", mathematical processing

By having sampled the body motion on a treadmill, the trajectory of the BCOM during each stride is expected to follow a *Lissajous contour*, i.e. a convoluted loop showing its 3D displacement with respect to the average position (see Appendix A). The advantages of a parametric representation (as the Lissajous contour) of the BCOM trajectory are that: a) the fourth variable, namely the time, is retained and allows the 3D visualization of the movement dynamics, b) the differentiation/integration of the trajectory can be inferred in order to obtain speeds, energies and path lengths, and c) whichever regression model is chosen to describe the time courses of the x (progression axis), y (vertical axis) and z (lateral axis) coordinates, the accuracy of the 3D fit benefits from the simultaneous equations, with the need of only a few regression coefficients per coordinate regardless of the complexity of the path.

The time course of each of the 3 BCOM coordinates is fit by a *Fourier Series* (see Appendix B), truncated at the 6^{th} harmonic (see below), with the time as the independent variable. Also, Crowe in 1993, used the Time Fourier Series in order to describe the oscillations of the BCOM during gait cycle (Crowe et al. 1993), while Thomson adopted the Fourier equations coefficients in order to calculated a symmetric index for the horses lameness (Halling Thomsen, Tolver Jensen 2010). The advantage of a truncated Fourier analysis, apart from the periodical nature of these equations, is that, differently from a polynomial regression, it is insensitive to further refinements.

Each extracted stride, with period *T*, is forced to become close loops, i.e.

$$x(T) = x(0),\ y(T) = y(0),\ z(T) = z(0)$$

by imposing the transformation:

$$x(t') = x(t') - \frac{t'}{T}\Delta_x,\ y(t') = y(t') - \frac{t'}{T}\Delta_y \text{ and } z(t') = z(t') - \frac{t'}{T}\Delta_z$$

where

$$\Delta_x = x(T) - x(0),\ \Delta_y = y(T) - y(0) \text{ and } \Delta_z = z(T) - z(0)$$

and *t'* is the absolute chronological time (s).
Those adjustments are successively used to evaluate the variability among strides as:

$$\overline{\Delta}_x = \frac{\sum_{j=1}^{n} \left|\Delta_{x,j}\right|}{n}, \ \overline{\Delta}_y = \frac{\sum_{j=1}^{n} \left|\Delta_{y,j}\right|}{n} \ \text{and} \ \overline{\Delta}_z = \frac{\sum_{j=1}^{n} \left|\Delta_{z,j}\right|}{n}$$

i.e. the average distance of the gaps to be filled between the start and the end points of each stride, for each coordinate, with their standard deviations ($\overline{\Delta}_x SD$, $\overline{\Delta}_y SD$, $\overline{\Delta}_z SD$).

Although not strictly necessary to the rest of the analysis the data sequence was cut to make the z coordinate (lateral axis) of the first stride to start close to mid-range and to deflect towards right with respect to the body progression in the sagittal (x-y) plane.

The x, y and z coordinates of each stride undertook then a Fourier Analysis truncated to the 6th harmonic:

$$\hat{x}(t) = a_0^x + \sum_{i=1}^{6} a_i^x \sin(i\,t) + b_i^x \cos(i\,t)$$

$$\hat{y}(t) = a_0^y + \sum_{i=1}^{6} a_i^y \sin(i\,t) + b_i^y \cos(i\,t)$$

$$\hat{z}(t) = a_0^z + \sum_{i=1}^{6} a_i^z \sin(i\,t) + b_i^z \cos(i\,t)$$

where

$$t = 2\pi \frac{t'}{T}$$

and *t'* is the absolute original time of each captured frame. The time standardization, by forcing all the cycle periods to range between 0 and 2π, has been introduced to allow an easier comparison among the harmonic phases (see below).

The average of the vertical coordinate, i.e. a_0^y, for each stride is collected as to calculate the mean value (for n strides) at each speed as:

$$\overline{a}_0^y = \frac{\sum_{j=1}^{n} a_{0,j}^y}{n}$$

while a_0 constants for x and z coordinates have been removed from the analysis (this corresponds to consider the progression and the lateral data of the stride as centered about the origin of those axes).
Since

$$a\sin(t) + b\cos(t) = c\sin(t + \phi)$$

where

$$c = \sqrt{a^2 + b^2}\ ,$$
$$\phi = \frac{\pi}{2}\operatorname{sgn}(b) - \arctan\left(\frac{b}{a}\right)$$

the Fourier Series can be also expressed, after removing the a_0 constant for the vertical axis, as:

$$\hat{x}(t) = \sum_{i=1}^{6} c_i^x \sin(i\,t + \phi_i^x)$$
$$\hat{y}(t) = \sum_{i=1}^{6} c_i^y \sin(i\,t + \phi_i^y)$$
$$\hat{z}(t) = \sum_{i=1}^{6} c_i^z \sin(i\,t + \phi_i^z)$$

This is called the 'phase angle form' of the Fourier Series and is more convenient than the original form as it contains just sine functions. The motion of BCOM would exhibit perfect right-left symmetry if it contained just even harmonics in the x (progression) and y (vertical) direction, and just odd harmonics in the z (depth) direction. This derives from the double frequency of the step (2 steps in a stride) in the sagittal plane and from the single sway of the stride in the frontal (y-z) plane.
Thus three indices of symmetry can be worked out as:

$$SI^x = \frac{c_2^x + c_4^x + c_6^x}{\sum_{i=1}^{6} c_i^x}, \quad SI^y = \frac{c_2^y + c_4^y + c_6^y}{\sum_{i=1}^{6} c_i^y} \quad \text{and} \quad SI^z = \frac{c_1^z + c_3^z + c_5^z}{\sum_{i=1}^{6} c_i^z}$$

and they are expected to be equal to 1 in case of perfect symmetry between right and left steps. Those indices are then averaged among strides as to obtain:

$$\overline{SI^x} = \frac{\sum_{J=1}^{n} S_j^x}{n}, \quad \overline{SI^y} = \frac{\sum_{J=1}^{n} S_j^y}{n} \quad \text{and} \quad \overline{SI^z} = \frac{\sum_{J=1}^{n} S_j^z}{n}$$

The average harmonic (single-sin) coefficients of a sequence of *n* strides can be calculated as:

$$\overline{c}_i^x = \frac{\sum_{j=1}^{n} c_{i,j}^x}{n}, \quad \overline{c}_i^y = \frac{\sum_{j=1}^{n} c_{i,j}^y}{n}, \quad \overline{c}_i^z = \frac{\sum_{j=1}^{n} c_{i,j}^z}{n}$$

together with their SDs. While this is a safe procedure only when all the strides have exactly the same duration, the approximation when averaging real strides is acceptable if they are extracted from the same homogeneous population as, for instance, for the same speed and gait.

Before averaging the phase values, the single-sin phases of each stride needs to be ‘aligned’ to minimize data variability. This means to choose a reference phase and express the others relative ($_R$) to it. The first harmonic in the lateral axis (z) was used for this purpose and all the others were recalculated as:

$$\phi_{iR}^x = i\left(\frac{\phi_i^x}{i} - \frac{\phi_1^z}{1}\right)$$

$$\phi_{iR}^y = i\left(\frac{\phi_i^y}{i} - \frac{\phi_1^z}{1}\right)$$

$$\phi_{iR}^z = i\left(\frac{\phi_i^z}{i} - \frac{\phi_1^z}{1}\right)$$

which corresponds, also, to impose

$$\phi_{1R}^z = 0$$

Averaging phases needs to be performed according to circular statistics, (Batschelet 1981), (see Appendix C). This procedure leads, for every experimental condition (speed/gait) and n strides, to average 3D Lissajous contours in the form of:

$$\bar{\hat{x}}(t) = \sum_{i=1}^{6} \bar{c}_i^x \sin(i\,t + \bar{\phi}_{iR}^x)$$
$$\bar{\hat{y}}(t) = \bar{a}_0^y + \sum_{i=1}^{6} \bar{c}_i^y \sin(i\,t + \bar{\phi}_{iR}^y)$$
$$\bar{\hat{z}}(t) = \sum_{i=1}^{6} \bar{c}_i^z \sin(i\,t + \bar{\phi}_{iR}^z)$$

where the symbol (¯) denotes the average of the predicted (^) value. This equation represent the 'digital locomotor signature', which contains general and individual features of a given gait condition. When symmetry is imposed, as for representing 'typical' contours for bipedal locomotion the odd harmonics should not be included in the first two equations (x & y axes), and the even ones should not be included in the third equation (z axis).

Whenever the true temporal range, rather than the standard interval 0-2π, would be preferred, the term *it* in the sine argument needs to be multiplied by $2\pi f$, where f is the stride frequency (Hz). Also, it is possible to reconstruct the real (on the walkway) 3D trajectory of BCOM by changing the equations for the Lissajous contour into:

$$\bar{\hat{x}}(t) = \bar{v}_x t' + \sum_{i=1}^{6} \bar{c}_i^x \sin(2\pi\, f\, i\, t' + \bar{\phi}_{iR}^x),$$
$$\bar{\hat{y}}(t) = \bar{a}_0^y + \sum_{i=1}^{6} \bar{c}_i^y \sin(2\pi\, f\, i\, t' + \bar{\phi}_{iR}^y)$$
$$\bar{\hat{z}}(t) = \sum_{i=1}^{6} \bar{c}_i^z \sin(2\pi\, f\, i\, t' + \bar{\phi}_{iR}^z)$$

where the average progression speed ($\bar{v}_x$) of the body has been included to ensure forward translation of the BCOM.

To summarize the analysis procedure, the parameters obtained from a stream of x, y and z coordinates of BCOM for each *.bcm file, are: n, f, $\bar{\Delta}_x$, $\bar{\Delta}_y$, $\bar{\Delta}_z$, $\bar{a}_0^y$, $\overline{SI^x}$, $\overline{SI^y}$, $\overline{SI^z}$ and 6 (harmonics) x [$\bar{c}_i^x$, $\bar{\phi}_{iR}^x$, $\bar{c}_i^y$, $\bar{\phi}_{iR}^y$, $\bar{c}_i^z$, $\bar{\phi}_{iR}^z$], each of which with the relevant SD, where n is the number of strides.

All the described mathematical steps are implemented in a LabVIEW ad hoc written program, called "*Lissajous Fourier BCM Trajectory*". Starting from the *.bcm file, it evaluates all the parameters listed above, (as shown in Figure 3.5 A) and also allows the pattern visualization of each stride, in order to check possible strides, designated to be deleted (Figure 3.5 B).

As we explained in section 3.2.1, for each subject three consecutive kinematic registrations were carried out for each velocity. It means that we have three *.bcm file for each subject, for each velocity. The values we are going to present in the next sections and chapters, will be indicated as $n, f, \overline{\Delta}_x, \overline{\Delta}_y, \overline{\Delta}_z, \overline{\Delta}_y, \overline{a}_0^y, \overline{SI^x}, \overline{SI^y}, \overline{SI^z}$, *dx, dy, dz* even if, from now, they will concern the mean value between the three registrations.

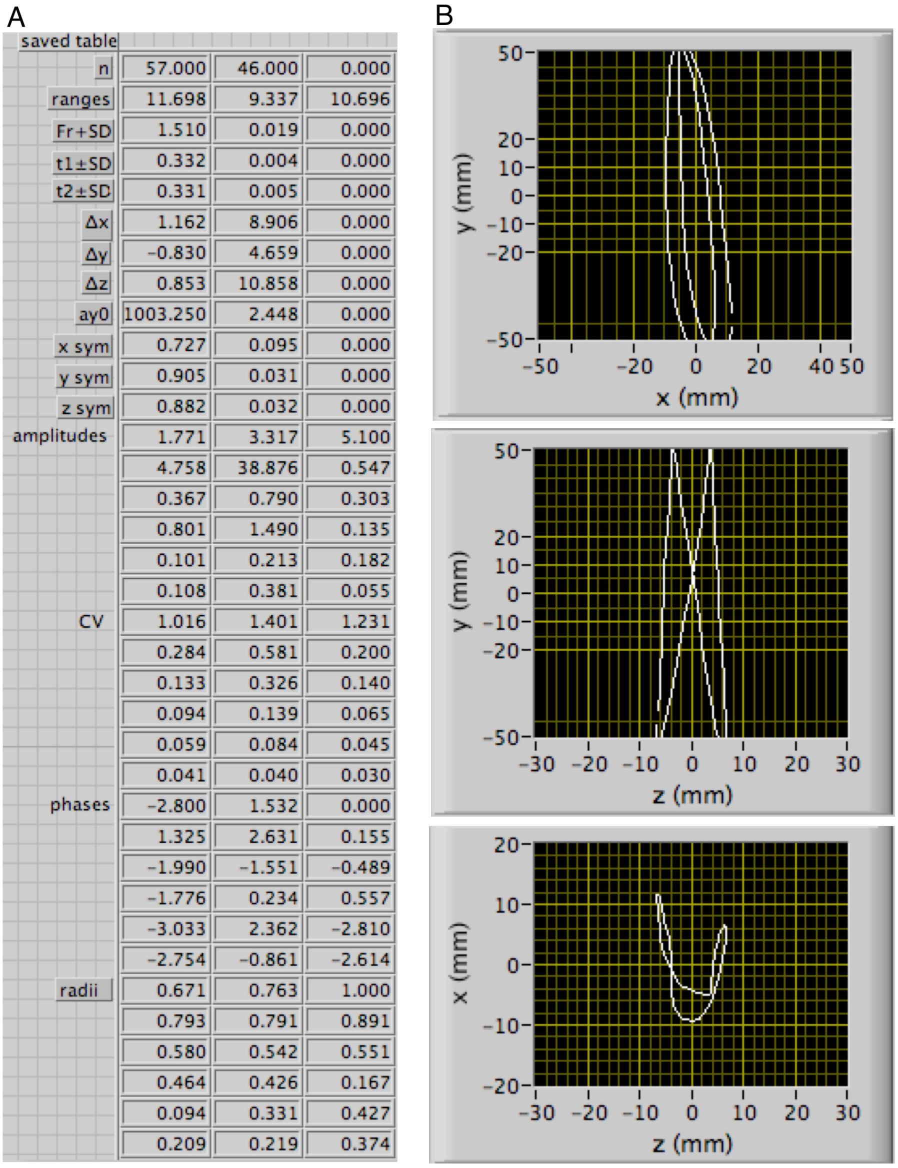

saved table			
n	57.000	46.000	0.000
ranges	11.698	9.337	10.696
Fr+SD	1.510	0.019	0.000
t1±SD	0.332	0.004	0.000
t2±SD	0.331	0.005	0.000
Δx	1.162	8.906	0.000
Δy	-0.830	4.659	0.000
Δz	0.853	10.858	0.000
ay0	1003.250	2.448	0.000
x sym	0.727	0.095	0.000
y sym	0.905	0.031	0.000
z sym	0.882	0.032	0.000
amplitudes	1.771	3.317	5.100
	4.758	38.876	0.547
	0.367	0.790	0.303
	0.801	1.490	0.135
	0.101	0.213	0.182
	0.108	0.381	0.055
CV	1.016	1.401	1.231
	0.284	0.581	0.200
	0.133	0.326	0.140
	0.094	0.139	0.065
	0.059	0.084	0.045
	0.041	0.040	0.030
phases	-2.800	1.532	0.000
	1.325	2.631	0.155
	-1.990	-1.551	-0.489
	-1.776	0.234	0.557
	-3.033	2.362	-2.810
	-2.754	-0.861	-2.614
radii	0.671	0.763	1.000
	0.793	0.791	0.891
	0.580	0.542	0.551
	0.464	0.426	0.167
	0.094	0.331	0.427
	0.209	0.219	0.374

Figure 3.5: A) List of the parameters evaluated by the *Lissajous-Fourier BCOM trajectory.vi*, B) Patterns of the BCOM in each plane in *Lissajous-Fourier BCOM trajectory.vi,* In all the graph and tables the harmonics amplitudes are expressed in millimeters, because of the small excursion of BCOM.

3.3.3 The Global Symmetry Index

In this section we are going to introduce a new parameter (the Global Symmetry Index) that together with the previous calculated variables will be useful to describe the dynamical symmetry of each subject. This index is a sort of average of the three single dynamic indices ($\overline{SI^x}$, $\overline{SI^y}$, $\overline{SI^z}$) weighted on each single displacement of the BCOM, i.e. dx, dy, dz, respectively. These measures are expressed in meters and calculated starting from the BCOM coordinates found in the *Lyssajous Countour* ($\bar{\hat{x}}(t), \bar{\hat{y}}(t), \bar{\hat{z}}(t)$) as

$$dx = \left[\max\left(\bar{\hat{x}}(t)\right) - \min\left(\bar{\hat{x}}(t)\right)\right] + \left(v \cdot \frac{1}{f}\right)$$

$$dy = \left[\max\left(\bar{\hat{y}}(t)\right) - \min\left(\bar{\hat{y}}(t)\right)\right] + \left(v \cdot \frac{1}{f}\right)$$

$$dz = \left[\max\left(\bar{\hat{z}}(t)\right) - \min\left(\bar{\hat{z}}(t)\right)\right] + \left(v \cdot \frac{1}{f}\right)$$

where *v* is the subject running speed, and *f* is the stride frequency previously obtained.

Similarly to the three dynamic indices ($\overline{SI^x}$, $\overline{SI^y}$, $\overline{SI^z}$), also the Global Index (GI), can assume values between 0 and 1 and is calculated as

$$GI = \frac{(dx \cdot \overline{SI^x}) + (dy \cdot \overline{SI^y}) + (dz \cdot \overline{SI^z})}{(dx + dy + dz)}$$

As for the single dynamic indices, also *GI* will be equal to 1 in case of perfect symmetry between right and left steps, while a value of 0 corresponds to complete asymmetry.

3.4 3D Images Processing

As we described previously (see section. 3.2.4), all the recorded MR images were saved in DICOM format file and subsequently analysed and processed with a custom, *ad hoc* program written in LabVIEW 8.6 (National Instrument, Austin, Texas, USA), in order to find out an index of the anatomical symmetry level for each subject, for each anatomical districts.

In the following sections we will describe the steps necessary to complete the processing algorithm that bring to compute the cross correlation index. As we will explain later, this index will be a measure of the level of symmetry between the right and the left side for each subject.

3.4.1 First step: open DICOM files

The DICOM file (Digital Imaging and Communications in Medicine) is from 1993 the ubiquitous standard in the radiology and diagnostic imaging industry for the exchange and management of images and image related information. It is also used for many other types of medical imaging. All modern digital radiology imaging equipment is available with a DICOM interface. DICOM digital images for clinical trials are transferred either across a wide area network (WAN) using a secure connection, or more commonly, a DICOM Compact Disc (CD) or Magneto-optical Disk (MOD) is sent by courier (Clunie 2000; Clunie 2007).

Each DICOM file includes information encoded in attributes, together with the actual pixel data (the image). These attributes compose the DICOM "header", containing identification subject information (such as name, weight, date of birth), management and acquisition technique information (such as the hospital name, date and time) and also parameters characterising the considered image. An example of a DICOM file structure is shown in Figure 3.6. These listed parameters have been obtained with the software Osiris v.3.3.2, a classical viewer for DICOM format images. As you can see in the picture, every line is described by an 8 digits sequence (the tag). This tag characterises the parameters within the DICOM file. Thought the software available for DICOM images visualisation are many, there are no standards for the encoding of information that accompanies the image and also often it is not possible to extract the single image.

For these reason we decided to open the DICOM files of the recorded MR images with a custom implemented program, in Labview 8.6. This programming language allows a simple interface for the user that needs to visualise images and to compute operation on them. In figure 3.7 is shown the first step of this procedure. We didn't extract all the parameters that characterised the file, as in figure 3.7, but only the ones necessary for our analysis.

Field Name	Tag	Content
▼DICOMObject		
MetaElementGroupLength	0002,0000	188
FileMetaInformationVersion	0002,0001	
MediaStorageSOPClassUID	0002,0002	1.2.840.10008.5.1.4.1.1.4
MediaStorageSOPInstanceUID	0002,0003	1.3.12.2.1107.5.2.6.22558.30000008013007492379600004320
TransferSyntaxUID	0002,0010	1.2.840.10008.1.2.1
ImplementationClassUID	0002,0012	1.3.12.2.1107.5.2
ImplementationVersionName	0002,0013	MR_2007A_VA30A
SpecificCharacterSet	0008,0005	ISO_IR 100
▼ImageType	0008,0008	ORIGINAL\PRIMARY\M\ND
value		ORIGINAL
value		PRIMARY
value		M
value		ND
SOPClassUID	0008,0016	1.2.840.10008.5.1.4.1.1.4
SOPInstanceUID	0008,0018	1.3.12.2.1107.5.2.6.22558.30000008013007492379600004320
StudyDate	0008,0020	20080130
SeriesDate	0008,0021	20080130
AcquisitionDate	0008,0022	20080130
ContentDate	0008,0023	20080130
StudyTime	0008,0030	195710.203000
SeriesTime	0008,0031	200723.312000
AcquisitionTime	0008,0032	200720.167491
ContentTime	0008,0033	200811.437000
Modality	0008,0060	MR
Manufacturer	0008,0070	SIEMENS
InstitutionName	0008,0080	Policlinico G.B.Rossi Verona
InstitutionAddress	0008,0081	10Piazzale L. A. Scuro, Verona a34ef9, Milano, 37126, IT
ReferringPhysiciansName	0008,0090	Policlinico G.B.Rossi Verona
StationName	0008,1010	MRC22558
StudyDescription	0008,1030	angio_head^tof_2d_veins
SeriesDescription	0008,103e	t1_tse_sag_S5_DIS2D
PerformingPhysiciansName	0008,1050	Sched.Med
ManufacturersModelName	0008,1090	Symphony
▼ReferencedImageSequence	0008,1140	1.2.840.10008.5.1.4.1.1.4\1.3.12.2.1...8.30000008013007492379600004293
▶item		1.2.840.10008.5.1.4.1.1.4\1.3.12.2.1...8.30000008013007492379600004291
▶item		1.2.840.10008.5.1.4.1.1.4\1.3.12.2.1...8.30000008013007492379600004303
▶item		1.2.840.10008.5.1.4.1.1.4\1.3.12.2.1...8.30000008013007492379600004293
PatientsName	0010,0010	MARCOLIN^GIUSEPPE
PatientID	0010,0020	2343523
PatientsBirthDate	0010,0030	19780327
PatientsSex	0010,0040	M
PatientsAge	0010,1010	029Y
PatientsWeight	0010,1030	77
ScanningSequence	0018,0020	SE
▼SequenceVariant	0018,0021	SK\SP\OSP
value		SK
value		SP
value		OSP
MRAcquisitionType	0018,0023	2D
SequenceName	0018,0024	*tse2d1_5
AngioFlag	0018,0025	N
SliceThickness	0018,0050	4
RepetitionTime	0018,0080	565
EchoTime	0018,0081	11
NumberofAverages	0018,0083	2
ImagingFrequency	0018,0084	63.679721
ImagedNucleus	0018,0085	1H
EchoNumbers	0018,0086	0
MagneticFieldStrength	0018,0087	1.5
SpacingBetweenSlices	0018,0088	4
NumberofPhaseEncodingSteps	0018,0089	210
EchoTrainLength	0018,0091	5
PercentSampling	0018,0093	65
PercentPhaseFieldofView	0018,0094	100
PixelBandwidth	0018,0095	130
DeviceSerialNumber	0018,1000	22558
SoftwareVersions	0018,1020	syngo MR A30 4VA30A
ProtocolName	0018,1030	t1_tse_sag_S5_DIS2D
DateofLastCalibration	0018,1200	20071127
TimeofLastCalibration	0018,1201	135004.000000
TransmitCoilName	0018,1251	Body
▼AcquisitionMatrix	0018,1310	0\320\208\0
value		0
value		320
value		208
value		0
In-planePhaseEncodingDirection	0018,1312	ROW
FlipAngle	0018,1314	150
VariableFlipAngleFlag	0018,1315	N

SAR	0018,1316	1.2739355564117
dB_dt	0018,1318	0
PatientPosition	0018,5100	FFS
Unknown	0019,0010	SIEMENS MR HEADER
Unknown	0019,1008	IMAGE NUM 4
Unknown	0019,1009	1.0
Unknown	0019,100b	46940
StudyInstanceUID	0020,000d	1.3.12.2.1107.5.2.6.22558.30000008013007431521800000032
SeriesInstanceUID	0020,000e	1.3.12.2.1107.5.2.6.22558.30000008013007492379600004306
StudyID	0020,0010	1
SeriesNumber	0020,0011	4
AcquisitionNumber	0020,0012	1
InstanceNumber	0020,0013	18
▼ImagePositionPatient	0020,0032	-230\7.1845927238464\217.89346218109
value		-230
value		7.1845927238464
value		217.89346218109
▼ImageOrientationPatient	0020,0037	1\0\0\0\0\-1
value		1
value		0
value		0
value		0
value		0
value		-1
FrameofReferenceUID	0020,0052	1.3.12.2.1107.5.2.6.22558.20080130195713312.0.0.5375
SliceLocation	0020,1041	7.1845927238464
SamplesperPixel	0028,0002	1
PhotometricInterpretation	0028,0004	MONOCHROME2
Rows	0028,0010	320
Columns	0028,0011	320
▼PixelSpacing	0028,0030	1.4375\1.4375
value		1.4375
value		1.4375
BitsAllocated	0028,0100	16
BitsStored	0028,0101	12
HighBit	0028,0102	11
PixelRepresentation	0028,0103	0
SmallestImagePixelValue	0028,0106	1
LargestImagePixelValue	0028,0107	1691
WindowCenter	0028,1050	501
WindowWidth	0028,1051	1079
WindowCenterWidthExplanation	0028,1055	Algo1
Unknown	0029,0010	SIEMENS CSA HEADER
Unknown	0029,0011	SIEMENS MEDCOM HEADER2
Unknown	0029,1008	IMAGE NUM 4
Unknown	0029,1009	20080130
Unknown	0029,1010	
Unknown	0029,1018	MR
Unknown	0029,1019	20080130
Unknown	0029,1020	
Unknown	0029,1160	com
RequestedProcedureDescription	0032,1060	angio_head tof_2d_veins
PerformedProcedureStepStartDate	0040,0244	20080130
PerformedProcedureStepStartTime	0040,0245	195710.281000
PerformedProcedureStepID	0040,0253	MR20080130195710
PerformedProcedureStepDescription	0040,0254	angio_head^tof_2d_veins
Unknown	0051,0010	SIEMENS MR HEADER
Unknown	0051,1008	IMAGE NUM 4
Unknown	0051,1009	1.0
Unknown	0051,100a	TA 46.94*4
Unknown	0051,100b	208*320
Unknown	0051,100c	FoV 460*460
Unknown	0051,100d	SP P7.2
Unknown	0051,100e	Cor
Unknown	0051,100f	PL2-4;PR2-4;SP2-6
Unknown	0051,1012	TP H375
Unknown	0051,1013	+LPH
Unknown	0051,1015	E
Unknown	0051,1016	M/ND
Unknown	0051,1017	SL 4.0
Unknown	0051,1019	A2
StorageMediaFile-setUID	0088,0140	1.3.12.2.1107.5.2.6.22558.30000008013014510543700000028
PixelData	7fe0,0010	

Figure 3.6: Example of DICOM structure, opened with the DICOM viewer Osiris 3.3.2.

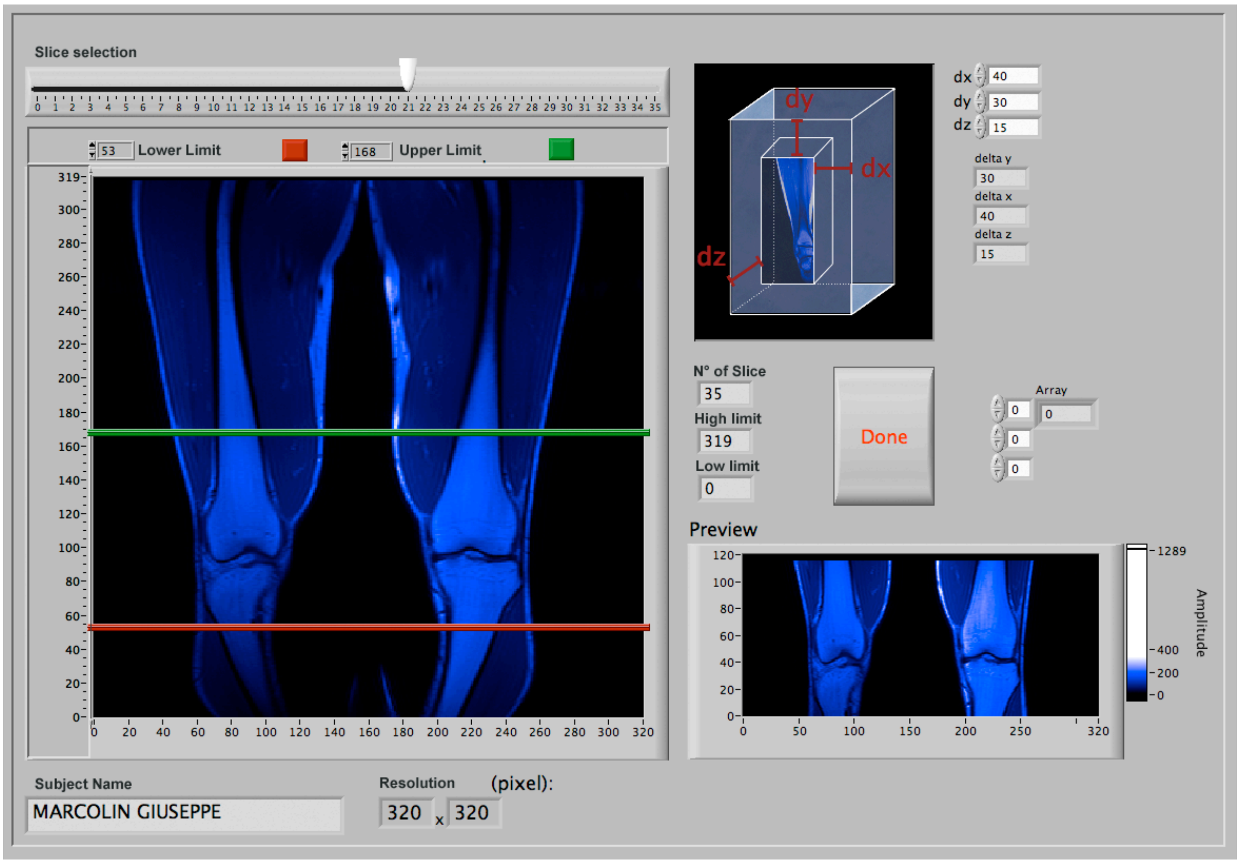

Figure 3.7: Labview first step interface: the user can select a DICOM file, which will be opened from the software. The selected image will be visualized together with some subject information. The green and the red horizontal bars in the left panel help the user two highlight the image region of interest, we want to analyze; we can see it in preview on the right panel.

The procedure we implemented exports for each districts 36 MR images (slices) as two-dimensional matrix of 320 X 320 pixels, (1.44 X 1.44 mm).

In the next pictures, we will represent the operations sequence applied only for the UD district, sized 320 X 320 pixels, but we followed the same steps also for the other two districts, (PD and LD) and for different sized volumes, as we will explain in the results.

3.4.2 Second step: the three-dimensional volume

Once the user has chosen the subject and the district of interest, mathematically the software, starting from the 36 single 2D images (320 X 320 pixel), builds a three-dimensional matrix, whose dimensions are (320 X 320 X 36 voxel). As shown in figure 3.8, the 36 coronal slices, for every district, assembled together, create a three-dimensional (3D) volume, whose elements (voxel) are values corresponding to a grey level intensity. We have 2^{12} grey levels, where 0 is black and 4096 is white.

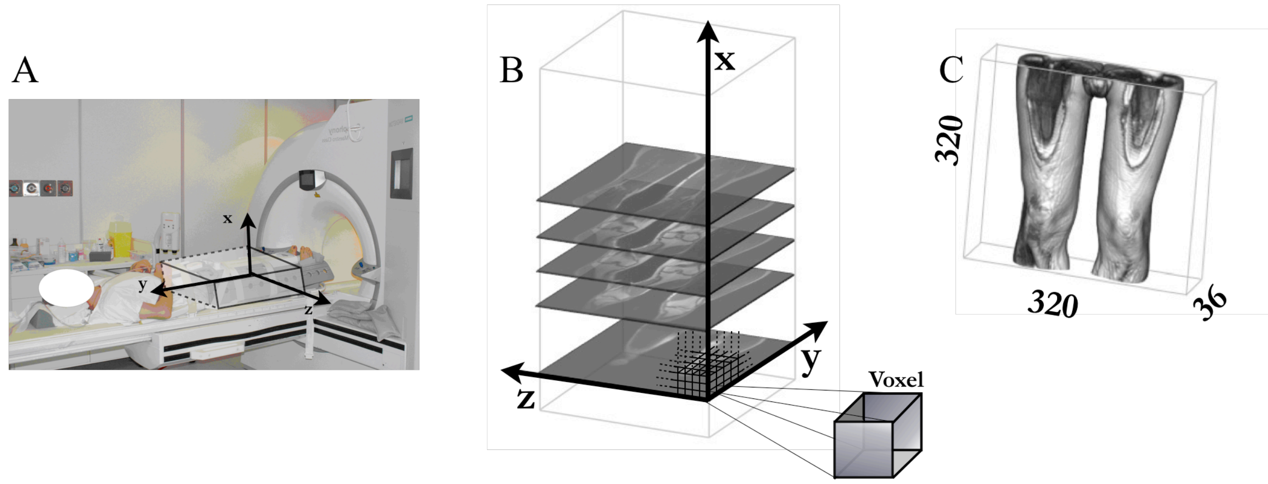

Figure 3.8: The three-dimensional volume: A) Volume of interest in the MR scan, B) The acquired images (slices), with the voxel representation, C) Total 3D Volume

3.4.3 Third step: obtaining two-separated volume

In order to compare the subject's left lower limb with the right one, firstly, the initial 3D volume has to be split in two separated volumes, right volume (**Rv**) and left volume (**Lv**), (Figure 3.10 A).

Throughout a Labview routine called *array subset*, we can obtain two different 3D matrices from the original one. The new two arrays will size 320 X 160 X 36.

3.4.4 Fourth step: volume reflection

Successively the Left Volume is reflected, on the sagittal plane as shown in figure 3.10 B. To achieve this aim in Labview, it's necessary to transpose the 2D array for every slice of the left volume, to reverse the pixels sequence for each array column, and then to transpose again the obtained matrix, like we show with a simple example in figure 3.9. The output, the user can see in the software is shown in figure 3.11.

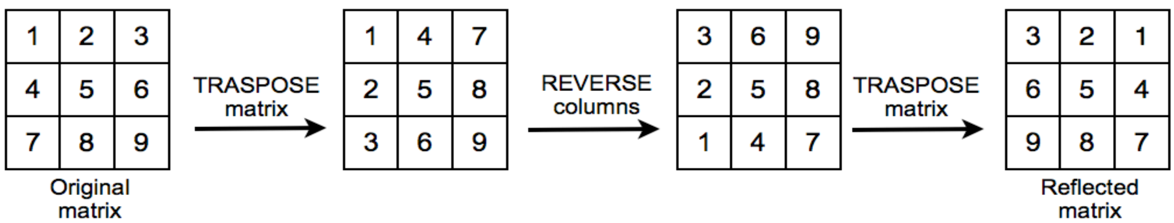

Figure 3.9: Example of the reflection process for a 2D simple matrix.

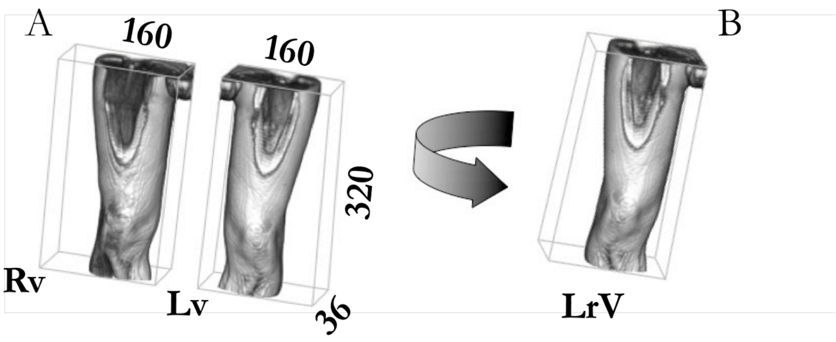

Figure 3.10: A) Separation of the global volume, B) Left reflected Volume on the sagittal plane

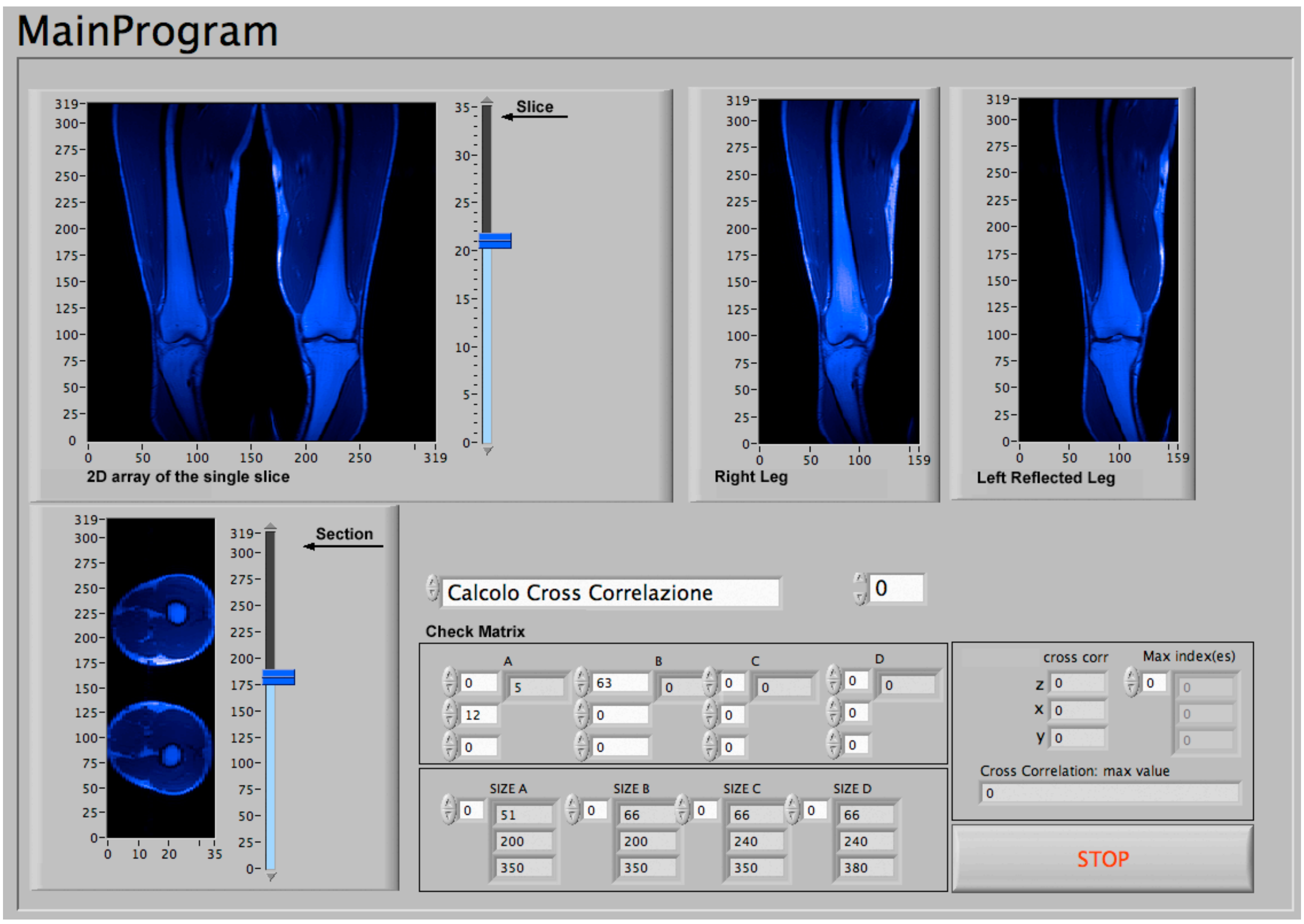

Figure 3.11: Main program user interface after the first fourth steps

3.4.5 Cross-correlation operation

In order to go on with the next step of the MR processing analysis, it is important to introduce the concept of *cross-correlation*. This term comes from statistics and it is a mathematical operation largely used in signal processing. It uses two signals to produce a third signal. This third signal is called the cross-correlation of the two input signals.

Cross correlation can be performed on time domain signals, but also often on frequency domain signals, in order to minimize the processing time. In this work we will only consider time domain cross-correlation operations.

For example, in the discrete time domain the cross correlation is a measure of similarity of two waveforms as a function of a time-lag (delay), applied to one of them. Considering two series x(i) and y(i), where i=0,1,2,…N-1, the cross correlation estimates the degree to which the two series are correlated. The cross correlation *r* at the delay *d* is defined as

$$r = \frac{\sum_i \left[(x(i) - \bar{x}) \cdot (y(i-d) - \bar{y}) \right]}{\sqrt{\sum_i (x(i) - \bar{x})^2} \sqrt{\sum_i (y(i-d) - \bar{y})^2}}$$

Where $\bar{x}$ and $\bar{y}$ are the means of the corresponding series. If *r* is computed for all delays *d = 0, 1, 2, ...N-1*, then it results in a cross correlation series of twice the length as the original series.

$$r(d) = \frac{\sum_i \left[(x(i) - \bar{x}) \cdot (y(i-d) - \bar{y}) \right]}{\sqrt{\sum_i (x(i) - \bar{x})^2} \sqrt{\sum_i (y(i-d) - \bar{y})^2}}$$

The denominator in the expression above serves to normalize the correlation coefficients such that $r(d)$ can assume values ranged from -1 to 1. Values as -1 or 1 indicate maximum correlation, while 0 indicates no correlation. A high negative correlation indicates a high correlation but of the inverse of one of the series.

As a simple example we can consider the two rectangular pulses shown below in blue and green, the correlation series is shown in red (Figure 3.12).

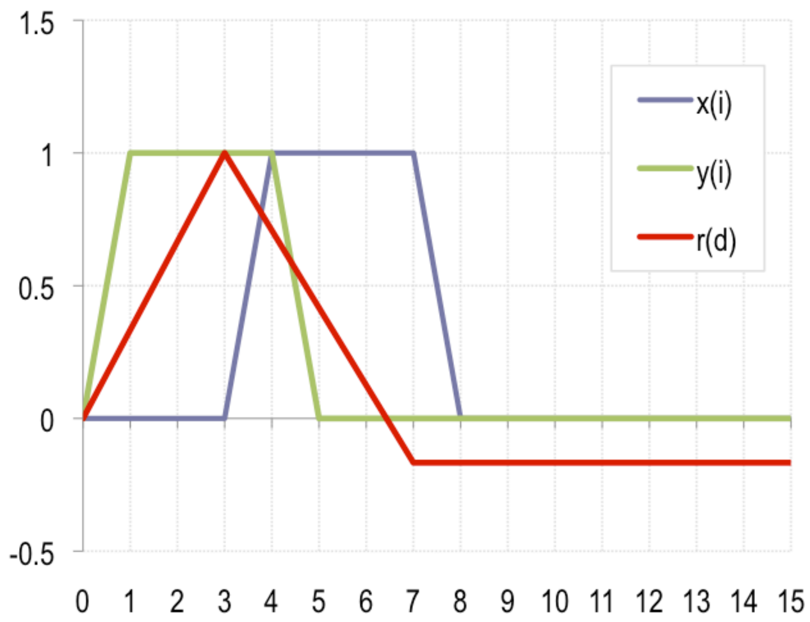

Figure 3.12: Example of cross-correlation between two signals x(i) and y(i) in the discrete time domain

The maximum correlation is achieved at a delay of 3. Considering the equations above, what is happening is the second series is being slid past the first, at each shift the sum of the product of the newly lined up terms in the series is computed. This sum will be large when the shift (delay) is such that similar structure lines up. This is essentially the same as the so-called *convolution* except for the normalization terms in the denominator. Cross-correlation procedure was also used in studies regarding symmetry in locomotion, for example to compare right and left EMG activity in lower limbs (Arsenault et al. 1986; Pierotti et al. 1991).

3.4.6 Autocorrelation

If a signal is correlated with itself, the resulting signal is instead called the *autocorrelation*. When the correlation is calculated between a series and a lagged version of itself, a high correlation is likely to indicate a periodicity in the signal of the corresponding time duration. The correlation coefficient at lag k of a series $x_0, x_1, x_2, \ldots x_{N-1}$ is normally given as

$$autocorr(k) = \frac{\sum_{i=0}^{N-1}(x_i - \bar{x}) \cdot (x_{i+k} - \bar{x})}{\sum_{i=0}^{N-1}(x_i - \bar{x})^2}$$

As an example of autocorrelation we reported a signal recorded during an electroencephalography examination (EEG), in particular derivation c3, as indicated in Figure 3.13.

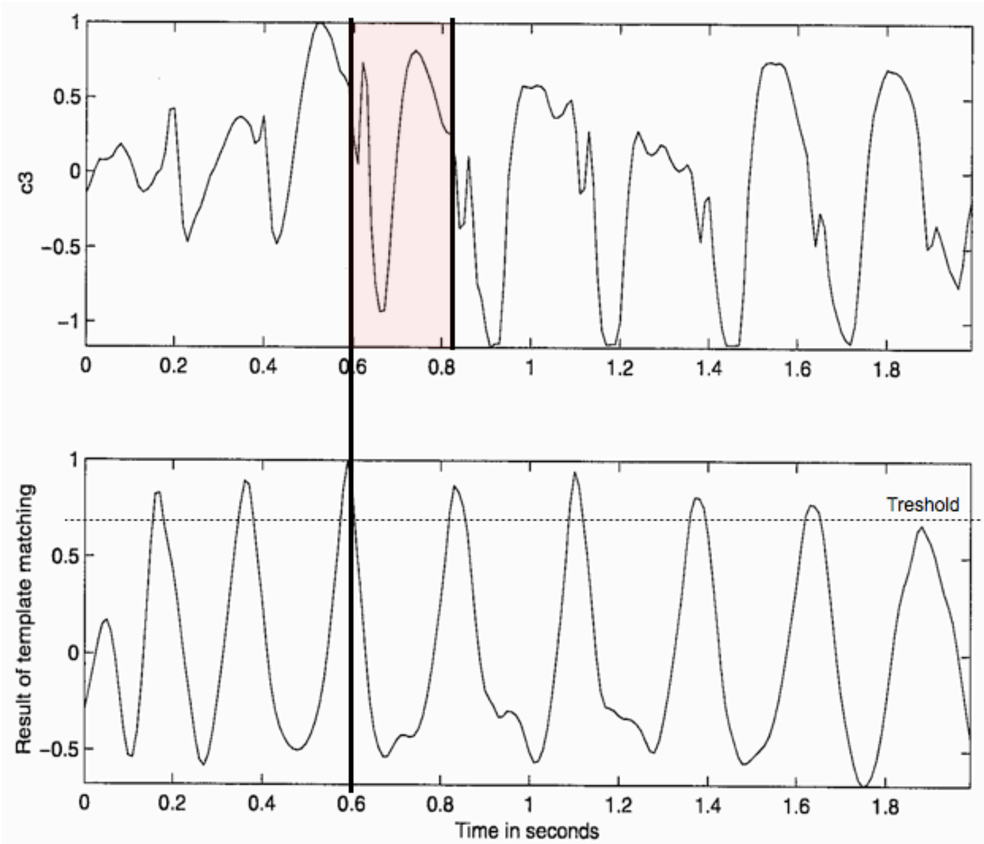

Figure 3.13: Example of auto-correlation

The waveform highlighted in the upper graph, ranged from 0.60 to 0.82 seconds, is a typical sign of epilepsy, and it is chosen as template. The autocorrelation in the graph below reaches the value of 1 at 0.60 seconds in correspondence with the template and presents a sequence of picks in the rest of the signal. In this way it is possible to detect the signal periodicity, and also, established a threshold, to identify the number of critical events.

3.4.7 2D Pattern Identification using Cross Correlation

To get closer to the form of cross-correlation we exploit in this work, it is useful to introduce this mathematical operation also in two-dimensions. Before we spoke about signals in the time domain, now we are going to speak about images, in the spatial domain.

One approach to identifying a pattern within an image uses the cross correlation of the image with a suitable mask. Where the mask and the pattern being sought are similar the cross correlation will be high. This kind of method is mostly used in patter identification, for example in diagnostic imaging or in the markers detection with optoelectronic systems.

If we consider the example of the marker detection, the original image is the single image/frame recorded by the camera and the mask is itself an image, which needs to have the same functional appearance as the pattern to be found, in this case the marker.

The original image and the mask (or template) are considered as a 2D array of pixel corresponding to a numeric value.

As described in figure 3.14, the 2D cross correlation consists of placing the pre-defined mask on a certain image area. Each point of the mask is then multiplied with its corresponding point on the image. All these products are added to obtain the correlation value, calculated as

$$\gamma(u,v)=\frac{\sum_{x,y}\left[f(x,y)-\bar{f}_{u,v}\right]\cdot\left[t(x-u,y-v)-\bar{t}\right]}{\sqrt{\sum_{x,y}\left[f(x,y)-\bar{f}_{u,v}\right]^{2}\cdot\sum_{x,y}\left[t(x-u,y-v)-\bar{t}\right]^{2}}}$$

where $\bar{t}$ is the mean of the template and $\bar{f}_{u,v}$ is the mean of $f(x,y)$ (original image) in the region under the template. The final output will be a 2D array of correlation values.

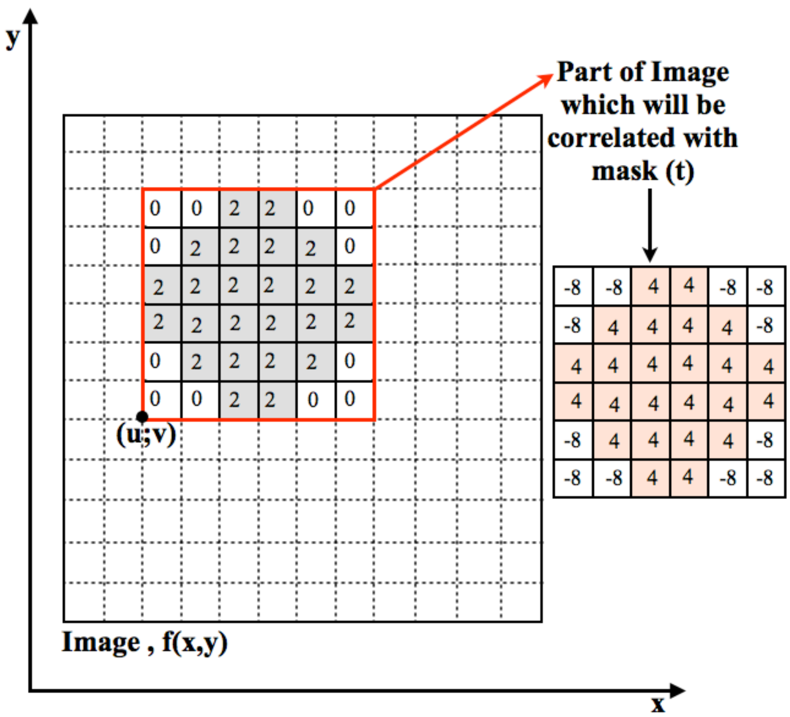

Figure 3.14: Example of 2D cross-correlation in markers detection

3.4.8 3D Fast normalized cross-correlation

Cross-correlation has been recently designed in three-dimensions in order to consider simultaneously the full anatomical volume information, to assist radiologist in providing correct diagnosis of metastases within the lung (Ambrosini et al. 2010; Lee et al. 2001; Wang et al. 2007), or brain (Ambrosini, Wang 2010). As in the 2D cross-correlation, also in these works we can speak about *pattern identification*. Infect the aim of the authors was to detect the metastasis (the pattern) inside the 3D anatomical volume built up after MRI scan. In this case the mask was a spherical volume with the same morphological feature of a metastasis (Figure 3.15). Following Lewis' approach, (Lewis 1996), they calculated a normalised cross-correlation coefficient (r), in order to identify the similarity degree between the possible candidate for being metastasis and the spherical mask.

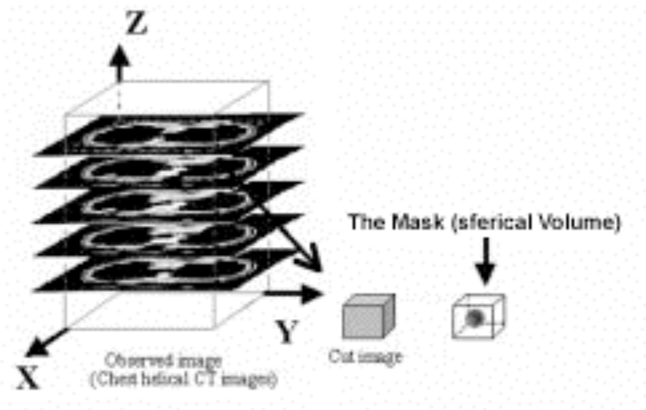

Figure 3.15 3D reconstructed volume and spherical pattern for the metastasis detection, (Lee, Hara 2001)

Analogously to the procedure adopted by above cited authors, we also exploited the Lewis approach, in order to find the best matching between the Right Volume (**Rv**) and the Left reflected Volume (**LrV**), i.e. the relative position between the two volumes that maximize the cross correlation value. The Right Volume (**Rv**) was bordered by zero intensity voxel, through a *zero-padding* operation. Therefore **Rv** was positioned inside a bigger volume whose dimensions are indicated in Figure 3.16 A). In this way the **LrV** could be virtually superimposed on the **Rv** (Figure 3.16 B). After the zero padding operation the custom software computed the cross correlation value r as

$$r(i,j,k) = \frac{\sum_{x,y,z}\left[Rv(x,y,z) - \overline{Rv}_{i,j,k}\right]\cdot\left[LrV(x-i,y-j,z-k) - \overline{LrV}\right]}{\sqrt{\sum_{x,y,z}\left[Rv(x,y,z) - \overline{Rv}_{i,j,k}\right]^2\cdot\sum_{x,y,z}\left[LrV(x-i,y-j,z-k) - \overline{LrV}\right]^2}}$$

$\overline{LrV}$ is the voxel mean value of the Left reflected Volume, and $\overline{Rv}_{i,j,k}$ is the voxel mean value of the Right Volume under the Left reflected Volume (position i,j,k), and summations are performed over x,y,z under the 3D window containing the Left reflected Volume positioned in i,j,k.

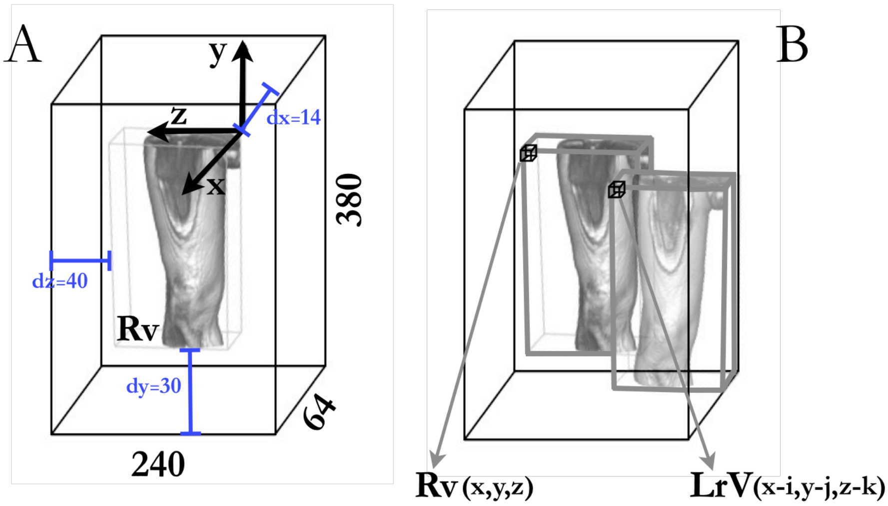

Figure 3.16: A) zero padding operation, B) LrV superimposed to Rv

The cross correlation index was evaluated for each relative position between the two considered volumes (64 X 380 X 240 times). Through the Labview custom software we could also monitor the value of r position by position as we shown in figure 3.17. In this panel we can see the graph of **r** in function of the elapsed time, the cross-correlation index **r** (the instant value and the maximum value) and the coordinates of relative position between the two volumes, which maximise the cross correlation value.

Finally the software allows a check of the computed results; it performs a subtraction of the **LrV** from the **Rv**. In Figure 3.18 it's possible to see (for the three anatomical planes) the difference between the two anatomical volumes, sited in the position that maximise the value of **r**; dark regions indicate high similarity between **LrV** and **Rv**.

As we explained in the previous sections, the cross correlation-value (**r**), can assume a range of values between -1 and 1, depending upon the similarity of the 3D analyzed volumes where a value of 1 indicates an exact matching of the **LrV** with the **Rv**, a value of -1 indicates an exact matching of the inverse of the **LrV** with the **Rv**, and a value of 0 indicates no correlation between the two volumes.

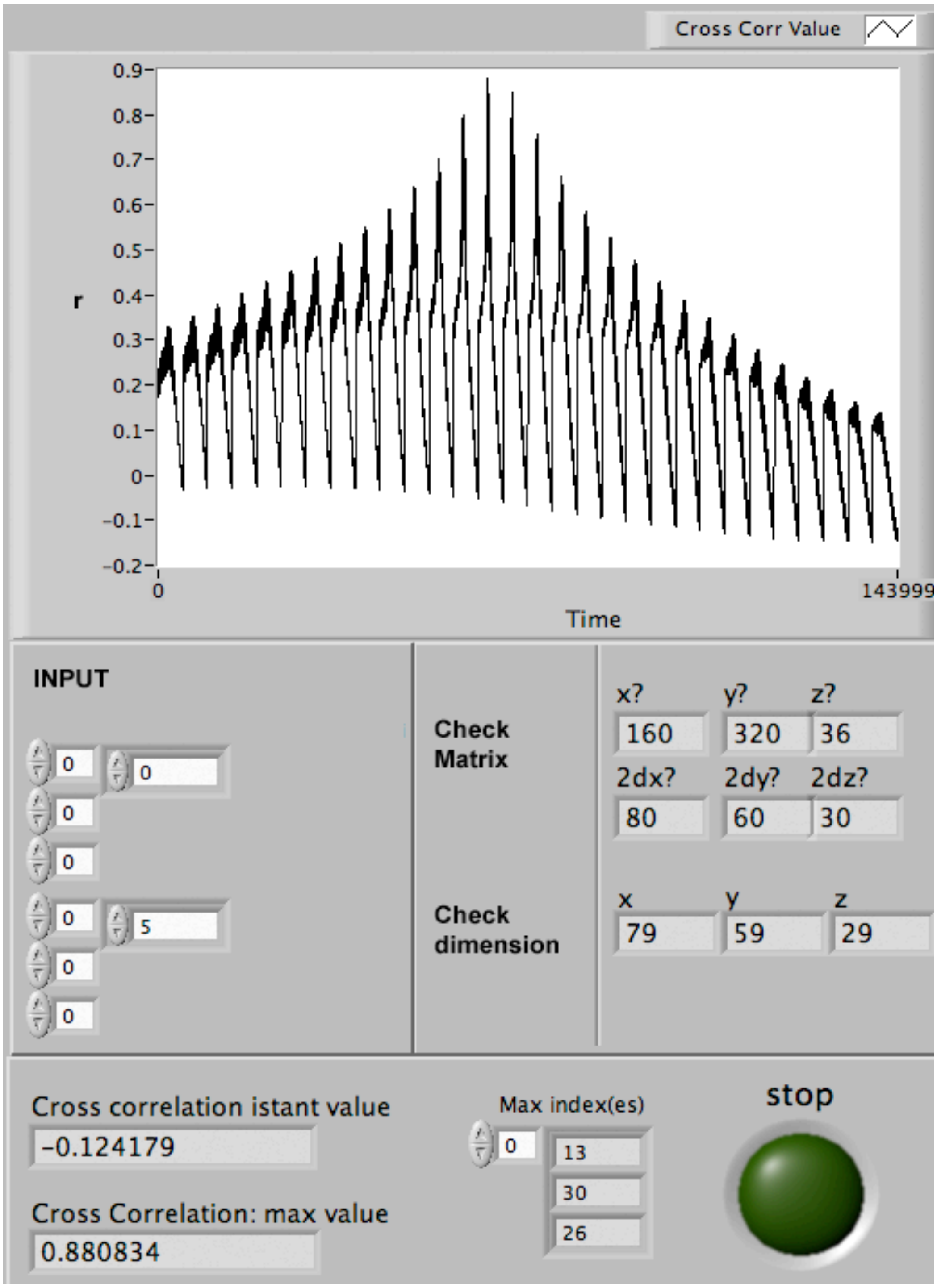

Figure 3.17 Labview Panel indicating the cross-correlation value r. This panel also allows to monitories the cross-correlation value position by position.

To validate the software accuracy, we tested our algorithm comparing the Right Volume of a specific subject, with the same Right reflected Volume of the same subject, obtaining, as we expected, the maximum value of cross-correlation (**r** = 1). In this case the difference between the two volumes in the position that maximise **r** is a completely dark pixels image.

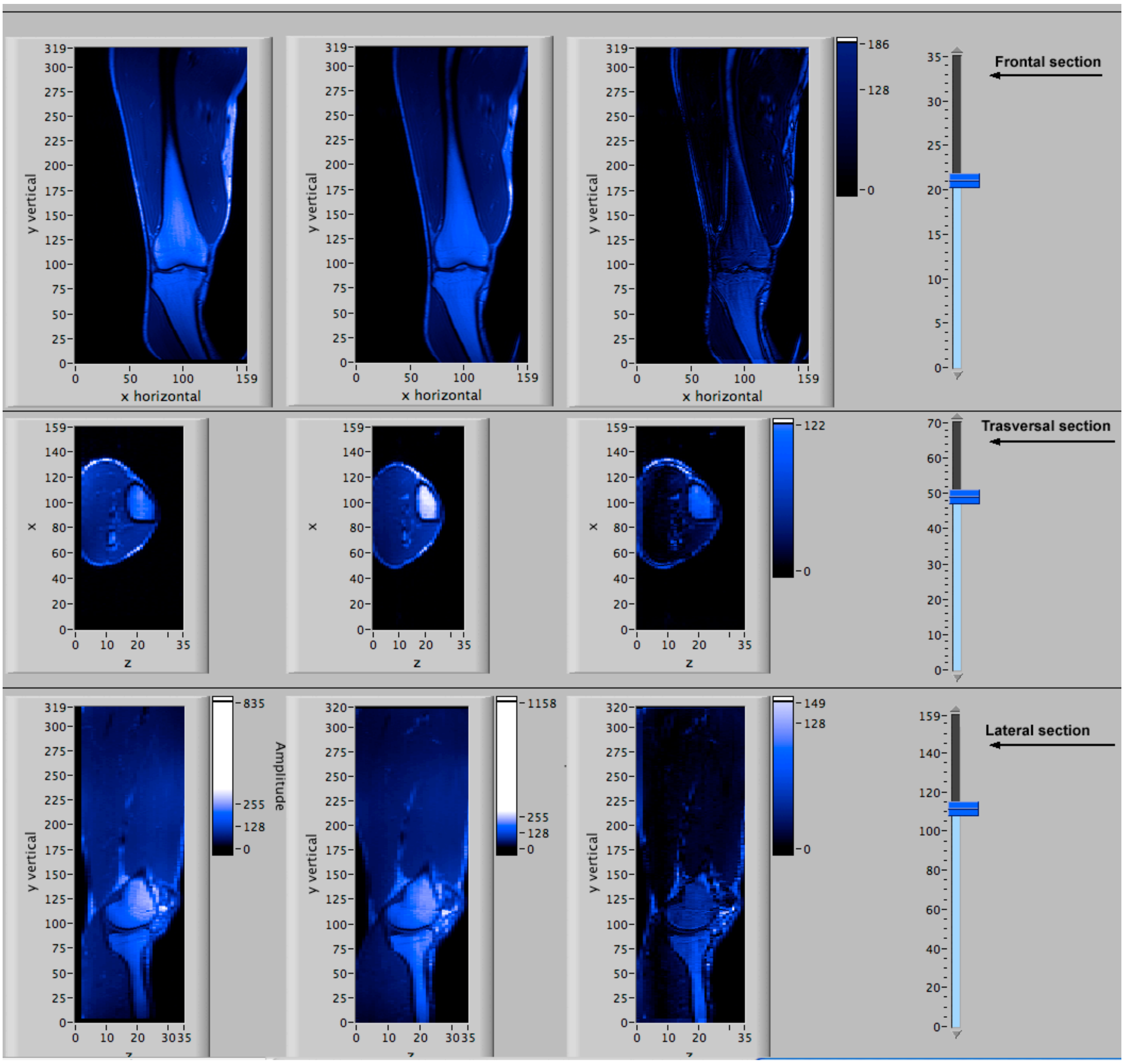

Figure 3.18: Subtraction of LvR from Rv. On the right panels we can observe the difference between the two volumes sited in the position that maximise the cross-correlation value. Dark pixels indicate high level of symmetry, while the bright pixels underline the differences between the two anatomical volumes.

Chapter 4

RESULTS

In this chapter we will show the results obtained, from the experimental protocols described in the previous chapter. Considering that only five SR and five TR were able to complete all the running protocol, up to 5.00 m/s, and other subjects stopped at the speed of 4.44 m/s, we didn’t consider for statistical analysis the highest speed level.

Difference across the five speeds were analysed using a two-ways ANOVA for repeated measures on speed. In addiction we performed a post-*hoc* Bonferroni correction to detect differences between single variables that will be analyzed in this chapter.

For other groups of variables, not dependent from velocity, we performed a one-way ANOVA in order to find difference between groups of subjects.

Relationships between variables were investigated using Pearson’s correlation coefficient. Statistical significance was accepted when p <0.05.

4.1 Characteristic of the subjects

Anthropometrical characteristic of the three different groups of subjects are shown in table 4.1, reporting the same value presented in chapter 3. One-way ANOVA (with a post-*hoc* Bonferroni correction) didn't show any significant difference, between OR, SR and TR, for the three anthropometrical variables (age, body mass and height).

	Occasional Runners (±SD)	**Skilled Runners (±SD)**	**Top Runners (±SD)**
Participants (n)	7	7	5
Age (y)	33.1 ± 13.2	31.9 ± 11.8	42.6 ± 7.4
Body Mass (Kg)	70.6 ± 3.4	67.3 ± 6.1	68.2 ± 4.9
Height (cm)	175.9 ± 4.7	177.3 ± 4.0	177.8 ± 4.4

Table 4.1: Number of participants, mean ± standard deviation (SD) of age (y), body mass (Kg), and height (cm) of the 3 different groups

4.2 Kinematics analysis

The results about kinematic analysis taking account of the parameters obtained from the stream of x, y and z coordinates of BCOM for each *.bcm file, have been calculated with the LabVIEW program "*Lissajous Fourier BCM Trajectory*" (see section 3.3.2) and then averaged on the three kinematic registration performed for each velocity, for each subject. In particular in this section we will put attention on the parameters that best underline the concept of symmetry:

- $\overline{SI^x}$, $\overline{SI^y}$, $\overline{SI^z}$: Single dynamic symmetry index for direction x, y and z respectively.
- *GI*: Global Symmetry Index.
- $\overline{\Delta}_x SD$, $\overline{\Delta}_y SD$, $\overline{\Delta}_z SD$: $\overline{\Delta}_x$, $\overline{\Delta}_y$ and $\overline{\Delta}_z$ Standard Deviation, where $\overline{\Delta}_x$, $\overline{\Delta}_y$, $\overline{\Delta}_z$ are the average distance of the gaps to be filled between the start and the end points of each stride, for each 'local' coordinate.

4.2.1 Single Dynamic Symmetry Indices

We collected in the following tables the Single Dynamic Indices $\overline{SI^x}$, $\overline{SI^y}$ and $\overline{SI^z}$. Every subject has six different indices, one for each running speed. Also we reported the mean value and the SD for each subject category and running velocity.

$\overline{SI^x}$	Running Speed (m/s)					
Subject	**2.22**	**2.78**	**3.33**	**3.89**	**4.44**	**5.00**
OR1	0.604	0.587	0.468	0.667	0.541	n.a
OR2	0.625	0.695	0.688	0.496	0.558	n.a
OR3	0.792	0.794	0.802	n.a	n.a	n.a
OR4	0.667	0.701	0.733	0.726	0.697	n.a
OR5	n.a	0.737	0.760	0.734	n.a	n.a
OR6	0.662	0.703	0.694	0.686	0.685	n.a
OR7	0.641	0.639	0.592	0.619	0.685	n.a
Mean	**0.665**	**0.694**	**0.676**	**0.655**	**0.633**	n.a
SD	**0.066**	**0.067**	**0.113**	**0.088**	**0.077**	n.a
SR1	0.742	0.796	0.821	0.757	0.857	0.806
SR2	0.726	0.752	0.763	0.763	0.756	0.594
SR3	0.735	0.732	0.743	0.745	0.783	0.735
SR4	0.623	0.674	0.670	0.666	0.768	n.a
SR5	0.715	0.753	0.793	0.799	0.725	0.714
SR6	0.668	0.681	0.727	0.749	0.697	n.a
SR7	0.642	0.689	0.709	0.765	0.786	0.728
Mean	**0.693**	**0.725**	**0.746**	**0.749**	**0.767**	**0.715**
SD	**0.048**	**0.046**	**0.051**	**0.041**	**0.051**	**0.077**

TR1	0.756	0.742	0.741	0.718	0.704	n.a
TR2	0.672	0.713	0.710	0.753	n.a	0.749
TR3	0.654	0.743	0.733	0.789	0.786	0.797
TR4	0.683	0.661	0.696	0.742	0.749	0.785
TR5	0.712	0.779	0.775	0.794	0.757	0.758
Mean	**0.695**	**0.727**	**0.731**	**0.759**	**0.749**	**0.772**
SD	**0.040**	**0.044**	**0.030**	**0.032**	**0.034**	**0.022**

Table 4.2: Single Symmetry Indices values with the relative Mean and SD, divided by group and running speed, for the forward (x) direction. (n.a. = not available results)

$\overline{SI^y}$	**Running Speed (m/s)**					
Subject	**2.22**	**2.78**	**3.33**	**3.89**	**4.44**	**5.00**
OR1	0.926	0.919	0.760	0.892	0.824	n.a
OR2	0.894	0.898	0.910	0.866	0.772	n.a
OR3	0.935	0.937	0.909	n.a	n.a	n.a
OR4	0.897	0.908	0.918	0.911	0.897	n.a
OR5	n.a	0.866	0.853	0.830	n.a	n.a
OR6	0.890	0.908	0.899	0.894	0.875	n.a
OR7	0.923	0.932	0.944	0.917	0.896	n.a
Mean	**0.911**	**0.910**	**0.885**	**0.885**	**0.853**	n.a
SD	**0.019**	**0.024**	**0.061**	**0.032**	**0.054**	n.a
SR1	0.934	0.939	0.929	0.919	0.915	0.920
SR2	0.858	0.865	0.850	0.837	0.824	0.752
SR3	0.898	0.881	0.876	0.885	0.884	0.898
SR4	0.887	0.878	0.864	0.870	0.848	n.a
SR5	0.923	0.926	0.930	0.924	0.892	0.863
SR6	0.901	0.907	0.905	0.895	0.872	n.a
SR7	0.873	0.874	0.896	0.870	0.895	0.903
Mean	**0.896**	**0.896**	**0.893**	**0.886**	**0.876**	**0.867**
SD	**0.027**	**0.028**	**0.031**	**0.030**	**0.031**	**0.068**
TR1	0.856	0.859	0.845	0.805	0.830	n.a
TR2	0.925	0.927	0.907	0.885	n.a	0.871
TR3	0.873	0.886	0.881	0.888	0.879	0.893
TR4	0.790	0.783	0.781	0.801	0.793	0.770
TR5	0.903	0.895	0.898	0.865	0.873	0.920
Mean	**0.869**	**0.870**	**0.862**	**0.849**	**0.844**	**0.864**
SD	**0.052**	**0.055**	**0.051**	**0.043**	**0.040**	**0.066**

Table 4.3: Single Symmetry Indices values with the relative Mean and SD, divided by group and running speed, for the vertical (y) direction. (n.a. = not available results)

$\overline{SI^z}$	Running Speed (m/s)					
Subject	**2.22**	**2.78**	**3.33**	**3.89**	**4.44**	**5.00**
OR1	0.861	0.861	0.828	0.809	0.791	n.a
OR2	0.920	0.917	0.922	0.816	0.860	n.a
OR3	0.938	0.910	0.914	n.a	n.a	n.a
OR4	0.953	0.949	0.943	0.922	0.916	n.a
OR5	n.a	0.855	0.824	0.788	n.a	n.a
OR6	0.920	0.914	0.889	0.795	0.733	n.a
OR7	0.902	0.857	0.861	0.907	0.865	n.a
Mean	**0.916**	**0.895**	**0.883**	**0.839**	**0.833**	n.a
SD	**0.032**	**0.037**	**0.047**	**0.059**	**0.072**	n.a
SR1	0.874	0.913	0.937	0.941	0.951	0.916
SR2	0.942	0.898	0.914	0.885	0.844	0.748
SR3	0.860	0.906	0.887	0.864	0.870	0.860
SR4	0.939	0.926	0.905	0.903	0.903	n.a
SR5	0.900	0.872	0.841	0.811	0.861	0.871
SR6	0.825	0.878	0.882	0.918	0.917	n.a
SR7	0.924	0.869	0.801	0.858	0.814	0.873
Mean	**0.895**	**0.895**	**0.881**	**0.883**	**0.880**	**0.854**
SD	**0.044**	**0.022**	**0.046**	**0.043**	**0.047**	**0.063**
TR1	0.838	0.772	0.729	0.726	0.687	n.a
TR2	0.914	0.885	0.875	0.846	n.a	0.797
TR3	0.840	0.843	0.816	0.805	0.797	0.800
TR4	0.823	0.796	0.786	0.784	0.759	0.776
TR5	0.837	0.832	0.809	0.792	0.760	0.796
Mean	**0.850**	**0.826**	**0.803**	**0.791**	**0.751**	**0.792**
SD	**0.036**	**0.044**	**0.053**	**0.043**	**0.046**	**0.011**

Table 4.4: Single Symmetry Indices values with the relative Mean and SD, divided by group and running speed, for the lateral (z) direction. (n.a. = not available results)

Results are presented as mean ± standard deviation (SD), in the graphs of Figures 4.1 and 4.2. Difference across running group and Single Symmetry Indices were analysed with a two-ways ANOVA with repeated measure on running speed (independent variable). In the first group of graphs (figure 4.1), we analysed differences between the symmetry single indices in the three different directions, ($\overline{SI^x}$, $\overline{SI^y}$, $\overline{SI^z}$), for each group of subjects.

In the second group of graphs (figure 4.2), we analysed instead, differences between running groups (OR, SR and TR) for each symmetry index.

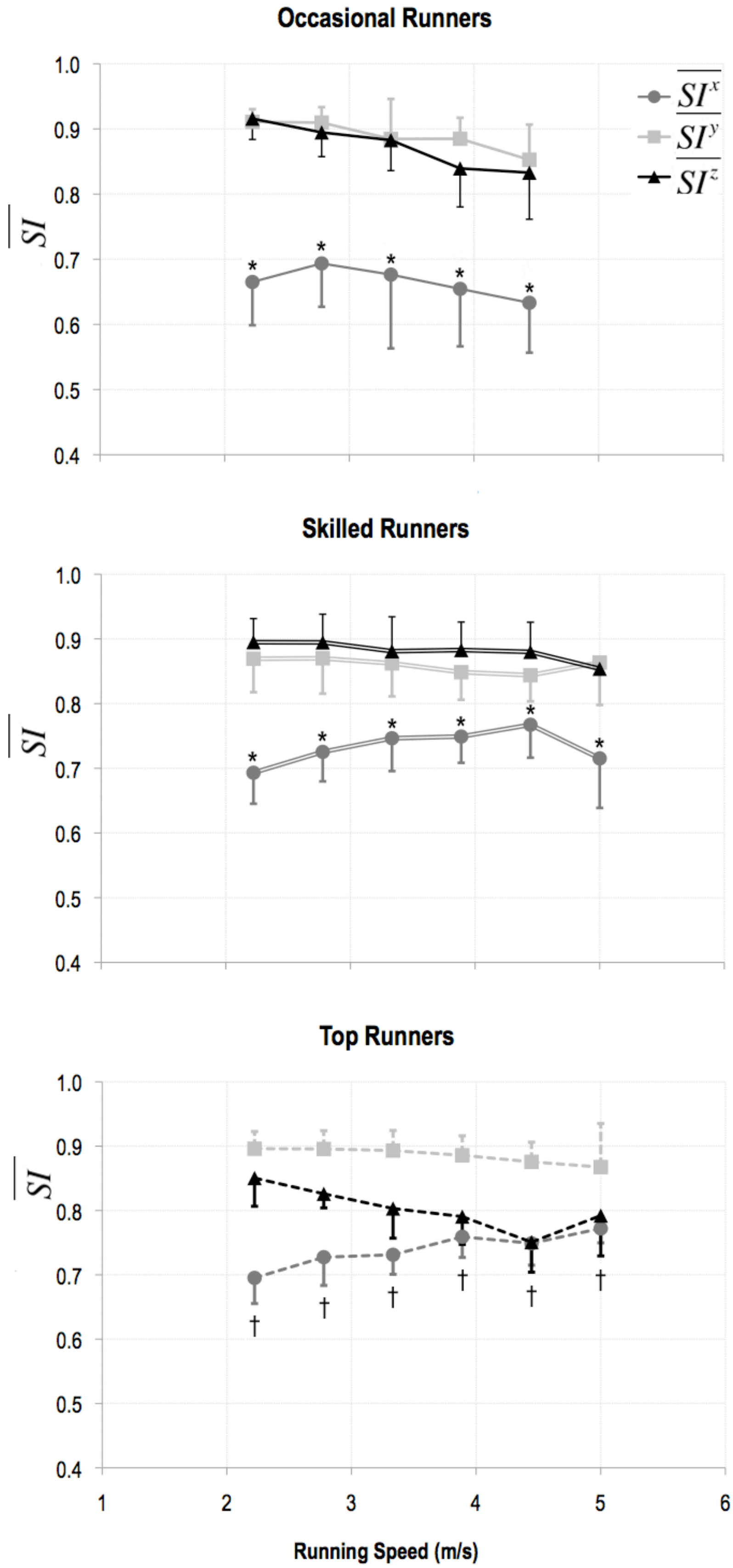

Figure 4.1: $\overline{SI}$ in function of running speed for the three coordinates divided for the three groups of subjects (OR, SR, TR). $\overline{SI^x}$ is always significantly lower ($p < 0.001$) than $\overline{SI^y}$ and $\overline{SI^z}$ for OR and SR (*), while for TR $\overline{SI^x}$ is statistically lower (†) than $\overline{SI^y}$, ($p < 0.001$).

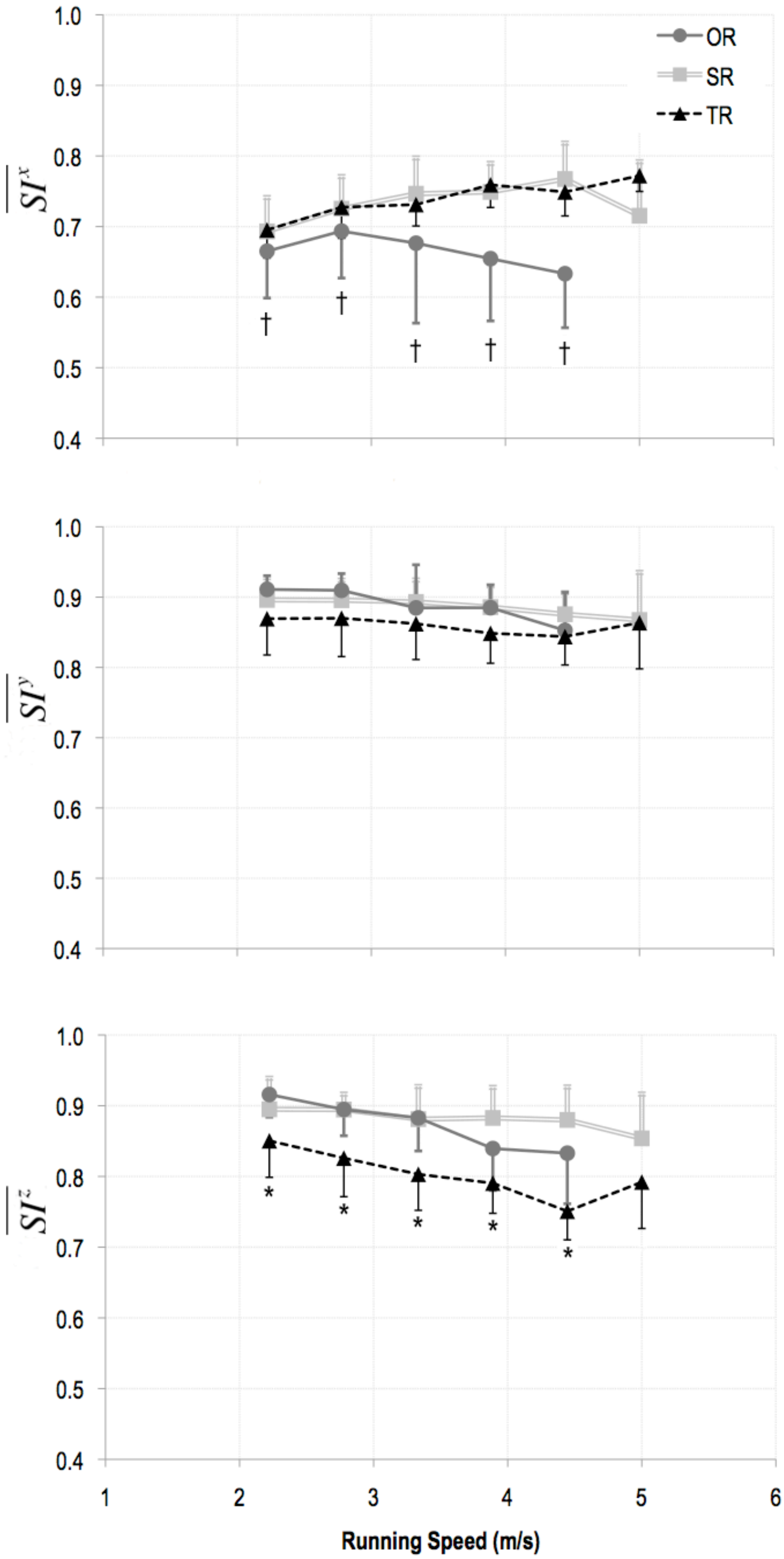

Figure 4.2: $\overline{SI^x}$, $\overline{SI^y}$ and $\overline{SI^z}$ for OR, SR and TR in function of running speed.

In x direction OR have a $\overline{SI}$ always lower than SR and TR (†), ($p < 0.001$), while in z direction TR have a $\overline{SI}$ always significantly lower, ($p < 0.001$) than OR.

Results about Symmetry single Indices can be summarized as:

- Dynamic Symmetry in the forward direction (x) is always lower than in lateral (z) and vertical (y) direction, independently from the running speed for OR and SR ($p < 0.001$). For TR, $\overline{SI^x}$ always lower than $\overline{SI^y}$ ($p < 0.001$), (Figure 4.1).
- OR in forward direction (x) present a lower value of $\overline{SI}$ than SR and TR, ($p < 0.001$). And also, even if not significantly $\overline{SI^x}$ seems to decrease with the running speed for OR (Figure 4.2, Top Panel).
- There is no significant difference across velocities and between groups of subjects in the vertical direction (y).
- In the lateral direction (z) TR have a $\overline{SI}$ always significantly lower than OR, ($p < 0.001$).

4.2.2 Global Index

Starting from the single values of $\overline{SI^x}$, $\overline{SI^y}$, $\overline{SI^z}$, collected in tables 4.2, 4.3 and 4.4, we evaluated the Global Symmetry Index as explained in section 3.3.3. Results are reported as mean ± standard deviation (SD) in table 4.5 and in the graph of the figure 4.3 A and B, for the three different groups of subjects. With the single Global Index values we performed a two-ways ANOVA for repeated measure on velocity. The independent variable was running speed and group and the dependent variable was GI. Statistical results are showed in figure 4.3 A and B, in particular OR have a GI significantly lower than SR and TR for each velocity, ($p < 0.001$). Also, the GI for OR seems to decrease with the increasing running velocity, even if not significantly.

GI	**Group of Running**		
Running Speed	**OR**	**SR**	**TR**
2.22	0.663 ± 0.065	0.684 ± 0.044	0.687 ± 0.043
2.78	0.690 ± 0.061	0.721 ± 0.047	0.717 ± 0.044
3.33	0.665 ± 0.132	0.742 ± 0.052	0.726 ± 0.027
3.89	0.633 ± 0.084	0.745 ± 0.041	0.748 ± 0.038
4.44	0.603 ± 0.098	0.759 ± 0.052	0.722 ± 0.068
5.00	n.a	0.706 ± 0.086	0.785 ± 0.009

Table 4.5: Results about Global Index values presented as mean ± SD , divided for groups of subjects and for running speed. (n.a. = not available results)

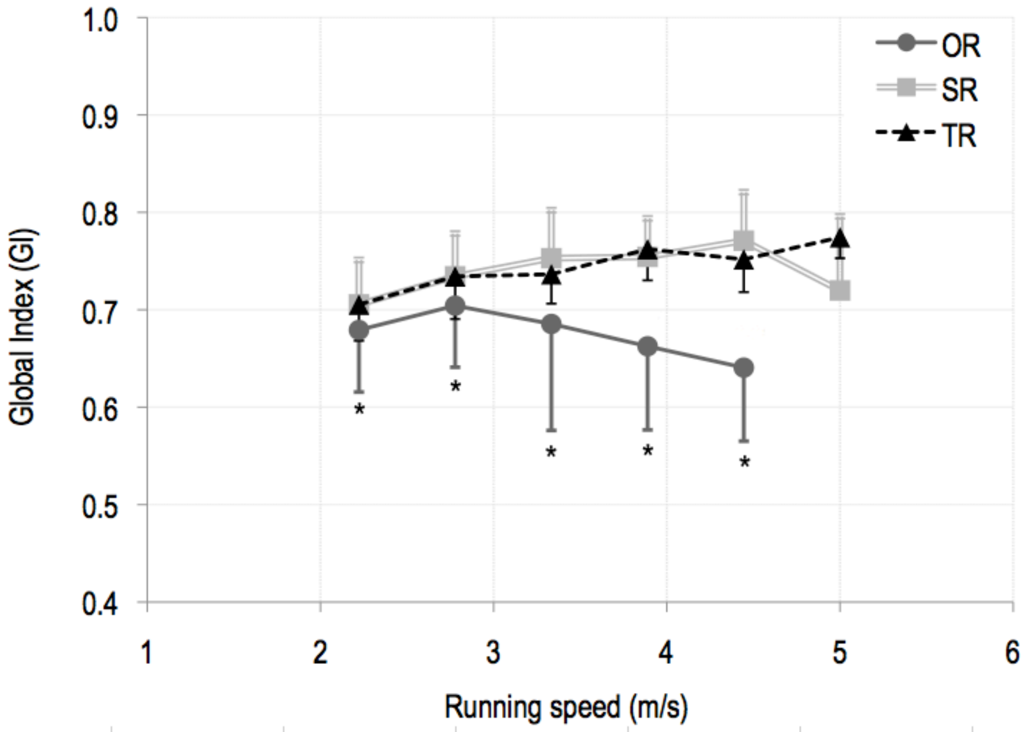

A

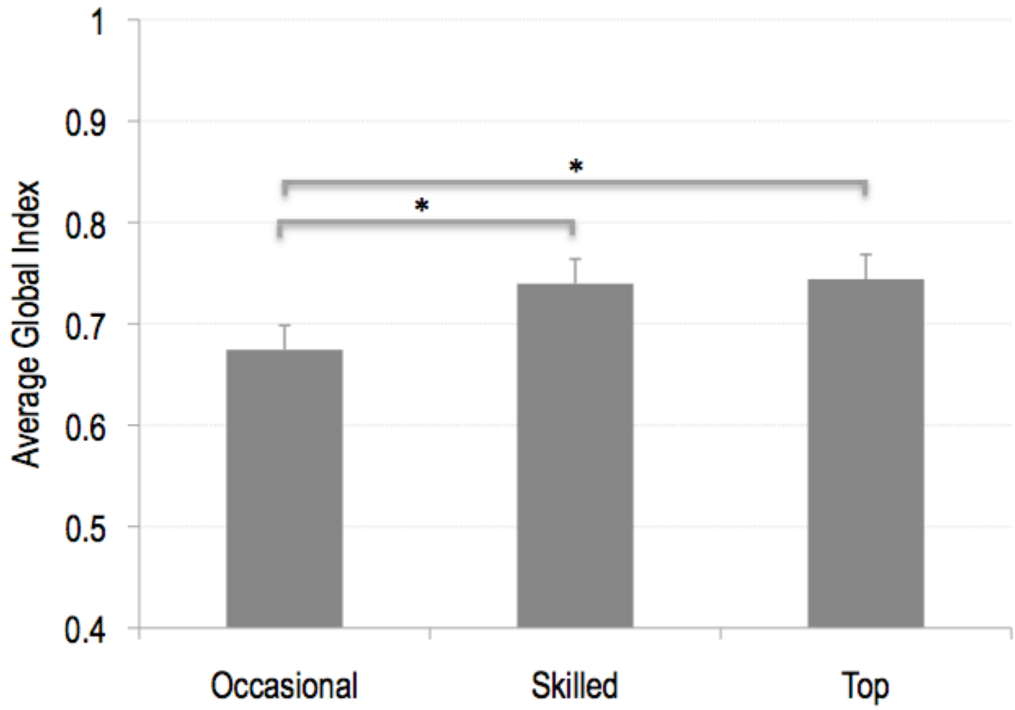

B

Figure 4.3: A) Global Symmetry Index in OR, SR and TR. The GI of OR is always lower respect to SR and TR, (* = p <0.001), independently from the running speed. B) Average Global Index for the three subjects categories.

4.2.3 $\overline{\Delta}_x$, $\overline{\Delta}_y$ and $\overline{\Delta}_z$ variability

The variability of the average distance of the gaps to be filled between the start and the end 3D BCOM position of each stride ($\overline{\Delta}_x$, $\overline{\Delta}_y$ and $\overline{\Delta}_z$) is represented by the standard deviation of these parameters ($\overline{\Delta}_x SD$, $\overline{\Delta}_y SD$ and $\overline{\Delta}_z SD$). The higher is the SD value, the smaller is the precision in matching the starting and ending 3D point of each stride, i.e. the considered subject is running more erratically.

Significant relationships between variables were founded in TR for *x* and *z* direction, in SR and OR for the vertical direction *y*. While TR decrease their variability with the increasing running speed, for OR and SR the variability increases significantly with the velocity (see Figure 4.4).

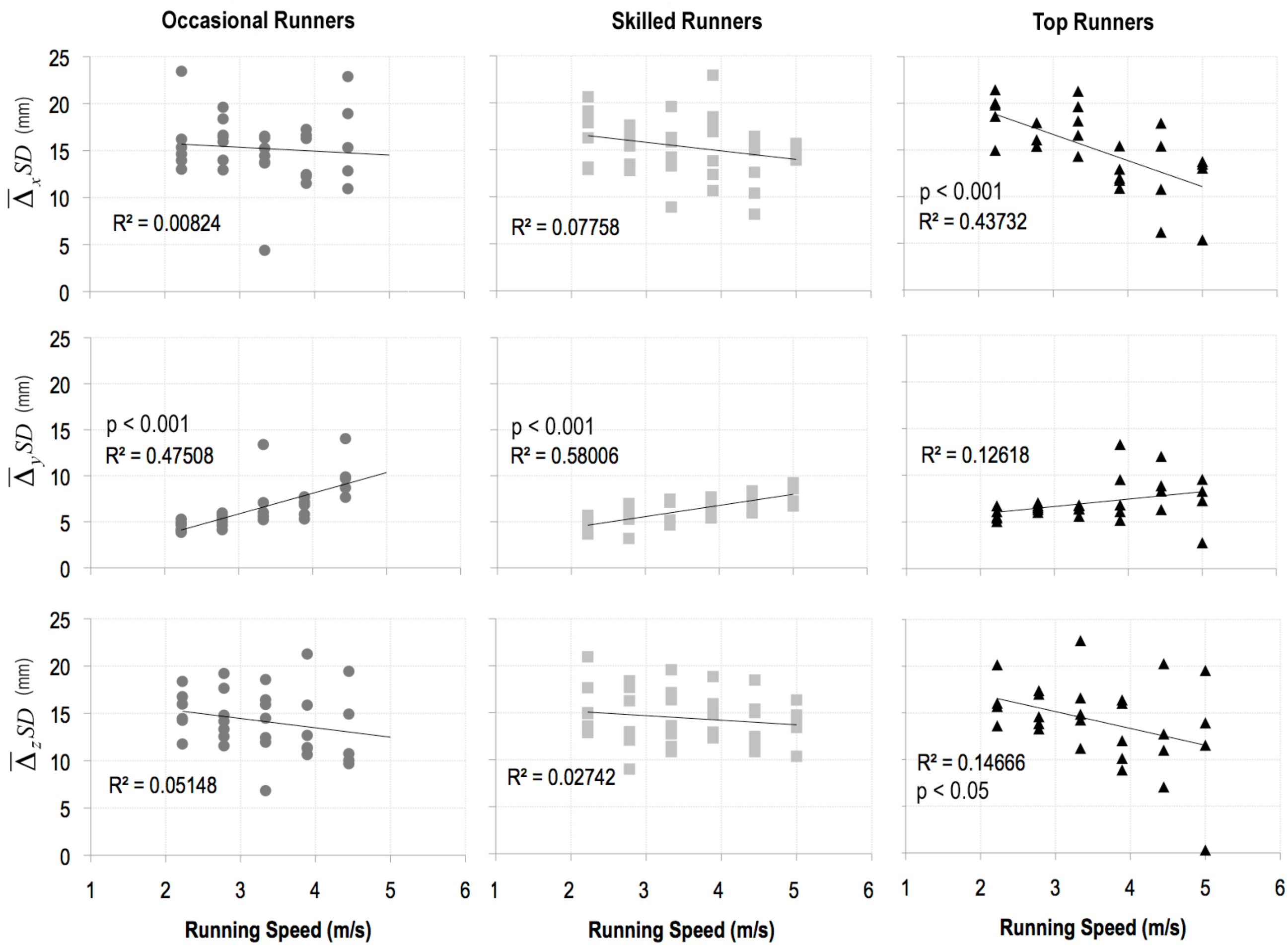

Figure 4.4: $\overline{\Delta}$ *SD* plotted against running speed, for *x*, *y* and *z* directions, for OR (solid grey circles), SR (solid grey squares) and TR (solid black triangles). Pearson's correlation coefficient and statistical significance is also indicated for each directions and group of subjects.

4.3 Running Economy

At the beginning of this paragraph we will report results about the metabolic cost (used to estimate running economy), together with the Heart Rate (HR) results. Secondly we will present the estimated $\dot{V}O_{2\,max}$ for the three groups of subjects, starting from their Cost of transport and from their record performance times obtained in National competitions. Finally we will dedicate the last part of this paragraph to the relationships between the cost of transport and the kinematic.

4.3.1 Cost of transport and Heart Rate

Statistical analysis was performed starting from the single metabolic cost/heart rate values of each subject, for each running velocity (values are collected in tables 4.6 and 4.7). A two-ways ANOVA for repeated measured on speed, with a post-hoc test of Bonferroni, was carried out in order to detect differences across speeds and between groups of subject. The independent variable was the progression speed. The chosen dependent variables were the Metabolic Cost (C) firstly and Heart Rate (HR) secondly. Statistic results are presented as mean ± standard deviation (SD) in figure 4.5.

$C(J/(Kg\cdot m))$	**Running Speed (m/s)**					
Subject	**2.22**	**2.78**	**3.33**	**3.89**	**4.44**	**5.00**
OR1	4.501	4.482	4.317	4.533	4.623	n.a.
OR2	5.590	5.197	4.809	5.888	5.941	n.a.
OR3	5.751	5.506	5.019	4.692	4.051	n.a.
OR4	4.069	4.197	4.285	4.500	4.225	n.a.
OR5	4.793	4.875	4.736	4.411	4.040	n.a.
OR6	4.871	5.300	5.434	4.969	4.753	n.a.
OR7	5.089	5.120	4.940	4.903	4.520	n.a.
Mean	**4.952**	**4.954**	**4.792**	**4.842**	**4.593**	n.a.
SD	**0.589**	**0.468**	**0.403**	**0.506**	**0.656**	n.a.
SR1	5.916	5.913	5.783	5.439	4.636	n.a.
SR2	5.553	5.226	4.556	4.552	4.152	4.093
SR3	4.626	5.035	5.185	5.190	5.191	4.581
SR4	6.080	5.114	4.907	4.691	4.629	n.a.
SR5	5.206	4.819	4.678	4.632	4.791	4.817
SR6	4.483	4.398	4.466	4.192	4.457	4.521
SR7	4.226	4.037	3.991	4.143	4.073	3.957
Mean	**5.156**	**4.934**	**4.795**	**4.691**	**4.561**	**4.394**
SD	**0.729**	**0.604**	**0.573**	**0.480**	**0.382**	**0.358**

TR1	5.447	5.067	4.887	4.997	5.139	4.811
TR2	4.944	4.742	4.579	4.787	4.778	n.a.
TR3	4.388	4.574	4.139	4.129	4.189	4.650
TR4	4.503	4.527	4.536	4.770	5.089	4.980
TR5	4.854	4.619	4.636	4.473	4.293	4.393
Mean	**4.827**	**4.706**	**4.555**	**4.631**	**4.698**	**4.709**
SD	**0.417**	**0.217**	**0.270**	**0.337**	**0.441**	**0.250**

Table 4.6: Single Metabolic Cost Values expressed in J/(Kg. m), with the relative Mean and SD. (n.a. = not available results).

HR(*bpm*)	**Running Speed (m/s)**					
Subject	**2.22**	**2.78**	**3.33**	**3.89**	**4.44**	**5.00**
OR1	n.a.	n.a.	n.a.	n.a.	n.a.	n.a.
OR2	144.172	150.941	162.806	172.500	182.435	n.a.
OR3	140.854	158.595	170.650	184.355	186.991	n.a.
OR4	123.860	138.430	158.950	169.820	181.730	n.a.
OR5	130.060	146.130	159.620	173.080	182.170	n.a.
OR6	133.500	158.290	183.171	199.191	201.306	n.a.
OR7	135.000	150.800	164.800	175.100	183.200	n.a.
Mean	**134.574**	**150.531**	**166.666**	**179.008**	**186.305**	n.a.
SD	**7.322**	**7.632**	**9.120**	**11.074**	**7.591**	n.a.
SR1	133.000	147.000	158.000	171.000	176.784	n.a.
SR2	113.483	131.243	141.561	154.227	168.397	170.462
SR3	116.300	133.300	148.500	170.500	187.600	197.200
SR4	140.700	140.100	158.700	168.500	180.200	n.a.
SR5	120.500	140.100	151.600	164.500	178.000	187.500
SR6	135.100	157.800	172.700	186.700	186.800	186.700
SR7	111.800	123.360	138.160	153.080	169.340	175.970
Mean	**124.412**	**138.986**	**152.746**	**166.930**	**178.160**	**183.566**
SD	**11.640**	**11.233**	**11.679**	**11.414**	**7.560**	**10.495**
TR1	105.185	117.630	126.813	140.536	154.465	156.850
TR2	133.628	146.163	159.261	163.880	178.096	n.a.
TR3	108.305	124.164	132.825	138.892	146.386	157.065
TR4	117.417	120.844	132.113	147.974	161.444	173.427
TR5	112.750	122.386	135.146	143.675	153.239	163.689
Mean	**115.457**	**126.237**	**137.232**	**146.991**	**158.726**	**162.758**
SD	**11.158**	**11.395**	**12.687**	**10.056**	**12.074**	**7.789**

Table 4.7: Single subject average heart rate (HR) value expressed in bpm, with the Mean and SD. (n.a. = not available results).

In the statistical results obtained with the two-ways ANOVA on the cost of transport, the hypothesis of sphericity was assumed, but we didn't find any significance across the velocity. As already widely demonstrated in literature (Margaria, Cerretelli 1963), the energy cost of running seems to be independent of speed, for each running group. Furthermore, among all groups, we found no statistical significant differences. Differently, for the Heart Rate, we found significant differences among groups of subjects, ($p < 0.001$). In particular TR had always higher HR values than SR and OR (figure 4.3.1). The hypothesis of sphericity was in this second test confirmed for the velocity, i.e. HR increases significantly ($p < 0.001$) with the running velocity for all the group of subjects.

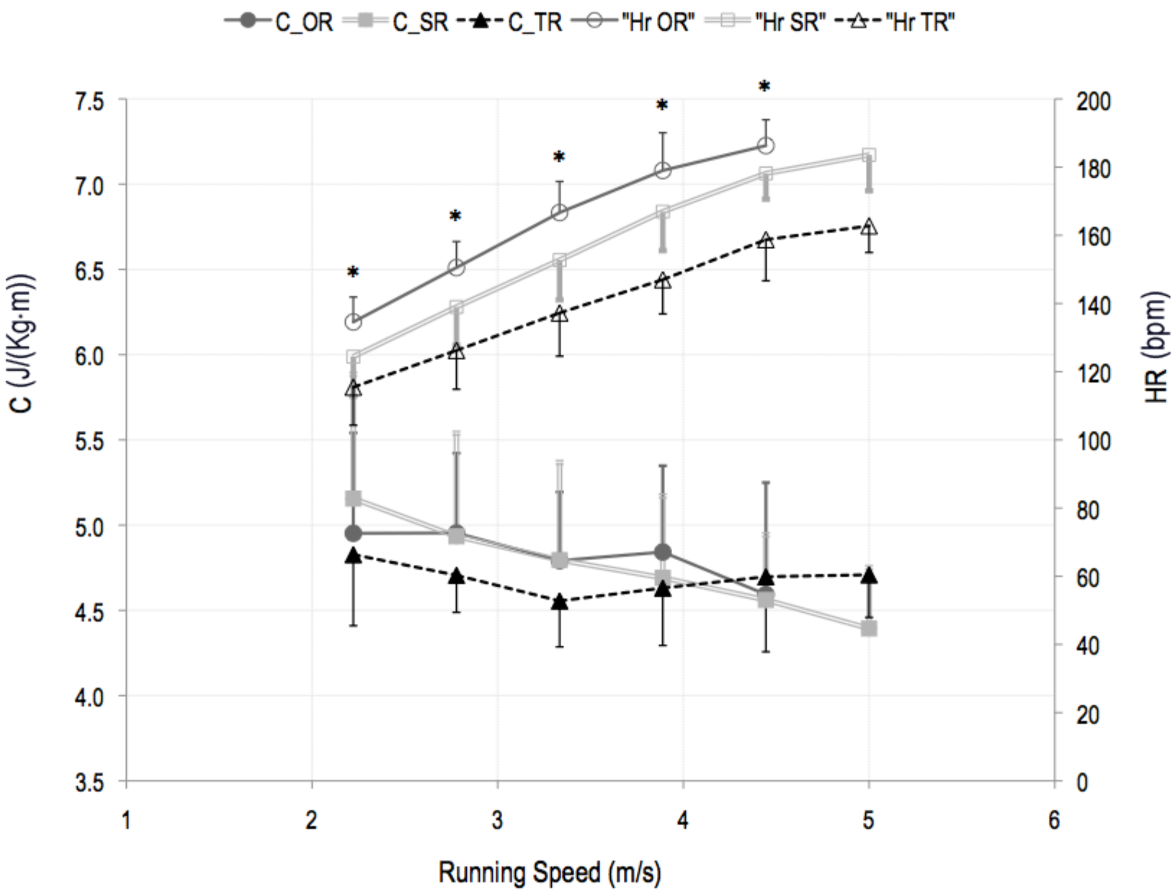

Figure 4.5: Mean ± SD for the Cost of Transport (C) (Lower Curves) and for the Heart rate (Upper curves). There is no significant difference between group of subject and across velocity for C, and the symbol * indicates that TR have a significantly higher Heart Rate ($p < 0.001$) than SR and than OR. In addition Heart Rate increases significantly with the running speed.

4.3.2 Cost of transport and estimated $\dot{V}O_{2\max}$

In order to better characterize the three different subjects categories (OR, SR and TR), we evaluated for each of them the estimated maximum oxygen consumption ($\dot{V}O_{2\max E}$).

We collected for each subject their best performance times ($t_{\lim}$) obtained during national competitions (marathon, half marathon or 10 Km competition). Starting from their record times we evaluated their maximum aerobic running velocity (**v_o**). Successively, using the data reported in table 4.6 we established the estimated Cost of transport (**C_E**) as the average Cost of Transport measured at the difference running velocity, for each runner. Values regarding **C_E** are reported in table 4.8.

Subject	C_E $(J/Kg \cdot m)$	$\dot{V}O_{2E}$ $(mlO_2/(Kg \cdot \min))$	$\%\dot{V}O_{2E}$ *(%)*	$\dot{V}O_{2\max E}$ $(mlO_2/(Kg \cdot \min))$
OR1	5.485	n.a.	n.a.	n.a.
OR2	4.255	50.196	0.845	59.381
OR3	5.004	48.386	0.821	58.909
OR4	4.571	n.a.	n.a.	n.a.
OR5	4.491	47.288	0.863	54.865
OR6	5.066	51.125	0.826	61.912
OR7	4.915	55.658	0.815	68.624
Mean	**4.827**	**50.531**	**0.834**	**60.738**
SD	**0.415**	**3.235**	**0.020**	**5.081**
SR1	4.419	63.360	0.904	70.125
SR2	4.689	55.440	0.793	69.751
SR3	5.537	71.082	0.814	87.394
SR4	5.084	54.594	0.838	65.123
SR5	4.968	65.847	0.818	80.609
SR6	4.824	73.518	0.907	81.085
SR7	4.071	58.646	0.864	67.861
Mean	**4.799**	**63.212**	**0.848**	**74.564**
SD	**0.473**	**7.424**	**0.045**	**8.373**
TR1	4.766	65.766	0.846	77.866
TR2	5.058	64.458	0.839	76.927
TR3	4.345	66.303	0.855	77.604
TR4	4.734	66.954	0.850	78.983
TR5	4.545	63.049	0.847	74.568
Mean	**4.690**	**65.306 ***	**0.848**	**77.190 ***
SD	**0.266**	**1.395**	**0.006**	**1.469**

Table 4.8: Results regarding the estimated parameter described in section 4.3.2. Significant differences were found between OR and TR, and OR and SR. In particular OR have lower $\dot{V}O_{2E}$ and $\dot{V}O_{2\max E}$ compared to the SR and TR (* = $p < 0.05$).

Using the definition of Cost of Transport (see chapter 2), we could calculate for each subject the estimated oxygen consumption during the competition as

$$\dot{V}O_{2E} = \mathbf{C_E} \cdot \mathbf{v_o} + \dot{V}O_{2rest}$$

In order to evaluate the portion of $\dot{V}O_{2E}$ characterizing each subject during the competitions, (**%** $\dot{V}O_{2E}$), we use the diagram proposed by di Prampero in 1985, (di Prampero 1985), showed in figure 4.6.

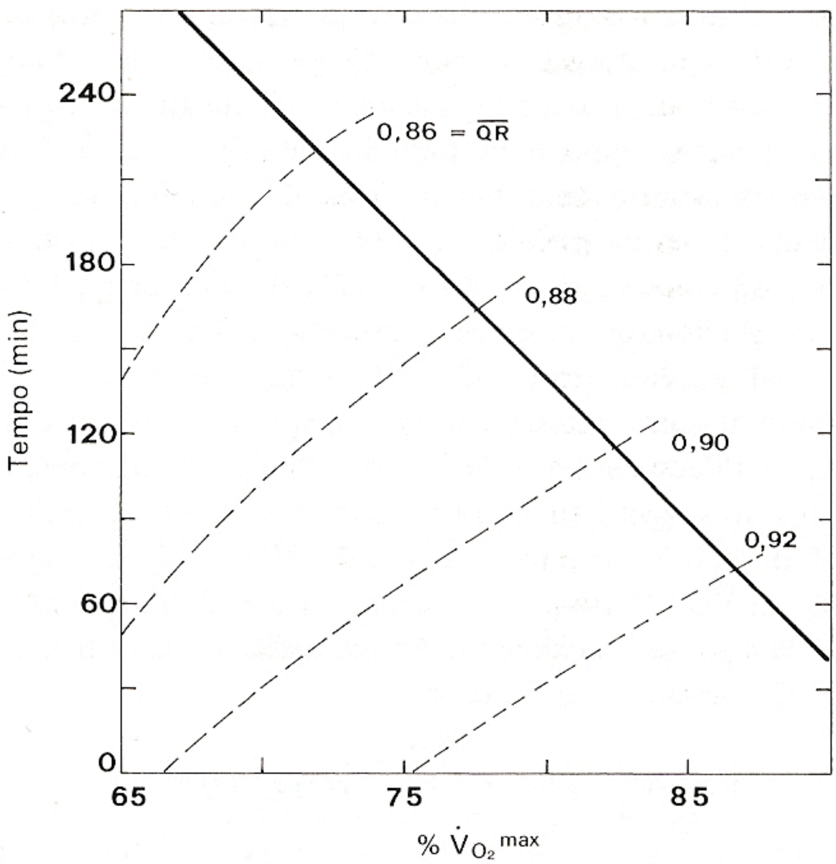

Figure 4.6: The portion of $\dot{V}O_{2E}$ plotted against the performance duration (record time) (di Prampero 1985). The dot lines represent the averaged Respiratory Quotient (RQ) that characterizes the exercise.

The record time $t_{\lim}$ (performance duration) is plotted against the sustained fraction of $\dot{V}O_{2\max E}$ In particular the black solid curve plotted in the graph of figure 4.6 is represented by the following equations

$$t_{\lim} = 15.7 - 16.7 \cdot \frac{\dot{V}O_{2E}}{\dot{V}O_{2\max E}}$$

where $t_{\lim}$, (in hours), is the record time (performance duration) and $\frac{\dot{V}O_{2E}}{\dot{V}O_{2\max E}}$ is the estimated portion of $\dot{V}O_{2\max E}$ during the competitions ($\%\dot{V}O_{2E}$).

In this way it’s simple to calculate the estimated maximum oxygen consumption ($\dot{V}O_{2\max E}$) for each subject as

$$\dot{V}O_{2\max E} = \frac{\dot{V}O_{2E}}{\%\dot{V}O_{2E}}$$

Results for the single estimated values are reported in table 4.8. We performed a one-way ANOVA between the three running groups (OR, SR and TR), in order to find differences, for the dependent variables $\dot{V}O_{2E}$ and $\dot{V}O_{2\max E}$.

Statistical results for the considered variables shown that TR have higher values for $\dot{V}O_{2E}$ and $\dot{V}O_{2\max E}$ compared to the OR ($p < 0.05$).

We didn’t find statistically significant differences between OR and SR, SR and TR for these variables.

Also, we didn’t find statistical differences between running groups for the Cost of Transport (C) and for the portion of $\dot{V}O_{2E}$ during the competitions ($\%\dot{V}O_{2E}$).

4.3.3 Cost of transport and kinematics

In figure 4.6 we reported the value of the single symmetry index for the three different directions in function of the cost of transport. We reported the single value of $\overline{SI^x}$, $\overline{SI^y}$ and $\overline{SI^z}$ for each velocity, for each athlete.

In order to find relationships between the symmetry single indices and the Cost of Transport C, we performed a correlation analysis between variables using Pearson’s correlation coefficient.

Results are represented in figure 4.7 with the relative Pearson coefficient. No significant relationships were founded between $\overline{SI}$ and the Cost of transport.

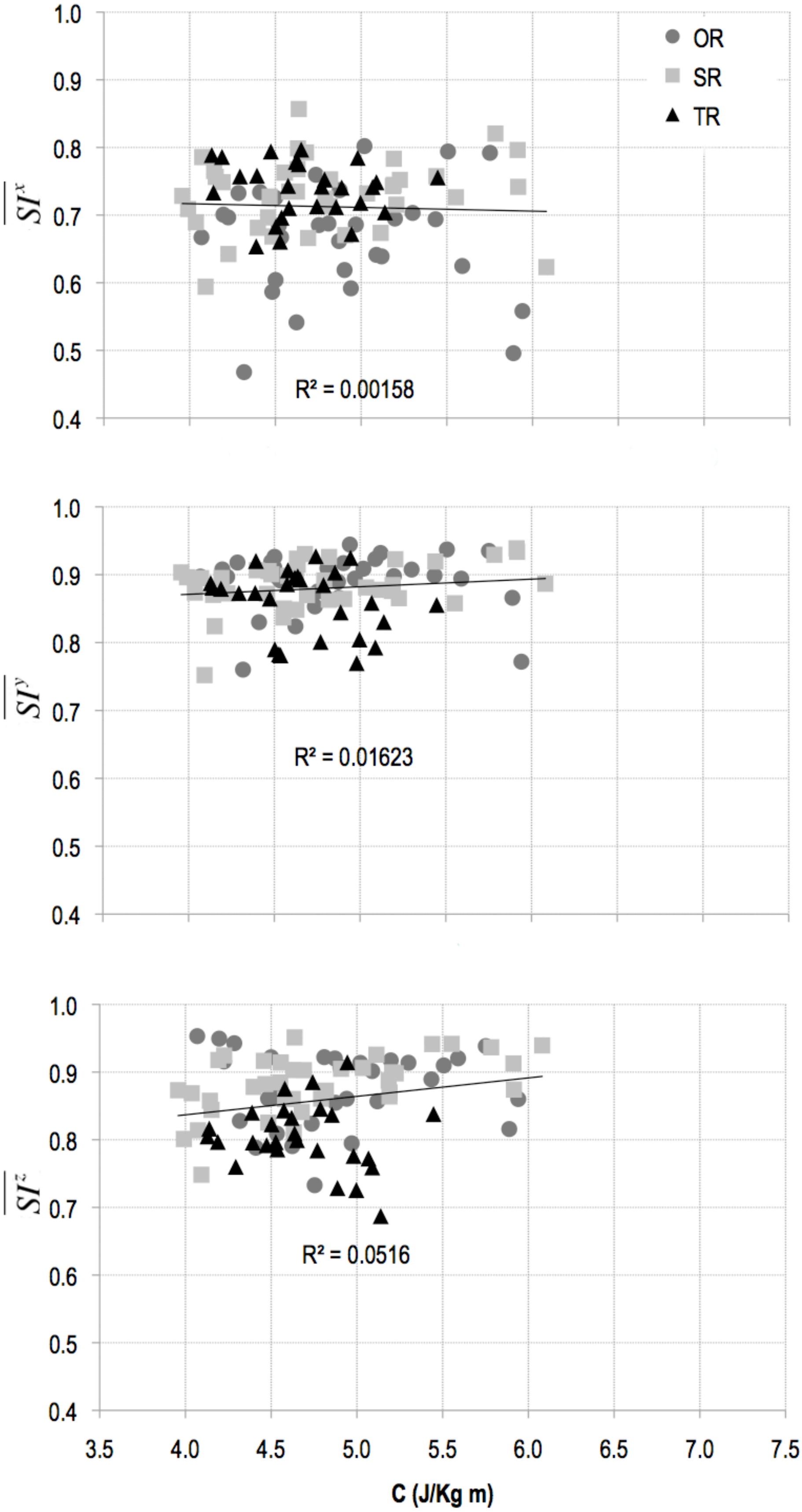

Figure 4.7: Cost of transport plotted against the 3 symmetry single indices $\overline{SI^x}$, $\overline{SI^y}$ and $\overline{SI^z}$ for all subjects. In particular we used solid grey circles for OR, solid grey squares for SR and solid black triangles for TR.

4.4 Anatomical symmetry index, the cross-correlation value

Results regarding the anatomical symmetry are limited to only seventeen subjects, because two MRI protocols (one for the OR and one for the TR), didn't give the correct output, due to technical problems. In this paragraph we will present the results obtained from the algorithm explained in paragraph 3.4.

The procedure, starting from the MR images of the subjects, computed the cross-correlation value (**r**), for the three different anatomical districts (PD, UD and LD). This index is a measure of the level of symmetry between the right and the left side for each subject in those districts. The closer **r** is to 1, the higher is symmetry between right and left side.

Furthermore for each district we didn't consider the whole image (320 X 320 pixels) because of the distortions caused by the magnetic field on the image boundaries (see Figures 4.8).

In order to delete this deformation, we considered only a portion of the global image. To do this, in the first step of the LabVIEW algorithm, we selected the region of interest we want to analyse (figure 3.8, section 3.4.1).

In particular as shown in figure 4.8

- For the PD, we deleted the first 100 pixels rows, starting from the bottom. We obtained the Pelvis district reduced (PDr).
- For the UD we deleted the first 28 pixels rows, starting from the bottom. We obtained the Upper District reduced (UDr).
- For the LD we considered only the first 280 pixel rows, starting from the bottom. We obtained the Lower District reduced (LDr).

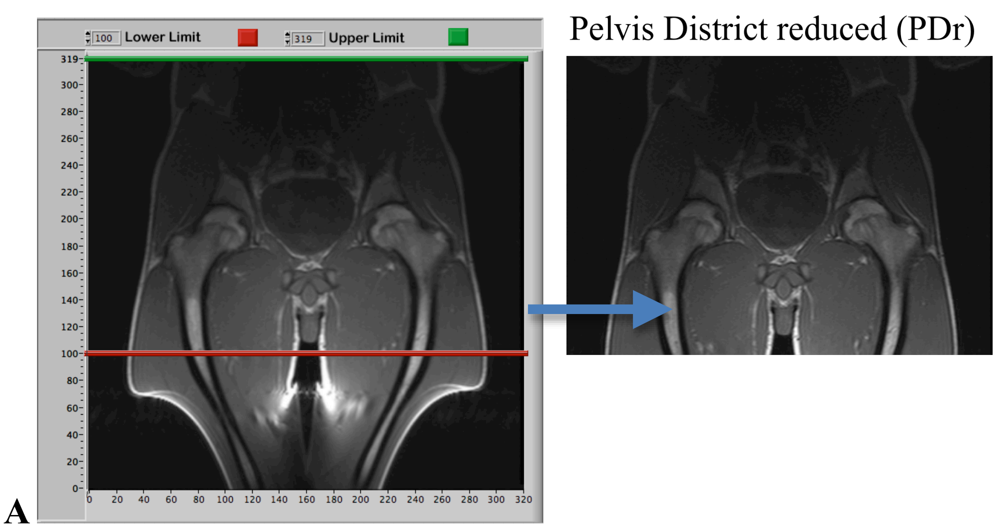

B
C
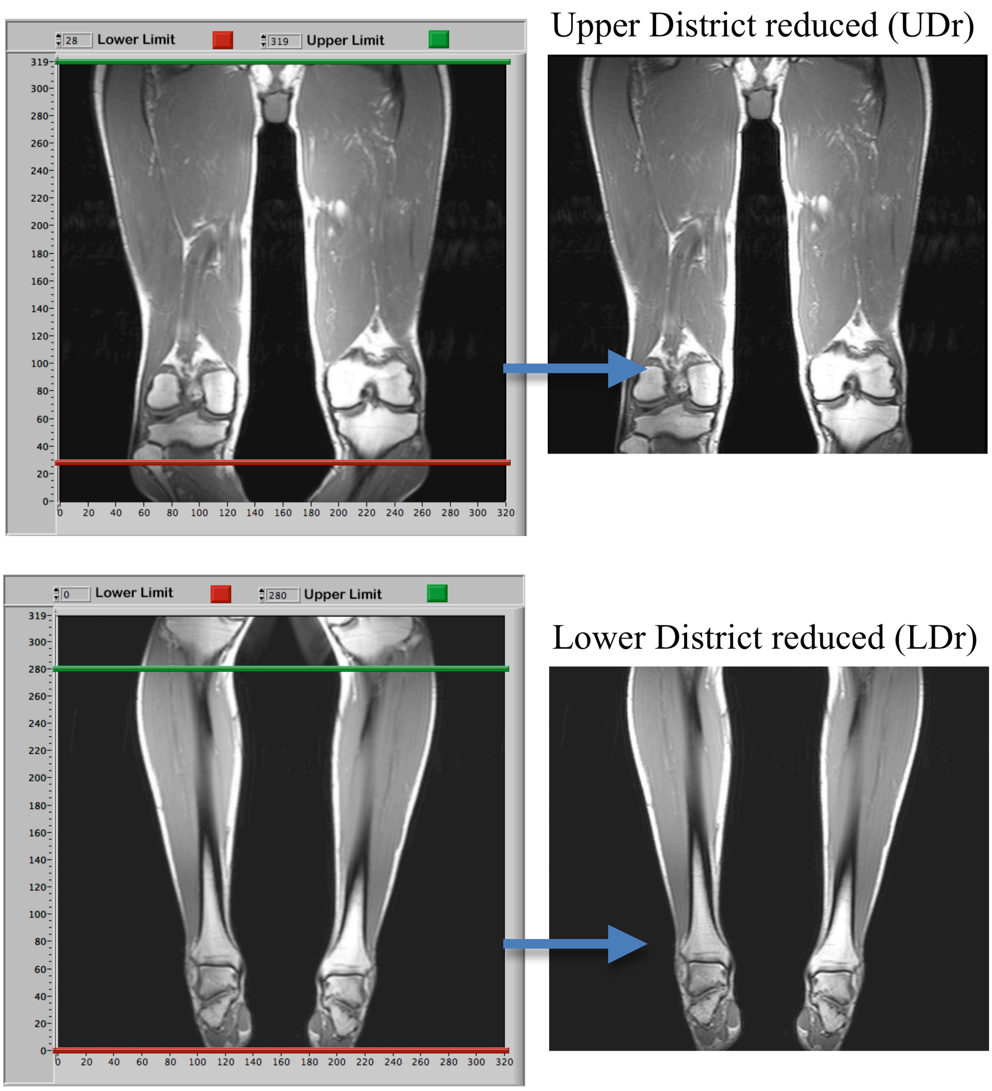

Figure 4.8: Reduction of the anatomical volume for the three acquired districts, PD, UP, and LD (A, B and C respectively. The new districts are indicated as PDr, UPr and LDr respectively.

We evaluated for every subject a single cross correlation value (**r**) for each district, and secondly a 'global' cross correlation value ($\mathbf{r_m}$) between the three districts (PDr, UPr and LDr).

$$r_m = \frac{r(PDr) + r(UDr) + r(LDr)}{3}$$

Results are presented in table 4.9. We performed a two-ways ANOVA (with a post-*hoc* Bonferroni correction). The dependent variable was (**r**), while the independent factors were running groups (OR, TR and TR) and anatomical regions (PDr, UDr and LDr). Results shown significant differences in **r** values, between PDr and UDr, and between PDr and LDr. The cross-correlation values (**r**), for the PDr, are statistically lower than the cross-correlation values (**r**) for UDr and LDr ($p < 0.05$), i.e. anatomical symmetry is higher in UDr and LDr. We didn't find any significance difference between the groups of subjects. We also evaluated differences between group of subjects for $\mathbf{r_m}$ cross-correlation value, (with one-way ANOVA), but we didn't find any significance.

Subject	r (PDr)	r (UDr)	r (LDr)	r_m	SD
OR1	n.a	n.a	n.a	n.a	n.a
OR2	0.741	0.788	0.836	0.788	0.047
OR3	0.927	0.882	0.838	0.882	0.044
OR4	0.723	0.877	0.909	0.836	0.099
OR5	0.699	0.839	0.726	0.755	0.075
OR6	0.831	0.827	0.880	0.846	0.029
OR7	0.606	0.833	0.848	0.762	0.136
Mean	**0.754**	**0.841**	**0.839**	**0.812**	
SD	**0.111**	**0.035**	**0.062**	**0.051**	
SR1	0.878	0.849	0.922	0.883	0.037
SR2	0.720	0.803	0.871	0.798	0.075
SR3	0.819	0.913	0.898	0.877	0.050
SR4	0.606	0.756	0.775	0.712	0.093
SR5	0.756	0.737	0.815	0.770	0.041
SR6	0.702	0.744	0.826	0.757	0.063
SR7	0.818	0.865	0.889	0.857	0.036
Mean	**0.757**	**0.810**	**0.857**	**0.808**	
SD	**0.091**	**0.068**	**0.053**	**0.066**	
TR1	0.785	0.810	0.818	0.805	0.017
TR2	0.785	0.779	0.805	0.790	0.014
TR3	n.a	n.a	n.a	n.a	n.a
TR4	0.826	0.866	0.890	0.861	0.033
TR5	0.794	0.835	0.784	0.804	0.027
Mean	**0.798**	**0.823**	**0.825**	**0.815**	
SD	**0.019**	**0.037**	**0.046**	**0.031**	
TOT MEAN	**0.766 ***	**0,824**	**0.843**	**0.811**	
TOT SD	**0.086**	**0.051**	**0.053**	**0.051**	

Table 4.9: ***Left Panel*****: Cross-correlation values for the three anatomical districts reduced (PDr, UDr and LDr), with their mean and standard deviation (SD). (*) = TOT MEAN of r(PDr) significantly lower than r(UDr) and r(LDr), (p <0.05).** ***Right Panel*****: 'Global' cross-correlation value (r mean) between districts.**

In the following sections we will investigate relationships between variables using Pearson's correlation coefficient. In particular we will correlate I) the three anatomical districts (PDr, UDr and LDr), II) kinematic ($\overline{SI}^x$, $\overline{SI}^y$, $\overline{SI}^z$ and GI) and anatomical indices, III) anatomical indices (PDr, UDr and LDr) and the cost of transport (C).

In table 4.10 we reported all the statistical results about the relationships between the analysed variables, each one with respective p-value and Pearson's correlation coefficient. In the next sections also, we will present a list of the most representative charts regarding the significant relationships between variables.

Correlations

		r (PDr)	r (UDr)	r (LDr)	rm	Age	$\overline{SI}$x	$\overline{SI}$y	$\overline{SI}$z	GI	C
r (PDr)	Pearson Correlation	1	.501*	.427	.871**	-.242	.651**	.110	-.094	.606**	.157
	Sig. (2-tailed)		.040	.087	.000	.349	.005	.675	.719	.010	.547
	N	17	17	17	17	17	17	17	17	17	17
r (UDr)	Pearson Correlation		1	.507*	.782**	-.287	.322	.003	.020	.357	-.114
	Sig. (2-tailed)			.038	.000	.263	.208	.990	.940	.160	.662
	N		17	17	17	17	17	17	17	17	17
r (LDr)	Pearson Correlation			1	-.748**	-.748**	.045	.103	.304	.046	.059
	Sig. (2-tailed)				.001	.001	.863	.694	.236	.860	.822
	N			17	17	17	17	17	17	17	17
rm	Pearson Correlation				1	-.485*	.487*	.095	.055	.473	.072
	Sig. (2-tailed)					.049	.048	.716	.834	.055	.785
	N				17	17	17	17	17	17	17
Age	Pearson Correlation					1	.099	-.276	-.303	.051	.188
	Sig. (2-tailed)						.686	.253	.207	.835	.442
	N					19	19	19	19	19	19
$\overline{SI}$x	Pearson Correlation						1	.186	.009	.992**	.005
	Sig. (2-tailed)							.447	.972	.000	.983
	N						19	19	19	19	19
$\overline{SI}$y	Pearson Correlation							1	.617**	.186	.105
	Sig. (2-tailed)								.005	.445	.668
	N							19	19	19	19
$\overline{SI}$z	Pearson Correlation								1	.012	.211
	Sig. (2-tailed)									.959	.385
	N								19	19	19
GI	Pearson Correlation									1	-.001
	Sig. (2-tailed)										.995
	N									19	19
C	Pearson Correlation										1
	Sig. (2-tailed)										
	N										19

*. Correlation is significant at the 0.05 level (2-tailed).

**. Correlation is significant at the 0.01 level (2-tailed).

Table 4.10: Total statistical correlation results between the analyzed variables. Data have been evaluated with SPSS statistics program (IBM company). Pearson Correlation coefficient is presented together with the relative p-value. Yellow squares indicate a p-value statistically significant. Bold box indicates a p-value really close to the significance.

4.4.1 Correlation between districts

Results about correlation between districts are shown in figure 4.9. The cross-correlation value for the Upper District reduced (UDr) is significantly correlated with the cross-correlation value of the Pelvis district reduced (PDr) and of the Lower District reduced (LDr), (p < 0.05). Also PDr and LDr seem to be positively correlated (see figure 4.9), even if not significantly. We can conclude therefore that the UDr anatomical symmetry influences positively the anatomical symmetry of the other two districts (PDr and LDr).

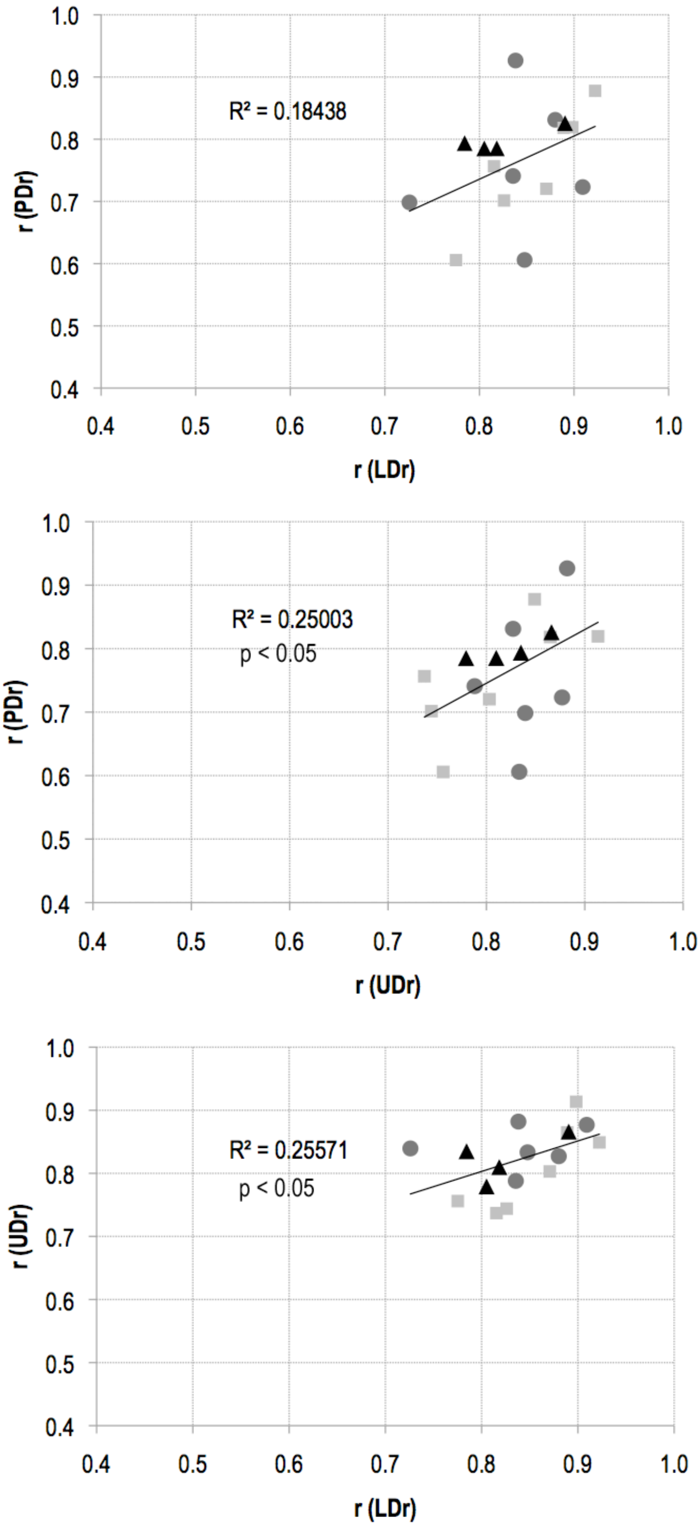

Figure 4.9: Relationships between the cross-correlation value r for the three anatomical districts with the correspondent Pearson coefficient and p-value.

4.4.2 Cross-Correlation values and kinematics

In order to compare the results about the anatomical symmetries with the ones regarding the kinematics, we performed a statistical correlation between the 'global' cross-correlation value $\mathbf{r_m}$ and the kinematics symmetry index. In particular we considered the values of *GI*, $\overline{SI^x}$, $\overline{SI^y}$ and $\overline{SI^z}$ averaged across the running speed, for each subject.

Results about the cross correlations are shown in the graphs of figure 4.10 and 4.11.

We didn't find significantly results for the correlation between $\mathbf{r_m}$ and *GI*, even if the *p*-value is very close to the significance threshold. By observing the scatter plot of figure 4.10, we can deduce that the two considered parameters are positively correlated, maybe not significantly because of the poor number of subjects.

As far as the single symmetry indices are concerned (figure 4.11), we notice that the only significant correlation we obtained is the ones between the mean cross correlation value $\mathbf{r_m}$ and the single symmetry index in forward direction, $\overline{SI^x}$.

Considering this last statistical results we can say for the three groups of subjects analyzed that the more the subject is anatomically symmetrical, the more he can run symmetrically in the forward (*x*) direction.

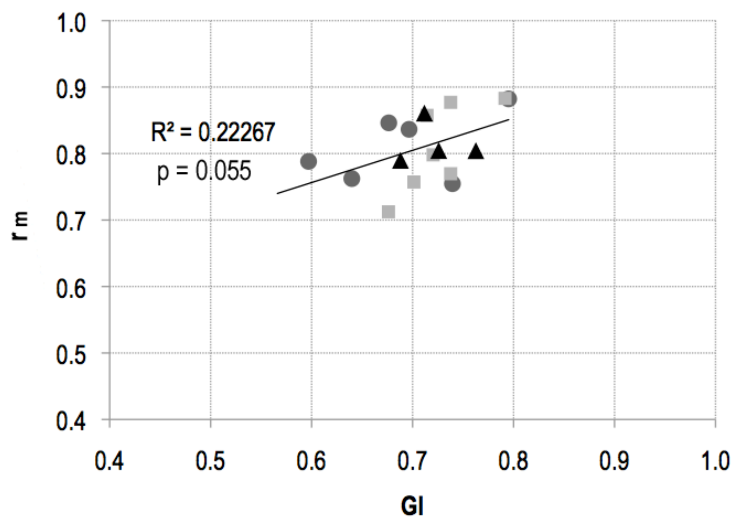

Figure 4.10: The Global Index *GI* is plotted against the Mean Cross-correlation value. We used solid grey circles for OR, solid grey squares for SR and solid black triangles for TR. The Pearson coefficient and the p-value are very close to the significance threshold. $\mathbf{r_m}$ seems to be positively correlated with the Global Symmetry Index.

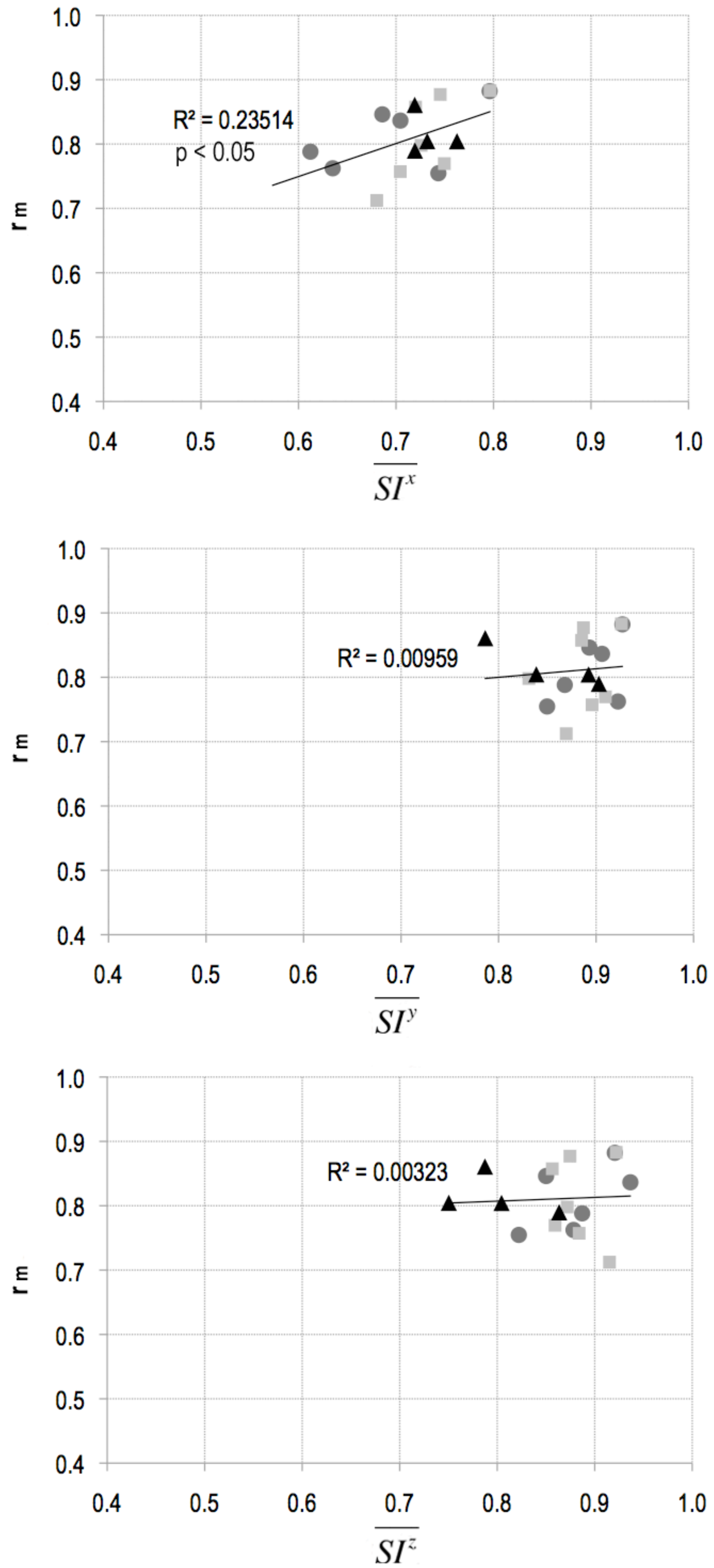

Figure 4.11: Relationships between the cross-correlation mean value and the three single symmetry indices, with the relative R^2 value and p-value when < 0.05

4.4.3 Cross-correlation values and Cost of Transport

Also for the cost of transport we performed a statistical correlation between variables. The considered parameters were the 'global' cross-correlation value **rm** and the cost of transport C. In particular we considered the mean cost of transport value, averaged across the running velocity for each subject.

Results are shown in figure 4.12, with no significantly relationship found between the two variables.

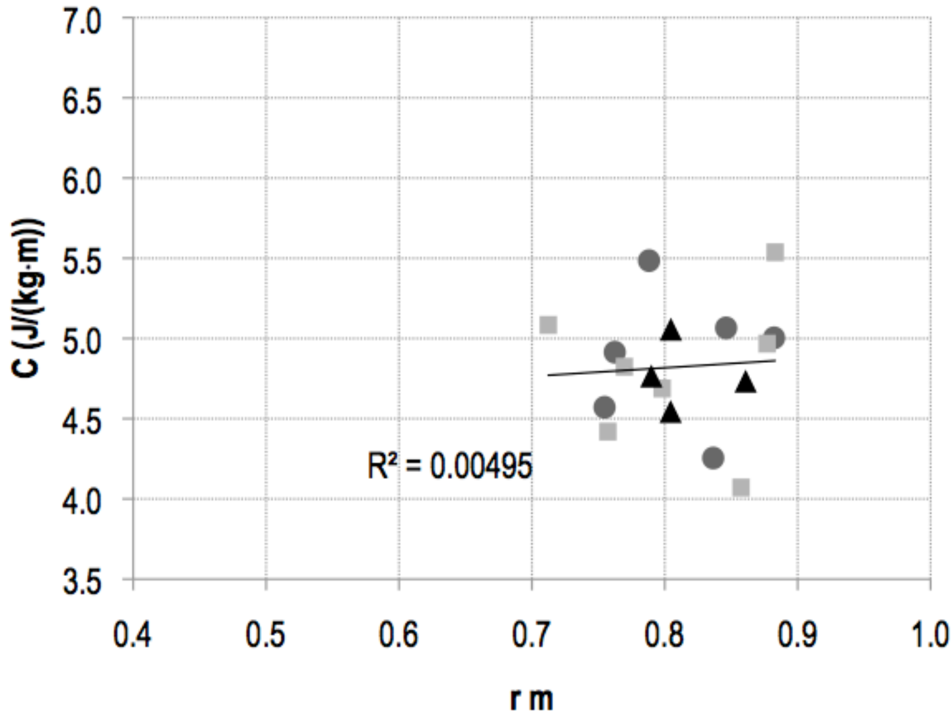

Figure 4.12: Cost of Transport plotted against the 'global' cross-correlation value rm

Chapter 5

DISCUSSION

In this chapter we will evaluate the outputs of this project, by comparing the obtained results with the expected hypotheses and with other studies. Finally, the limits of the present investigation and recommendations for further works will be proposed.

5.1 Subjects and the Cost of Transport

The main aim of our project was to answer to a series of questions, regarding the possible relationships among the energetic cost of transport, the dynamical symmetry of the BCOM displacement in running and the anatomical/structural symmetry of the lower limbs. Our hypothesis was inspired by the engineering of motor vehicles, where a structural symmetry could both influence the vehicles stability and keep low the fuel consumption. Also some works performed by Manning at the end of the 20^{th} century on horses (Manning & Ockenden 1994; Manning & Pickup 1998), suggested the possible relationships between body symmetry and performance during races.

Differently from previous studies concerning symmetry only in some anatomical features or in some specific biomechanical variables, we compared the symmetry of the whole limb anatomy and of running kinematics and evaluated their relationship with the cost of transport and the performance. In addition, we conducted that analysis in three groups of differently trained athletes.-Measuring the metabolic Cost of transport at incremental running velocity we obtained the graph of figure 4.5, (chapter 4); the energy cost values seems to be independent of speed, for each running group, as already widely demonstrated in literature (Margaria, Cerretelli 1963), (see chapter 2).

Among all groups, we didn't find statistical significant differences in C. It is possible, though, that the different subjects groups were characterized by a quite high similarity in training level. We have to consider that our study was a cross-sectional study similarly to many others, in general reporting no training effect on C (Bourdin, Pastene 1993; Dolgener 1982; Margaria, Cerretelli 1963; McGregor, Busa 2009; Slawinski & Billat 2004). Maybe a longitudinal experimental design, considering a homogeneous group of subjects analysed before and after a training period, could either identify statistical differences.

Differently, for the Heart Rate that better reflects metabolic power, we found significant differences among groups of subjects, in particular TR had always higher HR values than SR and OR. HR increases linearly and significantly with the running velocity for all the group of subjects. Differences were found also between groups of subject in $\dot{V}O_{2E}$ e and $\dot{V}O_{2\max E}$. In particular OR have lower $\dot{V}O_{2E}$ and $\dot{V}O_{2\max E}$, compared to the SR and TR. In fact, according to the literature, the principal features of the cardiovascular responses to training include an increase in maximal oxygen uptake, stroke volume and cardiac output with a decreasing of the maximal Heart Rate (Cerretelli 2001).

5.1.1 Cost of Transport and Anatomical Symmetries

In order to find correlations between C and the anatomical symmetries we considered the 'global' cross-correlation value **rm**, as anatomical index, and the mean cost of transport value, averaged across the running velocity for each subject, but no significantly relationship was found between the two considered variables (figure 4.12).

This result is confuting our beginning hypothesis regarding possible relations between structural asymmetry and energetic consumption, and also brings a different message if compared with the study of Manning regarding the individual performance. But we need to formulate some considerations.

While Manning in his works considered the Fluctuant Asymmetry, (FA) as anatomical index and he limited his investigation to measure some anthropometric trait in the right and left side of the individuals, in our work we evaluated a global structure asymmetry, taking in account muscles, bones and the surrounding tissues of the lower limbs. Also we measured the legs length of each subject in order to evaluate the absolute discrepancy (Δ_{length}) between right and left leg. Results are shown in Table 5.1 with mean and SD for each group of subject.

In chapter 2, we referred about experiments regarding discrepancies in the lower limbs, showing the relationship between structural asymmetry and locomotion asymmetry, but there was no correlation with the energetic cost (Boyadjian, Marin 1999; Lund 1930; Souman, Frissen 2009).

In 2001, Gurney presented a study about the effect of limb-length on gait economy. He showed that some physiological parameter like oxygen consumption and the rate of perceived exertion (Heart Rate) were greater with a 2 cm limb-length discrepancy, see their figure 2.7 A and 2.7 B (Gurney, Mermier 2001).

The values reported in Table 5.1 indicate that the average value of discrepancy for the subjects analyzed in this thesis was always lower than the threshold of 2 cm established from Gurney in order to find significant difference both in HR and in some energetic parameter as the $\dot{V}O_{2E}$. In fact, as in the work of Gurney et al., we didn't find any relationships between HR and **rm** and between $\dot{V}O_{2E}$ and **rm** as we shown in figure 5.1 A and 5.1 B.

This could be a possible explanation of the lack of relations between Cost of Transport and anatomical structure symmetry, even if the reasons for these results can be different.

	Right Leg Length	**Left Leg Length**	Δ_{length}
Subject	**cm**	**cm**	**cm**
OR1	82.24	83.64	1.40
OR2	82.35	80.03	2.32
OR3	86.80	86.77	0.04
OR4	79.93	78.65	1.28
OR5	78.10	78.65	0.55
OR6	88.15	87.10	1.05
OR7	84.01	85.14	1.13
Mean	**83.08**	**82.85**	**1.11**
SD	**3.57**	**3.71**	**0.71**
SR1	81.51	79.56	1.95
SR2	88.48	86.54	1.94
SR3	81.56	81.33	0.23
SR4	76.99	77.37	0.38
SR5	87.33	86.97	0.36
SR6	85.84	84.02	1.82
SR7	86.43	85.48	0.95
Mean	**84.02**	**83.04**	**1.09**
SD	**4.12**	**3.69**	**0.80**
TR1	76.37	74.35	2.02
TR2	83.61	80.81	2.80
TR3	87.70	88.60	0.90
TR4	93.39	92.73	0.66
TR5	87.78	87.50	0.28
Mean	**85.77**	**84.80**	**1.33**
SD	**6.30**	**7.24**	**1.04**

Table 5.1: Right and Left Leg Length for the three groups of subjects, evaluated starting from the kinematic registration. No difference between groups of subject was found.

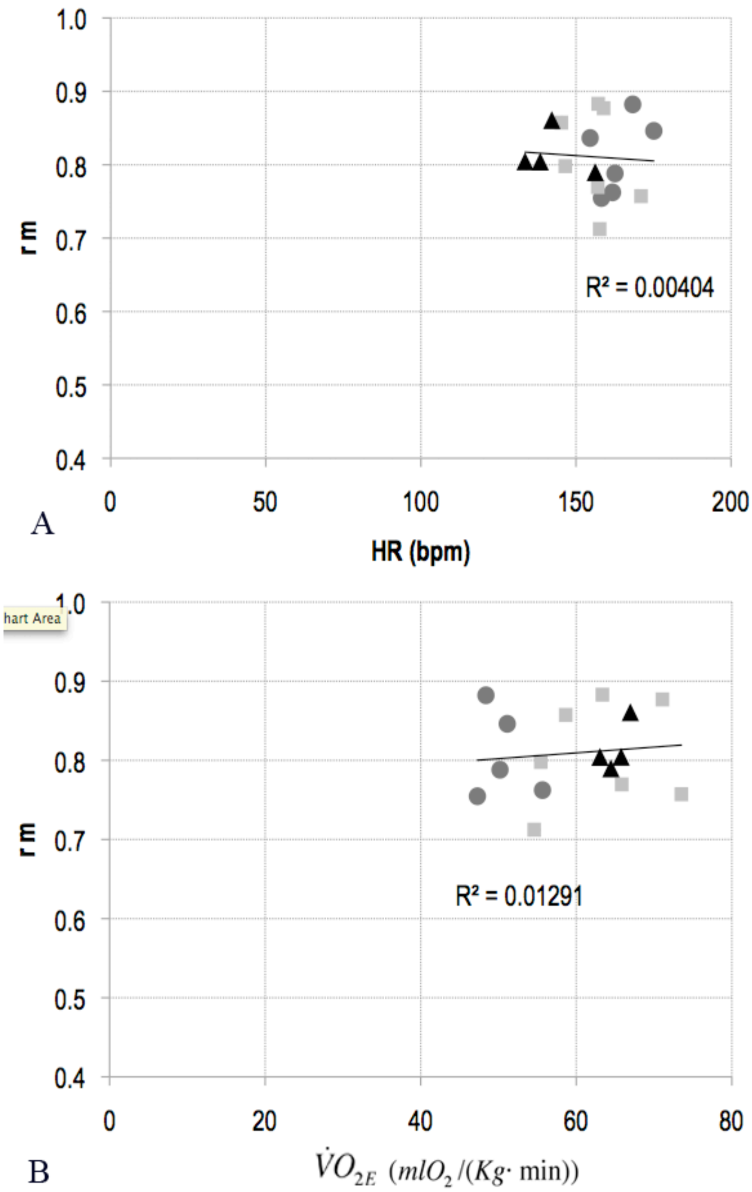

Figure 5.1: Relationships between the mean cross correlation value rm with the Heart Rate (Upper graph) and the estimated Oxygen consumption (Lower Graph). No significant relationship was found between variables. We used solid grey circles for OR, solid grey squares for SR and solid black triangles for TR, in order to distinguish the three different subjects categories.

We can suppose also, that the number of participants was low in comparison with other studies regarding anatomical symmetry and performance (Manning & Ockenden 1994; Manning & Pickup 1998). Furthermore we considered for our analysis not a homogenous group of subject. SR and TR lower limbs are more prejudiced and susceptible compared with the OR, because of the training. The prolonged exercise could have changed the lower limbs structure. Muscles mass changes and joints overuse could have induced asymmetries between right and left leg in TR and SR but not in OR. The absence of correlation between anatomical symmetry and energetic cost could mean that the anatomical asymmetry was not so great as the leg discrepancies showed by Gurney, or that our body can compensate for imperfections in the mechanics of our legged system, with no influence on the metabolic cost of transport also because as we saw in the literature all the individuals are characterized by a physiological asymmetry in the behavior of the lower limbs (Sadeghi, Allard 2000). For these reasons, both for Skilled and Top Runners, and for Occasional Runners we didn't observe any change in the cost of transport related to the possible anatomical symmetries.

As we said before, a longitudinal study performed on a group of homogenous subjects, could better detect potential differences in the Cost of transport.

5.1.2 Cost of Transport and Kinematics

No significant relationships were found between $\overline{SI}$ in the three different directions and the Cost of transport as shown in figure 4.7, in chapter 4. Also no significant relationship was found between C and the global symmetry index (GI), and between C and $\overline{\Delta}_x SD$, $\overline{\Delta}_y SD$ and $\overline{\Delta}_z SD$.

The reasons of the lack of correlation between the energetic cost of transport and the dynamical symmetry indices could be the same assumed in the previous section for the cost of transport, but also a further discussion will be presented in the next paragraph.

5.2 Kinematics

In this paragraph we will discuss the displacement of the BCOM and the indices used to quantify its dynamical asymmetries.

Results about symmetry single indices are summed in figure 4.1 and 4.2 of chapter 4. Values of symmetry for $\overline{SI^x}$ (forward direction, x) were always lower compared with the one in lateral (z) and vertical (y) direction, independently from the running speed. Also, $\overline{SI^y}$ and $\overline{SI^z}$ seemed to be positively correlated. That mean that in general it is simpler to run maintaining a symmetrical displacement of the BCOM in vertical and lateral direction rather in forward direction; maybe it could be related to the constrain of running on the treadmill. In fact the values of *dx*, *dy* and *dz*, evaluated in chapter 3 in order to calculate the Global Symmetry Index were significantly higher for the forward direction x, compared with the other two directions. The lowest values were found for the vertical displacement.

In forward direction, also, we observed that the group of the occasional runners, (OC) presented lower values for the single symmetry index compared to y and z directions and also, even if not significantly, $\overline{SI^x}$ seems to decrease with the running speed for OR. These results could suggest that the more trained subjects (SR and TR) were able to maintain high symmetry during fast running. Differently in the lateral direction (z) TR shown $\overline{SI^z}$ values significantly lower than OR, and the Global Index-follows the same behavior of $\overline{SI^x}$.

Statistical results were showed in figure 4.3 A and B, in particular OR had a GI significantly lower than SR and TR for each velocity. Also, the GI for OR seems to decrease with the increasing running velocity, even if not significantly. At high running velocity, it seems more difficult to keep a symmetric locomotion; the step frequency grows up and, also, the physical effort could induce in the subjects a sense of fatigue that avoid them to maintain a symmetrical gaits.

5.2.1 $\overline{\Delta_x}$, $\overline{\Delta_y}$ and $\overline{\Delta_z}$ variability

The program evaluating the Lissajous Contour calculated also the average distances of the gaps to be filled between the start and the end 3D BCOM trajectory, in local coordinates, of each stride ($\overline{\Delta}_x$, $\overline{\Delta}_y$ and $\overline{\Delta}_z$). Their variability is represented by the standard deviation of these parameters ($\overline{\Delta}_x SD$, $\overline{\Delta}_y SD$ and $\overline{\Delta}_z SD$). The higher was the SD value, the lower was the precision in the starting and ending 3D point for each stride, i.e. the dynamical variability increases with the increasing standard deviation values. To evaluate the effect of the running speed on the $\overline{\Delta}_x$, $\overline{\Delta}_y$ and $\overline{\Delta}_z$ variability, we correlated running velocity with the SD value for $\overline{\Delta}_x$, $\overline{\Delta}_y$ and $\overline{\Delta}_z$ (mm), for each running group as we showed in figure 4.4, in chapter 4.

While TR decreased their variability with the increasing running speed (in z and x direction), for OR and SR the variability increased significantly with their velocity (vertical direction y). Thus we could conclude that training can be useful to improve the subject's capacity of running consistently.

5.3 Anatomical symmetry

Results about anatomical/structural symmetries are represented by the cross-correlation value **r** (for single anatomical districts) and $\mathbf{r_m}$ (for the 'global' symmetry). These two indices can assume a range of values between -1 and 1, depending upon the similarity of the 3D analyzed volumes where a value of 1 indicates an exact matching of the right side with the left side. Anatomical symmetry results are summarized in table 4.10. In this section we will discuss the main significant results regarding the anatomical/structural symmetry and its practical effects.

5.3.1 Anatomical Symmetry is independent from the investigated district and decreases with age

As shown in figure 4.9, the cross-correlation values evaluated for the three analysed anatomical districts (Pelvis district reduced (PDr), Upper District reduced (UDr) and Lower District reduced (LDr)) seem to be positively correlated among each other. In particular the significant correlation between UDr and LDr and between UDr and PDr, supports the hypothesis that a subject symmetry (or asymmetry) would be independent from a specific anatomical district.

This finding could be very useful for future developments of this study. If the symmetry of the different anatomical districts is independent from the evaluated region, the number of possible MR images acquired could be reduced, minimizing in this way the acquisition times and the costs. Analysing only one district also would be useful in order to focalize the attention in specific anatomical structures. For example, increasing the MR images resolution it would be possible to separate the different tissues and also compare single structures as bones or muscles.

The second important result regards the correlation between anatomical symmetry and the subjects' age. In fact, as indicated in table 4.10, both the cross-correlation value for the PDr and the mean cross-correlation value $\mathbf{r_m}$ are significantly (and negatively) correlated with the subject's age (see also figure 5.3).

We know from literature that muscles strength (Frontera et al. 2000) and maximal shortening velocity (D'Antona et al. 2003), decrease with age. Also other studies, directly measuring power output in lower limbs showed that the generated power by the lower limbs muscles is lower for older subjects. In addition, during dynamic contractions, the asymmetry of the generated power in right and left legs was greater for older subjects compared to the younger ones (Perry et al. 2007). Furthermore, as already mentioned, the prolonged usage could cause some wearing process and change the lower limbs structure. Muscles mass changes and joints overuse could have induced asymmetries between right and left legs during the years, or also the effect of asymmetry could be due to a bad posture of the subject. No differences were found between groups of subjects. It could be interesting to perform a longitudinal study with a homogeneous group of subjects, or to plan anatomical MRI analysis on the same subject in different growing phases to reduce the bias due to the inter-subject variability.

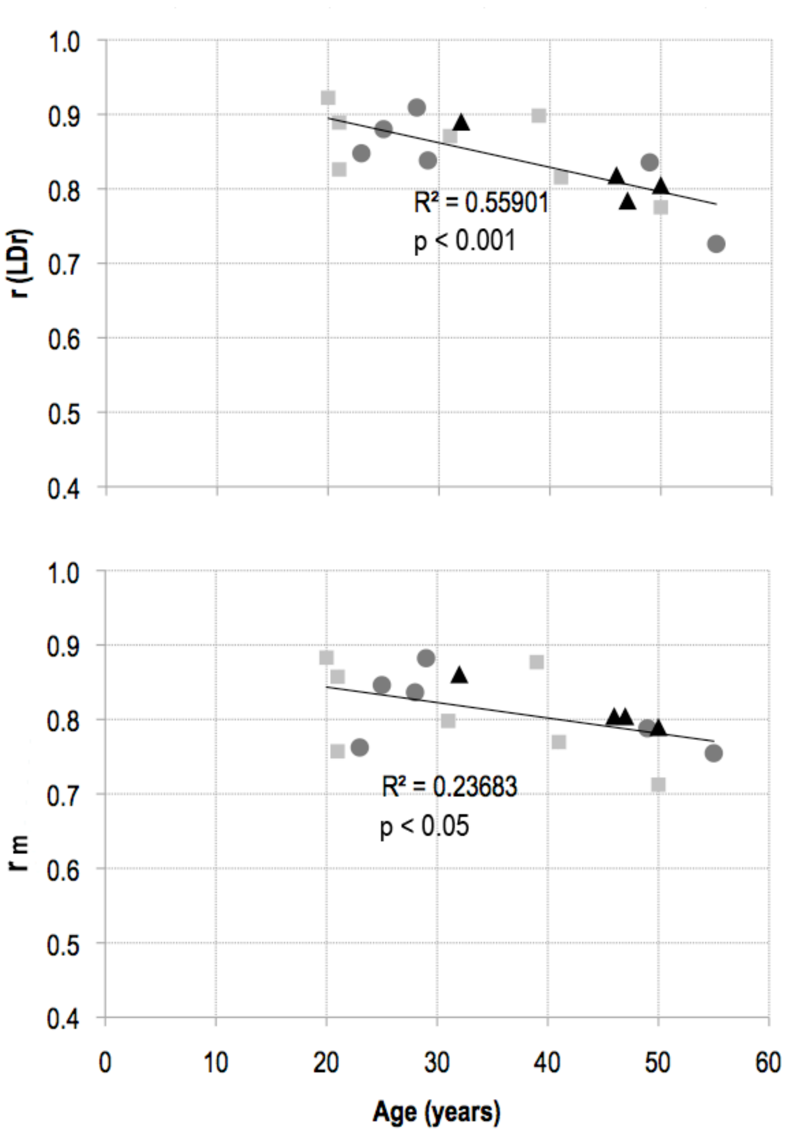

Figure 5.3: Negative correlation between Anatomical symmetry indices and subjects' age. We used solid grey circles for OR, solid grey squares for SR and solid black triangles for TR, in order to distinguish the three different subjects categories.

5.3.2 Anatomical symmetry and kinematics

A statistical correlation between the ‘global’ anatomical cross-correlation value $\mathbf{r_m}$ and the kinematics symmetry indices *GI*, $\overline{SI^x}$, $\overline{SI^y}$ and $\overline{SI^z}$ was performed.

Results about the cross correlations are shown in the graphs of figure 4.10 and 4.11 in chapter 4 and they shown a positive correlation between the anatomical symmetry index and the dynamical symmetry indices. In particular significant results were found for the forward direction ($\overline{SI^x}$).

We didn’t find a significant correlation between $\mathbf{r_m}$ and *GI*, even if the *p*-value is very close to the significance threshold (0.055). The two considered parameters are positively correlated on the scatter plot of figure 4.10, with the lack of significance possibly due to the low sample size.

We can assume for the three groups of subjects analyzed that the more the subject is anatomically symmetrical, the more he can run symmetrically in the forward (x) direction. This finding is in accordance with our initial hypothesis comparing human body and motor vehicles. Similarly to cars, where structural symmetry can help to maintain driving stability, with no tendency towards veering when travelling on a flat terrain, symmetrical anatomical structure could help humans (and animals) to maintain the desired direction during running.

5.3.3 Anatomical cross-correlation values and Cost of Transport

Results regarding the cross-correlation values and the energetic cost have been already discussed in section 5.1.1. We can add also that maybe our experiments were performed in a too much shorter running time. Indeed, some physiological differences could occur after a more prolonged running time so that only few minutes of running could not be a time enough to determine evident discrepancies as a function of running ability. A suggestion for the next development of this study is to investigate a single speed for a longer duration to better isolate and investigate physiological adjustments in different trained runners.

5.4 Conclusion and Further development

In the introduction of this work, we listed a group of questions regarding the possible interactions between anatomical symmetries, dynamical symmetries and the energetic Cost of Transport in human running. These questions, arising from to the world of the motor vehicles and from previous literature, found some answers with the results obtained in this work.

The human body and the mechanical vehicle seem to have some similarity regarding the structure stability. In a car, wheel balance/alignment and homogeneous tyre wearing, is necessary in order to maintain driving stability and reduce the fuel consumption. Also in the human body, a structural/anatomical symmetry is accompanied by a high level of dynamical symmetry, during running locomotion, but, differently from the motor vehicles, the energetic consumption doesn't change with the level of anatomical and dynamic symmetry. Furthermore, training seems to be an important element in the stability and in the dynamical symmetry of running, even if no metabolic benefit was found.

As we know from literature, the asymmetrical behaviour of the lower limbs reflect natural functional differences between the lower extremities (Sadeghi, Allard 2000). It is possible that some physiological adaptations of the human machinery compensate for small imperfections in the mechanics of our legged system, with no influence on the metabolic cost of transport, while larger anatomical imperfection, like length leg discrepancy higher than 2cm (Gurney, Mermier 2001) or a body mass not uniformly distribuited like a load carried on the back in a rucksack (Saibene & Minetti 2003), or also prosthesis and support (Mattes, Martin 2000) for pathological situations, could have a significant effect on the energetic cost of transport.

Even if we think that this work brings new insights in the study of symmetry in locomotion, further developments could be carried out in order to deepen the understanding of the results already obtained. The number of partecipans should increase and a longitudinal work could be carried out in order to find out differences between groups (for example, before and after a training period or in different period of the individual growing).

In addition, it would be important to use other physiological and biomechanical parameters, which provide information about both the human symmetry, and the metabolic profile of the subjects. For example, as suggested by Manning (Manning & Pickup 1998), the measured $\dot{V}O_{max}$, could be a good estimator of the considered relationships. Also muscle power appears to be a good indicator of a person's ability both to propel the body and to control balance during gait (Sadeghi, Allard 2000).

Appendices

APPENDIX A: *The Lissajous Contour*

As we saw in chapter 3 (section 3.3.2), the individual three-dimensional trajectory of the BCOM while moving on a treadmill, is a periodic function, mathematically described by harmonics characterizing the Digital Locomotory Signature. A close loop can represent this trajectory, i.e. the Lissajous *contour*, following the same pattern at each stride.
In Mathematics, Lissajous *contours* (Emmerton 1986), are a family of curves described by the parametric following equations:

$$x(t) = a\cdot(\cos\omega_x t - \varphi_x)$$
$$y(t) = b\cdot(\cos\omega_y \mathrm{t} - \varphi_\mathrm{x})$$

which describe complex harmonic motion; sometimes also written in the forms:

$$x(t) = a\cdot(\sin\omega t + \varphi)$$
$$y(t) = b\cdot(\sin t)$$

where *A* and *φ* are the coefficient amplitude and the phase, respectively. The appearance of the curve is highly sensitive to the ratio *a*/*b*. For a ratio of 1, the figure is an ellipse, with special cases including circles (a = b; φ = π/2 radians) and lines (φ = 0), (see figure A3).
Another simple Lissajous figure is the parabola (a/b = 2; φ = π/2). Other ratios produce more complicated curves, which are closed only if *a*/*b* is rational. See Figure A1, and A2.

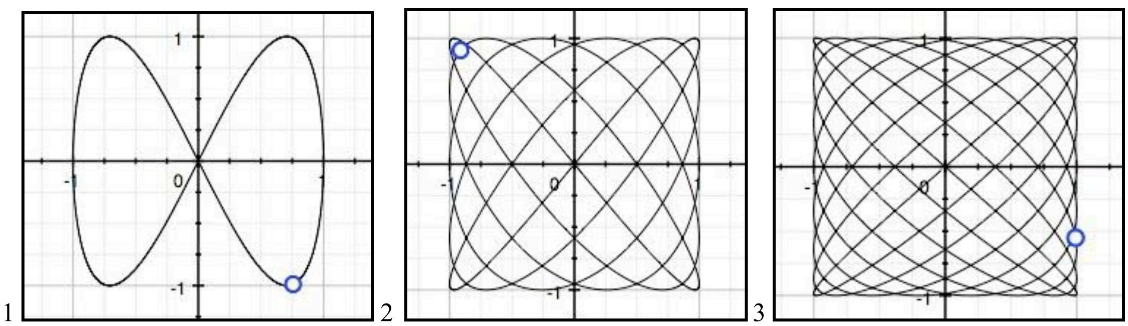

Figure A1. Some simple Lissajous curves in 2D; respectively in panel 1, 2, 3, *a* is 1, 5 and 9 and *b* is 2, 6 and 8.

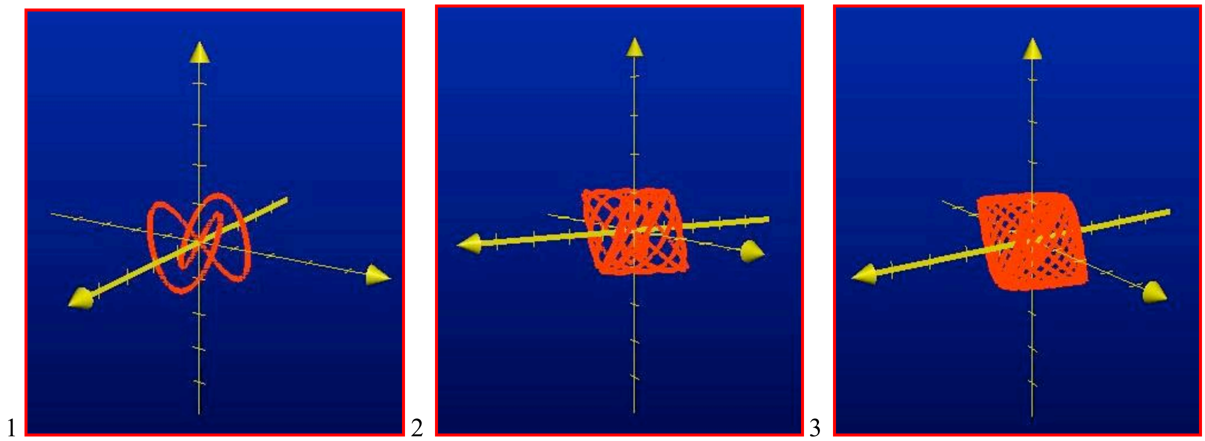

Figure A2. Some simple Lissajous curves in 3D. Respectively in panel 1, 2, 3, *a* is 1, 5 and 9 and *b* is 2, 6 and 8.

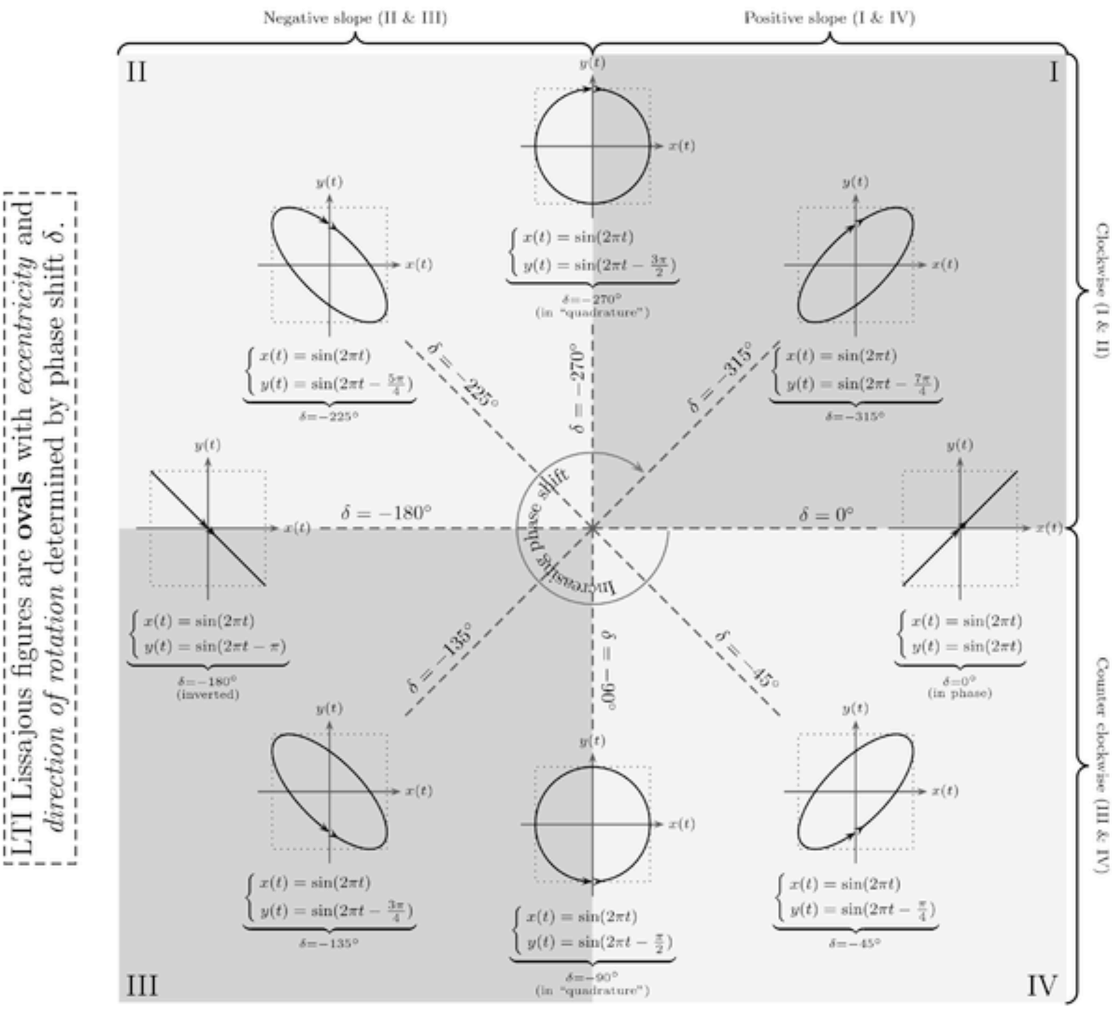

Figure A3: Examples of different *Lissajous* contourns when a=b. The figure summarizes how the Lissajous figure changes over different phase shifts.

APPENDIX B: *The Fouries analysis*

The mathematics of Fourier analysis has been used for many years to study physical phenomena coming from a wide variety of scientific and engineering fields. The theory of Fourier series truly began with the profound work of Fourier on heat conduction at the beginning of the 19th century. Fourier in his "*Théorie analytique de le chaleur*" dealt with the problem of describing the evolution of the temperature of a thin wire in a spatial direction and in time. He proposed that the function of the temperature could be expanded in a series of *sine* functions. The Fourier sine series, so defined in the 19th century, was a special case of a more general concept: the Fourier series for a *periodic function.*

Periodic functions arise in the study of wave motion, when a basic waveform repeats itself periodically. In mathematics, a periodic function is a function that repeats its values in regular intervals or periods. The most important examples are the trigonometric functions, which repeat over intervals of length 2π. Also the individual three-dimensional trajectory of the BCOM while moving on a treadmill is a periodic function and we exploited Fourier analysis in order to describe the locomotion signature of the BCOM.

Considering a function f(t), it is said to have a period T, if $f(t + T) = f(t)$ for all t.

By forcing all the cycle periods to range between 0 and 2π, the function f (t), will have a period T of 2π, and its Fourier series will be In other words, the technique of Fourier analysis, which is only valid for periodic (cyclic) functions, involves the derivation of a series of sine and cosine terms to represent the frequency content of a signal. However, a non-periodic signal can be numerically converted to a periodic signal, and subjected to a Fourier analysis.

$$f(t) = a_0 + \sum \left(a_i \cos \frac{2\pi i}{T} t + b_i \sin \frac{2\pi i}{T} t \right)$$

with a_0, a_i and b_i defined by the integrals

$$a_0 = \int \left(y(t) \cos \frac{2\pi i}{T} t \cdot dt \right)$$

$$a_i = \frac{2}{T} \int \left(y(t) \cos \frac{2\pi i}{T} t \cdot dt \right)$$

$$b_i = \frac{2}{T} \int \left(y(t) \sin \frac{2\pi i}{T} t \cdot dt \right)$$

In other words, the technique of Fourier analysis, which is only valid for periodic functions, involves the derivation of a series of sine and cosine terms to represent the frequency content of a signal (see figure B1). However, a non-periodic signal can be numerically converted to a periodic signal, and subjected to a Fourier analysis.

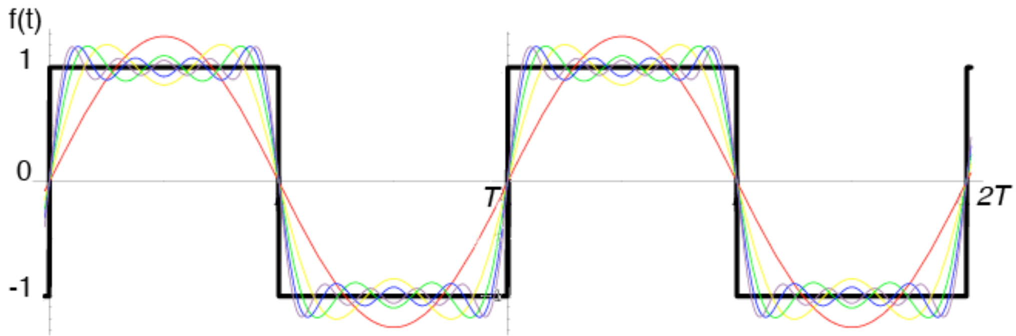

Figure 1B: An example of Fourier analysis applied on a square wave: the original periodic signal *f* (t) is decomposed in a sum of sinusoids with different frequency. The sum of the different trigonometric function (colored signals), estimates the original square waveform (black signal).

All these coefficients are defined in the range from -T/2 to T/2. The absolute value of each coefficient reflects its importance in determining the over-all shape of the original waveform. Thus, the larger the value of the coefficient, the more effect it has in determining the shape of the waveform. The fundamental frequency represents the single cosine + sine term, that best describes how the signal varies during one cycle:

$$f(t) = a_1 \cos \frac{2\pi}{T} t + b_1 \sin \frac{2\pi}{T} t$$

where a_1 and b_1 are the fundamental cosine and sine frequency coefficients, respectively. The sine coefficients give the magnitudes of the waveforms that complete all the cycles during the movement and oscillate about the mean of the measurements, while the cosine coefficients give the magnitudes of waveforms that complete all the cycles during the movement, 90 degrees out of phase with the corresponding sinusoidal waveforms but otherwise identical in shape. Multiples of the fundamental frequency are referred to as harmonics:

$$f(t) = a_i \cos \frac{2\pi i}{T} t + b_i \sin \frac{2\pi i}{T} t$$

where a_n and b_n are the n derivative cosine and sine frequency coefficients. Once the fundamental frequency has been determined, the curve-fitting procedures are then used to determine the size of the respective harmonics that are needed to approximate the signal. In general, it is necessary to scale the contribution of each harmonic to the function. This contribution decreases as harmonic number increases for human movement; and it is weighted by means of a coefficient.

Polar form: It is also possible to mathematically represent the Fourier Series of a periodic function in a polar form, as:

$$f(t) = C_0 + C_n \sin(t + \varphi_n)$$

where C_0 represents the equivalent of a_0 (the eventual constant term); C_n and φ_n are respectively the coefficients harmonics (amplitudes) and the phases of the function, instead of a_i and b_i Fourier Series coefficients. This is the mathematical form we used to fully describe the three-dimensional displacement of the BCOM:

$$x(t) = Ax_1 \sin(t + \varphi_1) + Ax_2 \sin(t + \varphi_2) + Ax_3 \sin(t + \varphi_3) + Ax_4 \sin(t + \varphi_4) + Ax_5 \sin(t + \varphi_5) + Ax_6 \sin(t + \varphi_6)$$

$$y(t) = Ay_1 \sin(t + \varphi_1) + Ay_2 \sin(t + \varphi_2) + Ay_3 \sin(t + \varphi_3) + Ay_4 \sin(t + \varphi_4) + Ay_5 \sin(t + \varphi_5) + Ay_6 \sin(t + \varphi_6)$$

$$z(t) = Az_1 \sin(t + \varphi_1) + Az_2 \sin(t + \varphi_2) + Az_3 \sin(t + \varphi_3) + Az_4 \sin(t + \varphi_4) + Az_5 \sin(t + \varphi_5) + Az_6 \sin(t + \varphi_6)$$

where x(t), y(t) and z(t) constitute the mathematical polar forms (or harmonics) of Fourier Series in forward, vertical and lateral direction, respectively; A represents the amplitude coefficient and φ the phase coefficient, in each movement direction.

We decided to truncate the Fourier Series to the 6th harmonic according to Parseval's Theorem

- similar equations characterize well enough the real pattern of human locomotion;
- if this approach will be further used, the same Fourier coefficients and phases will be calculated. This is set out in Fourier analysis
- coefficients past the sixth had very little influence of the final waveform. Moreover, it will be possible to add further harmonics without changing the values of the previous ones.

APPENDIX C: *Circular Statistics*

Averaging phases needs to be performed according to circular statistics (Batschelet 1981), to avoid, for instance, that extreme values within the $(0, 2\pi)$ interval, which represent similar phases, will result in an incorrect average of about π. Thus, we applied the following transformation:

$$A_{iR}^{x} = \sin\left(\phi_{iR}^{x}\right),\ B_{iR}^{x} = \cos\left(\phi_{iR}^{x}\right)$$
$$A_{iR}^{y} = \sin\left(\phi_{iR}^{y}\right),\ B_{iR}^{y} = \cos\left(\phi_{iR}^{y}\right)$$
$$A_{iR}^{z} = \sin\left(\phi_{iR}^{z}\right),\ B_{iR}^{z} = \cos\left(\phi_{iR}^{z}\right)$$

then the average values for the *n* strides were obtained as:

$$\overline{A}_{iR}^{x} = \frac{\sum_{j=1}^{n} A_{iR,j}^{x}}{n},\ \overline{B}_{iR}^{x} = \frac{\sum_{j=1}^{n} B_{iR,j}^{x}}{n}$$
$$\overline{A}_{iR}^{y} = \frac{\sum_{j=1}^{n} A_{iR,j}^{y}}{n},\ \overline{B}_{iR}^{y} = \frac{\sum_{j=1}^{n} B_{iR,j}^{y}}{n}$$
$$\overline{A}_{iR}^{z} = \frac{\sum_{j=1}^{n} A_{iR,j}^{z}}{n},\ \overline{B}_{iR}^{z} = \frac{\sum_{j=1}^{n} B_{iR,j}^{z}}{n}$$

From them the average 'relative' phases were calculated as:

$$\overline{\phi}_{iR}^{x} = ATAN\left(\overline{B}_{iR}^{x}, \overline{A}_{iR}^{x}\right)$$
$$\overline{\phi}_{iR}^{y} = ATAN\left(\overline{B}_{iR}^{y}, \overline{A}_{iR}^{y}\right)$$
$$\overline{\phi}_{iR}^{z} = ATAN\left(\overline{B}_{iR}^{z}, \overline{A}_{iR}^{z}\right)$$

Also phase variability needs to be calculated according to circular statistics (Batschelet 1981). For each single-sin harmonic of the 3 Fourier series the variables (radii):

$$r_{iR}^{x} = \left[\left(A_{iR}^{x}\right)^{2} + \left(B_{iR}^{x}\right)^{2}\right]^{1/2},\ r_{iR}^{y} = \left[\left(A_{iR}^{y}\right)^{2} + \left(B_{iR}^{y}\right)^{2}\right]^{1/2} \text{and } r_{iR}^{z} = \left[\left(A_{iR}^{z}\right)^{2} + \left(B_{iR}^{z}\right)^{2}\right]^{1/2}$$

are equal to 1 if there was no variability among phases, and to 0 if the averaged phases were uniformly distributed in the interval $(0, 2\pi)$. Then the phase SDs are computed as:

$$s_{iR}^{x} = \left[2\left(1 - r_{iR}^{x}\right)\right]^{1/2},\ s_{iR}^{y} = \left[2\left(1 - r_{iR}^{y}\right)\right]^{1/2} \text{and } s_{iR}^{z} = \left[2\left(1 - r_{iR}^{z}\right)\right]^{1/2}$$

The above procedure leads, for every experimental condition (speed/gait) and *n* strides, to average 3D Lissajous contours in the form of:

$$\bar{\hat{x}}(t) = \sum_{i=1}^{6} \bar{c}_{i}^{x} \sin(it + \bar{\phi}_{iR}^{x}),\ \bar{\hat{y}}(t) = \bar{a}_{0}^{y} + \sum_{i=1}^{6} \bar{c}_{i}^{y} \sin(it + \bar{\phi}_{iR}^{y}) \text{ and } \bar{\hat{z}}(t) = \sum_{i=1}^{6} \bar{c}_{i}^{z} \sin(it + \bar{\phi}_{iR}^{z})$$

where the symbol (¯) denotes the average of the predicted (^) value. This equation represent the 'digital locomotor signature', which contains general and individual features of a given gait condition.

References

Agostoni E. *Compendio di fisiologia della respirazione (Seconda Edizione)*. Raffaello Cortina Editore ed 1996.

Allen WK, Seals DR, Hurley BF, Ehsani AA, Hagberg JM. Lactate threshold and distance-running performance in young and older endurance athletes. *J Appl Physiol*. 1985: **58**: 1281-1284.

Ambrosini R, Wang P, O'Dell W. Computer-aided detection of metastatic brain tumors using automated three-dimensional template matching. *J Magn Reson Imaging*. 2010: **31**: 85-93.

Anderson FC, Pandy MG. Dynamic optimization of human walking. *J Biomech Eng*. 2001: **123**: 381-390.

Ardigo LP, Goosey-Tolfrey VL, Minetti AE. Biomechanics and energetics of basketball wheelchairs evolution. *Int J Sports Med*. 2005: **26**: 388-396.

Armitage M, Larkin D. Laterality, motor asymmetry and clumsiness in children. *Human Movement Science*. 1993: **12**: 155-177.

Arsenault AB, Winter DA, Marteniuk RG. Bilateralism of EMG profiles in human locomotion. *Am J Phys Med*. 1986: **65**: 1-16.

Batschelet E. *Circular statistic in biology*. Academic Press ed: San Diego, CA 1981.

Beneke R, Hutler M. The effect of training on running economy and performance in recreational athletes. *Med Sci Sports Exerc*. 2005: **37**: 1794-1799.

Billat VL, Flechet B, Petit B, Muriaux G, Koralsztein JP. Interval training at VO2max: effects on aerobic performance and overtraining markers. *Med Sci Sports Exerc*. 1999: **31**: 156-163.

Bourdin M, Pastene J, Germain M, Lacour JR. Influence of training, sex, age and body mass on the energy cost of running. *Eur J Appl Physiol Occup Physiol*. 1993: **66**: 439-444.

Boyadjian A, Marin L, Danion F. Veering in human locomotion: the role of the effectors. *Neurosci Lett*. 1999: **265**: 21-24.

Bramble D, Lieberman D. Endurance running and the evolution of Homo. *Nature*. 2004: **432**: 345-352.

Bransford DR, Howley ET. Oxygen cost of running in trained and untrained men and women. *Med Sci Sports*. 1977: **9**: 41-44.

Brown WM, Price ME, Kang J, Pound N, Zhao Y, Yu H. Fluctuating asymmetry and preferences for sex-typical bodily characteristics. *Proc Natl Acad Sci U S A*. 2008: **105**: 12938-12943.

Cavagna G. Symmetry and asymmetry in bouncing gaits. *Symmetry*. 2010: **2(3)**: 1270-1321.

Cavagna GA. The two asymmetries of the bouncing step. *Eur J Appl Physiol*. 2009: **107**: 739-742.

Cavagna GA, Legramandi MA, Peyre-Tartaruga LA. The landing-take-off asymmetry of human running is enhanced in old age. *J Exp Biol*. 2008: **211**: 1571-1578.

Cavagna GA, Saibene FP, Margaria R. MECHANICAL WORK IN RUNNING. *J Appl Physiol*. 1964: **19**: 249-256.

Cerretelli P. *Fisiologia dell'esercizio: Sport, Ambiente, Età, Sesso.* Società Editrice Universo ed. Roma 2001.

Chen TC, Nosaka K, Lin MJ, Chen HL, Wu CJ. Changes in running economy at different intensities following downhill running. *J Sports Sci*. 2009: **27**: 1137-1144.

Clunie D, A. *DICOM Structured Reporting*: PixelMed Publishing 2000.

Clunie DA. DICOM structured reporting and cancer clinical trials results. *Cancer Inform*. 2007: **4**: 33-56.

Conley DL, Krahenbuhl GS. Running economy and distance running performance of highly trained athletes. *Med Sci Sports Exerc*. 1980: **12**: 357-360.

Cotes J, Meade F. The energy expenditure and mechanical energy demand in walking. *Ergonomics*. 1960: **3**: 97-120.

Crowe A, Schiereck P, de Boer R, Keessen W. Characterization of gait of young adult females by means of body centre of mass oscillations derived from ground reaction forces. *Gait & Posture*. 1993: **1**: 61-68.

D'Antona G, Pellegrino MA, Adami R, Rossi R, Carlizzi CN, Canepari M, Saltin B, Bottinelli R. The effect of ageing and immobilization on structure and function of human skeletal muscle fibres. *J Physiol*. England, 2003:499-511.

Daniels J, Krahenbuhl G, Foster C, Gilbert J, Daniels S. Aerobic responses of female distance runners to submaximal and maximal exercise. *Ann N Y Acad Sci*. 1977: **301**: 726-733.

Daniels J, Oldridge N. Changes in oxygen consumption of young boys during growth and running training. *Med Sci Sports*. 1971: **3**: 161-165.

Daniels JT. A physiologist's view of running economy. *Med Sci Sports Exerc*. 1985: **17**: 332-338.

Dempster WT, Gabel WC, Felts WJ. The anthropometry of the manual work space for the seated subject. *Am J Phys Anthropol*. 1959: **17**: 289-317.

di Prampero P. *La locomozione umana su terra, in acqua, in aria. Fatti e teorie.* Edi-Ermes ed. Milano 1985.

di Prampero PE. The energy cost of human locomotion on land and in water. *Int J Sports Med*. 1986: **7**: 55-72.

di Prampero PE, Capelli C, Pagliaro P, Antonutto G, Girardis M, Zamparo P, Soule RG. Energetics of best performances in middle-distance running. *J Appl Physiol*. 1993: **74**: 2318-2324.

di Prampero PE, Salvadego D, Fusi S, Grassi B. A simple method for assessing the energy cost of running during incremental tests. *J Appl Physiol*. 2009: **107**: 1068-1075.

Doke J, Donelan JM, Kuo AD. Mechanics and energetics of swinging the human leg. *J Exp Biol*. 2005: **208**: 439-445.

Dolgener F. Oxygen cost of walking and running in untrained, sprint trained, and endurance trained females. *J Sports Med Phys Fitness*. 1982: **22**: 60-65.

Emmerton J. The pigeon's discrimination of movement patterns (Lissajous figures) and contour-dependent rotational invariance. *Perception*. 1986: **15**: 573-588.

Falls HB, Humphrey LD. Energy cost of running and walking in young women. *Med Sci Sports*. 1976: **8**: 9-13.

Fourier, J. *The Analytical Theory of Heat.* Dover, New York. 1955

Frontera WR, Hughes VA, Fielding RA, Fiatarone MA, Evans WJ, Roubenoff R. Aging of skeletal muscle: a 12-yr longitudinal study. *J Appl Physiol*. 2000: **88**: 1321-1326.

Gabbard C, Hart S. Probing Previc's theory of postural control (foot dominance). *Brain Cogn*. 1996: **30**: 351–353.

Gangestad SW, Thornhill R. Facial masculinity and fluctuating asymmetry. *Evolution and Human Behavior*. 2003: **24**: 231-241.

Gentry V, Gabbard C. Foot-preference behavior: a developmental perspective. *J Gen Psychol*. 1995: **122**: 37-45.

Grammer K, Thornhill R. Human (Homo sapiens) facial attractiveness and sexual selection: the role of symmetry and averageness. *J Comp Psychol*. 1994: **108**: 233-242.

Gurney B, Mermier C, Robergs R, Gibson A, Rivero D. Effects of limb-length discrepancy on gait economy and lower-extremity muscle activity in older adults. *J Bone Joint Surg Am*. 2001: **83-A**: 907-915.

Halling Thomsen M, Tolver Jensen A, Sorensen H, Lindegaard C, Haubro Andersen P. Symmetry indices based on accelerometric data in trotting horses. *J Biomech*. 2010: **43**: 2608-2612.

Herzog W, Nigg BM, Read LJ, Olsson E. Asymmetries in ground reaction force patterns in normal human gait. *Med Sci Sports Exerc*. 1989: **21**: 110-114.

Hildebrand M. Analysis of asymmetrical gaits. *Journal of Mammalogy*. 1977: **58**: 131-156.

Jones AM, Doust JH. A 1% treadmill grade most accurately reflects the energetic cost of outdoor running. *J Sports Sci*. 1996: **14**: 321-327.

Kaneko M. Mechanics and energetics in running with special reference to efficiency. *J Biomech*. 1990: **23 Suppl 1**: 57-63.

Karman T, Gabrielli G. What price speed? Specific power required for propulsion of vehicles. *Mech Eng*. 1950: **72**: 775-771.

Katsarkas A, Smith H, Galiana H. Postural instability on one foot in patients with loss of unilateral peripheral vestibular function. *J Vestib Res*. 1994: **4**: 153-160.

Knierim U, Van Dongen S, Forkman B, Tuyttens FA, Spinka M, Campo JL, Weissengruber GE. Fluctuating asymmetry as an animal welfare indicator -- a review of methodology and validity. *Physiol Behav*. 2007: **92**: 398-421.

Koopman B, Grootenboer HJ, de Jongh HJ. An inverse dynamics model for the analysis, reconstruction and prediction of bipedal walking. *J Biomech*. 1995: **28**: 1369-1376.

Lake MJ, Cavanagh PR. Six weeks of training does not change running mechanics or improve running economy. *Med Sci Sports Exerc*. 1996: **28**: 860-869.

Lavcanska V, Taylor NF, Schache AG. Familiarization to treadmill running in young unimpaired adults. *Hum Mov Sci*. 2005: **24**: 544-557.

Leary RF, Allendorf FW. Fluctuating asymmetry as an indicator of stress: Implications for conservation biology. *Trends in Ecology & Evolution*. 1989: **4**: 214-217.

Lee Y, Hara T, Fujita H, Itoh S, Ishigaki T. Automated detection of pulmonary nodules in helical CT images based on an improved template-matching technique. *IEEE Trans Med Imaging*. 2001: **20**: 595-604.

Lejeune TM, Willems PA, Heglund NC. Mechanics and energetics of human locomotion on sand. *J Exp Biol*. 1998: **201**: 2071-2080.

Lewis J. Fast normalized cross-correlation. Industrial Light and Magic, 1996.

Liikavainio T, Isolehto J, Helminen HJ, Perttunen J, Lepola V, Kiviranta I, Arokoski JP,

Komi PV. Loading and gait symmetry during level and stair walking in asymptomatic subjects with knee osteoarthritis: importance of quadriceps femoris in reducing impact force during heel strike? *Knee*. England, 2007:231-238.

Liljestrand G, Stenstrom N. Respirationversuche beim Gehen, Laufen, ski und Shlittschuhlaufen. 1920: **39**: 167-206.

Lund FH. Physical asymmetries and disorientation. The American journal of Psychology, 1930:51-62.

MacDougall JD, Roche PD, Bar-Or O, Moroz JR. Maximal aerobic capacity of Canadian schoolchildren: prediction based on age-related oxygen cost of running. *Int J Sports Med*. 1983: **4**: 194-198.

Mahaudens P, Detrembleur C, Mousny M, Banse X. Gait in adolescent idiopathic scoliosis: energy cost analysis. *Eur Spine J*. 2009: **18**: 1160-1168.

Manning J, Ockenden L. Fluctuating asymmetry in racehorses. *Nature*. 1994: **370**: 185-186.

Manning JT. Fluctuating asymmetry and body weight in men and women: Implications for sexual selection. *Ethology and Sociobiology*. 1995: **16**: 145-153.

Manning JT, Chamberlain AT. Fluctuating asymmetry in gorilla canines: a sensitive indicator of environmental stress. *Proc Biol Sci*. 1994: **255**: 189-193.

Manning JT, Koukourakis K, Brodie DA. Fluctuating asymmetry, metabolic rate and sexual selection in human males. *Evolution and Human Behavior*. 1997: **18**: 15-21.

Manning JT, Pickup LJ. Symmetry and performance in middle distance runners. *Int J Sports Med*. 1998: **19**: 205-209.

Margaria R. Sulla fisiologia e specialmente sul consumo energetico, della marcia e della corsa a varie velocità ed inclinazioni del terreno. *Atti Acc Naz Lincei*. 1938: **7**: 299-368.

Margaria R, Cerretelli P, Aghemo P, Sassi G. Energy cost of running. *J Appl Physiol*. 1963: **18**: 367-370.

Mattes SJ, Martin PE, Royer TD. Walking symmetry and energy cost in persons with unilateral transtibial amputations: matching prosthetic and intact limb inertial properties. *Arch Phys Med Rehabil*. 2000: **81**: 561-568.

Maupas E, Paysant J, Martinet N, Andre J. Asymmetric leg activity in healthy subjects during walking, detected by electrogoniometry. *Clin Biomech (Bristol, Avon)*. 1999: **14**: 403-411.

Mayhew JL. Oxygen cost and energy expenditure of running in trained runners. *Br J Sports Med*. 1977: **11**: 116-121.

McGregor SJ, Busa MA, Yaggie JA, Bollt EM. High resolution MEMS accelerometers to estimate VO2 and compare running mechanics between highly trained inter-collegiate and untrained runners. *PLoS One*. 2009: **4**: e7355.

Mian O, Thom J, Ardigò L, Narici M, Minetti A. Metabolic cost, mechanical work, and efficiency during walking in young and older men. *Acta Physiol (Oxf)*. 2006: **186**: 127-139.

Minetti A, Cazzola D, Seminati E, Giacometti M, ROI S. Skyscraper running. *Comparative biochemistry and physiology a-molecular & integrative Physiology*. 2008: **150**: S67-S68.

Minetti AE. The biomechanics of skipping gaits: a third locomotion paradigm? *Proc Biol Sci*. 1998: **265**: 1227-1235.

Minetti AE. The mathematical description (Lissajous contour) of the 3D trajectory of the body centre of mass: A locomotor 'signature' for the physiology, biomechanics and pathology of human and animal gaits. Gait & Posture, 2009:S153-S153.

Minetti AE, Ardig OL, Reinach E, Saibene F. The relationship between mechanical work and energy expenditure of locomotion in horses. *J Exp Biol*. 1999: **202**: 2329-2338.

Minetti AE, Ardigo LP, Saibene F. Mechanical determinants of gradient walking energetics in man. *J Physiol*. 1993: **472**: 725-735.

Minetti AE, Ardigo LP, Saibene F. The transition between walking and running in humans: metabolic and mechanical aspects at different gradients. *Acta Physiol Scand*. 1994: **150**: 315-323.

Minetti AE, Cazzola D, Seminati E, Giacometti M, Roi GS. Skyscraper running: physiological and biomechanical profile of a novel sport activity. *Scand J Med Sci Sports*. 2009.

Minetti AE, Pinkerton J, Zamparo P. From bipedalism to bicyclism: evolution in energetics and biomechanics of historic bicycles. *Proc Biol Sci*. 2001: **268**: 1351-1360.

Minetti AE, Saibene F. Mechanical work rate minimization and freely chosen stride frequency of human walking: a mathematical model. *J Exp Biol*. 1992: **170**: 19-34.

Moller AP, Thornhill R. Bilateral symmetry and sexual selection: a meta-analysis. *Am Nat*. 1998: **151**: 174-192.

Ortega JD, Farley CT. Individual limb work does not explain the greater metabolic cost of walking in elderly adults. *J Appl Physiol*. 2007: **102**: 2266-2273.

Perry MC, Carville SF, Smith IC, Rutherford OM, Newham DJ. Strength, power output and symmetry of leg muscles: effect of age and history of falling. *Eur J Appl Physiol*. 2007: **100**: 553-561.

Petray C, Krahenbuhl G. Running Training, Instruction on Running Technique, and Running Economy in 10-year-old Males. *Res Q Exerc Sport*. 1985: **56**: 251-255.

Pierotti SE, Brand RA, Gabel RH, Pedersen DR, Clarke WR. Are leg electromyogram profiles symmetrical? *J Orthop Res*. 1991: **9**: 720-729.

Potdevin F, Gillet C, Barbier F, Coello Y, Moretto P. Propulsion and braking in the study of asymmetry in able-bodied men's gaits. *Percept Mot Skills*. 2008: **107**: 849-861.

Raibert M. Symmetry in Running. *Science*, 1986:1292-1294.

Ralston HJ. Energy-speed relation and optimal speed during level walking. *Int Z Angew Physiol*. 1958: **17**: 277-283.

Rudel RG, Healey J, Denckla MB. Development of motor co-ordination by normal left-handed children. *Dev Med Child Neurol*. 1984: **26**: 104-111.

Sadeghi H, Allard P, Prince F, Labelle H. Symmetry and limb dominance in able-bodied gait: a review. *Gait & Posture*. 2000: **12**: 34-45.

Saibene F, Minetti AE. Biomechanical and physiological aspects of legged locomotion in humans. *Eur J Appl Physiol*. 2003: **88**: 297-316.

Sawicki GS, Ferris DP. Mechanics and energetics of level walking with powered ankle exoskeletons. *J Exp Biol*. 2008: **211**: 1402-1413.

Schmidt-Nielsen K. Locomotion: energy cost of swimming, flying, and running. *Science*. 1972: **177**: 222-228.

Slawinski JS, Billat VL. Difference in mechanical and energy cost between highly, well, and nontrained runners. *Med Sci Sports Exerc*. 2004: **36**: 1440-1446.

Smith TP, McNaughton LR, Marshall KJ. Effects of 4-wk training using Vmax/Tmax on VO2max and performance in athletes. *Med Sci Sports Exerc*. 1999: **31**: 892-896.

Souman JL, Frissen I, Sreenivasa MN, Ernst MO. Walking straight into circles. *Curr Biol*. 2009: **19**: 1538-1542.

Steudel-Numbers KL, Wall-Scheffler CM. Optimal running speed and the evolution of hominin hunting strategies. *J Hum Evol*. 2009: **56**: 355-360.

Van Valen L. A Study of Fluctuating Asymmetry. Evolution, 1962:125-142.

VanZant RS, McPoil TG, Cornwall MW. Symmetry of plantar pressures and vertical forces in healthy subjects during walking. *J Am Podiatr Med Assoc*. 2001: **91**: 337-342.

Waller. *Journal of Physiology*. 1919: **52**.

Wang P, DeNunzio A, Okunieff P, O'Dell WG. Lung metastases detection in CT images using 3D template matching. *Med Phys*. 2007: **34**: 915-922.

Whittington J, Richards P. The stability of children's laterality prevalences and their relationship to measures of performance. *Br J Edu Psychol*. 1987: **57**: 45–55.

Winter D. *Biomechanics of human movement*: New York: John Wiley & Sons 1979.

Winter D. *Biomechanics and motor control of human movement*: New York, John Wiley and Sons, Inc, Third Edition 2005.

Yong J, Smith R, Hatano L, Hillmansen S. What Price Speed - REVISITED. *Ingenia.* 2005: **22**: 46-51

Zamparo P, Carignani G, Plaino L, Sgalmuzzo B, Capelli C. Energy balance of locomotion with pedal-driven watercraft. *J Sports Sci*. 2008: **26**: 75-81.

Zarrugh MY, Radcliffe CW. Predicting metabolic cost of level walking. *Eur J Appl Physiol Occup Physiol*. 1978: **38**: 215-223.

Zarrugh MY, Todd FN, Ralston HJ. Optimization of energy expenditure during level walking. *Eur J Appl Physiol Occup Physiol*. 1974: **33**: 293-306.

Acknowledgements

Just arrived at the end of this work, it's common tradition to dedicate some lines to thank all the people, this thesis would not have been possible unless.
This page is addressed to all the person helped me in the course of these three years. Also in my opinion, most of times this is the only section that is read from people not directly involved in the project, relatives, friends or any other interested in this. For this reason I decided to go on with this text using my native language, Italian.
Un grande ringraziamento va al Prof. Alberto Minetti, tutor di questa tesi di dottorato. In questi 3 anni di studio e collaborazione è stato per me una guida, un'insegnante, una persona che definirei "stimolante".
Insieme con lui ringrazio tutte le persone coinvolte principalmente nel lavoro presentato; il Luca Ardigò dell'Università di Verona, anche se a distanza ha potuto aiutarmi con preziosi consigli e Paola Zamparo per i suggerimenti. Il Dott. Niccolò Faccioli dell'Ospedale di Borgo Roma (Verona) e Lauro (tecnico radiologo) per la loro disponibilità "elastica" nell'effettuare tutte le risonanze magnetiche. Un grazie speciale va alla Dottoressa Francesca Nardello, indispensabile nella parte sperimentale di questa tesi e alla tesista Alessandra. Ringrazio inoltre tutti i soggetti che hanno preso parte agli esperimenti, in particolare alla nostra "cavia" preferita, Gaspare. Ringrazio Cristine (mi raccomando si legge CRIS-CINI!), per la consulenza statistica e non solo. Ringrazio inoltre tutti coloro che hanno saputo rispondere a dubbi, incertezze e momenti di panico durante questo lavoro di ricerca, il prof Caiani del Politecnico di Milano, Ezio, causa principale di questo dottorato, Fico Federico, che viene citato anche solo per il nome, Dario e tutti gli insegnanti della National Instrument.
Grazie a tutto il gruppo del Prof. Minetti che si è allargato in questi anni. Grazie ragazzi perché insieme siamo come una squadra! Grazie al mio compagno di scrivania (per fortuna ce ne sono due separate!), Grazie Carlo per la tua pazienza, i consigli e gli "strappi" in stazione; grazie a Riccardo (ottima scelta gli amaretti), grazie a Gaspare che di mestiere fa il sosia e la cavia, ma è anche un buon programmatore, grazie Fabrizio per la consulenza clinica, e grazie ancora a Cristine per questi splendidi 6 mesi.

Non posso non ricordare in questi ringraziamenti tutte le persone del dipartimento, dalle segretarie del secondo piano Sandra, Marina ed Anna, ai tecnici, senza i quali il laboratorio non potrebbe andare avanti. Grazie a Riccardo, Pietro, Mario e Roberto.

Grazie a tutti gli altri dottorandi e tesisti che come me cercano di imparare la fisiologia (o lo hanno già fatto..). Grazie a Leonardo, Antonio, Ario, Dario, Francesco, Carmelo, Marta e Sara. Grazie a chi già è ricercatore, Matteo Pecchiari, un uomo con la risposta giusta al momento giusto, Darione e Gabriella, perchè senza di voi la pausa pranzo non avrebbe più senso. Ringrazio particolarmente tutti i professori del dipartimento di Fisiologia, quelli che qui hanno lavorato e quelli che oggi continuano a farlo all'interno di una struttura un po' vecchiotta ma ricca di storia.

Infine non posso dimenticare in questo elenco una componente fondamentale che mi ha accompagnato in questa esperienza. Ringrazio la mia famiglia; i miei genitori e le mie sorelle per avermi sempre dato fiducia e per aver creduto nelle mie scelte. Con loro ringrazio tutti i miei parenti e amici che mi sono stati vicini in questi 3 anni.

Ecco. Ultimo nell'elenco, ma non per importanza, grazie a chi ha condiviso con me le difficoltà ("strademoralizzanti") e le soddisfazioni incontrate in questo percorso di crescita "scientifica" e umana.